UNIVERSITAT DE BARCELONA

Functional analysis of EXD2 in mitochondrial homeostasis

Joana Raquel Faria da Silva

UNIVERSITAT DE BARCELONA

FACULTAT DE FARMÀCIA

Programa de doctorat en Biomedicina

INSTITUT DE RECERCA BIOMÈDICA (IRB) DE BARCELONA

FUNCTIONAL ANALYSIS OF EXD2 IN MITOCHONDRIAL HOMEOSTASIS

Memòria presentada per Joana Raquel Faria da Silva per optar al grau de doctor per la Universitat de Barcelona

Director

Travis H. Stracker

Tutor

Albert Tauler Girona

Joana Silva

Barcelona, 2016

TABLE OF CONTENTS

SUMMARY

Mitochondria function as bioenergetic, biosynthetic and signaling organelles within cells. Despite having their own genome, mitochondria also rely on nuclear encoded genes for their function. Our work focuses on the study of the uncharacterized protein Exonuclease 3'-5' domain like 2 (EXD2), a nuclear encoded gene that has been previously implicated in DNA repair and recombination. Interestingly, we found that EXD2 localizes to mitochondria and its depletion results in lower oxygen consumption, defects in metabolism and reduced mtDNA. EXD2 does not associate with known replication proteins and its depletion does not affect mtDNA replication. Instead, we found that EXD2 interacts with several subunits of Complex I of the electron transport chain and the mitoribosome and its depletion impairs mitochondrial translation, causing widespread metabolic abnormalities. Depletion of *Drosophila* EXD2 led to developmental defects, premature attrition of germ stem cells (GSCs) and problems with fecundity, which was accompanied by a significant increase in female lifespan. All phenotypes could be reversed by an anti-oxidant diet, supporting the idea that depletion of EXD2 triggers increased oxidative stress. Finally, we observed that EXD2 deficiency impairs breast tumor growth in *xenografts*, possibly by rendering the cells glutamine dependent or sensitive to hypoxia. Together, our data indicate that EXD2 is a novel mitochondrial translation factor and that its depletion results in defective oxidative phosphorylation and accumulation of ROS. We propose that EXD2 mutations may underlie undiagnosed metabolic disease and that it could be used as a biomarker/target for human cancer.

RESUMEN

Las mitocondrias son orgánulos celulares con una función bioenergética, biosintética y de señalización. A pesar de tener su propio genoma, las mitocondrias requieren genes codificados en el núcleo para su correcto funcionamiento. Nuestro trabajo se centra en el estudio de una proteína no caracterizada llamada *Exonuclease 3'-5' domain like 2* (EXD2), codificada por un gen nuclear que ha sido previamente asociado con la recombinación y reparación del daño en el DNA. Curiosamente, observamos que EXD2 localiza en la mitocondria y que su reducción en los niveles de expresión resulta en un consumo de oxígeno más bajo, defectos en el metabolismo y mtDNA reducido. EXD2 no parece asociarse con proteínas de replicación conocidas y su reducción no afecta la replicación del mtDNA. En cambio, encontramos que EXD2 interacciona con diferentes subunidades del Complejo I de la cadena de transporte electrónico y el mitoribosoma y que su reducción afecta la traducción mitocondrial causando anormalidades metabólicas. Un mal funcionamiento de EXD2 en *Drosophila* conlleva a defectos en el desarrollo, un desgaste prematuro de las células madre germinales (GSCs) y problemas de fertilidad, los cuales son acompañados de un incremento significante de esperanza de vida. Todos los fenotipos pueden ser revertidos con una dieta anti-oxidante, apoyando la idea de que la reducción de EXD2 genera estrés oxidativo.

Finalmente, observamos que una deficiencia en EXD2 afecta al crecimiento de tumores de mama en xenoinjertos, posiblemente por la rendición de células dependientes de glutamina o sensibles a hipoxia. Nuestra hipótesis es que EXD2 afecta a la traducción mitocondrial, y su inhibición resulta en una deficiencia en la fosforilación oxidativa y una acumulación de especies reactivas de oxígeno (ROS). Proponemos que las mutaciones en EXD2 podrían subyacer a una enfermedad metabólica sin diagnosticar y ello podría tener una aplicación como biomarcador o diana en cáncer humano.

LIST OF ABBREVIATIONS

A	Adenine
ADP	Adenosine diphosphate
ATP	Adenosine triphosphate
BioID-MS	BioID mass spectrometry
BN-PAGE	Blue Native Polyacrylamide Gel Electrophoresis
C	Cytosine
cDNA	Complementary DNA
ChIP	Chromatin immunoprecipitation
CO	Cytochrome c oxidase
CoA	Coenzyme A
CORR	Co-localization for redox regulation
CPT	Camptothecin
CR	Calorie restriction
D-loop	Displacement loop
DDR	DNA damage response
DDX28	DEAD-box helicase 28
DNA	Deoxyribonucleic acid
ECAR	Extracellular acidification rates
EcR	Ecdysone receptor
EF	Elongation factor
ELAC2	ElaC ribonuclease 2
ER	Endoplasmic reticulum
ERAL1	Era G-protein-like 1
ETC	Electron transport chain
EXD2	Exonuclease 3’-5’ domain containing 2
FAD	Flavin adenine dinucleotide
FASTKD2	FAST kinase domains 2
G	Guanine
GFP	Green fluorescent protein
Glc	Glucose
Gln	Glutamine
GLS	Glutaminase
GRSF1	G-rich sequence binding factor 1

GSC	Germ stem cell
GSH	Reduced glutathione
GSSG	Oxidized glutathione
GTP	Guanosine-5’-triphosphate
H-strand	Heavy-strand
HSP	Heavy strand promoter
IF	Initiation factor
IM	Inner membrane
IMS	Intermembrane space
InR	Insulin receptor
IRS	Insulin receptor substrates
KO	Knock out
L-strand	Light-Strand
LRPPRC	Leucine rich pentatricopeptide repeat containing
LSP	Light strand promoter
LSU	Large subunit
MFRTA	Mitochondrial free radical theory of aging
MMC	Mitomycin C
MPP	Mitochondrial processing peptidase
mRNA	Messenger RNA
mtDNA	Mitochondrial DNA
mtPAP	Mitochondrial poly(A) polymerase
mtRF1a	Mitochondrial release factor 1a
mtRNA	Mitochondrial RNA
mtRRF	Mitochondrial ribosome recycling factor
MTS	Mitochondrial-targeting sequence
NAC	N-acetyl cysteine
NAD	Nicotinamide adenine dinucleotide
NCR	Noncoding region
ND	NADH dehydrogenase
NMR	Nuclear magnetic resonance
OCR	Oxygen consumption rates
OM	Outer membrane
OXPHOS	Oxidative phosphorylation
Paraquat	PQT

PDE12	Phophodiesterase 12
PEPA	Position Enrichment by Proton Analysis
PET	Positron emission tomography
PNPase	Polynucleotide phosphorylase
POLRMT	Mitochondrial RNA polymerase
RNA	Ribonucleic acid
ROS	Reactive oxygen species
RPA	Replication protein A
rRNA	Ribosomal RNA
SF	Strep-Flag
sh	Short hairpin
SSU	Small subunit
T	Thymine
TCA	Tricarboxylic acid
TF2BM	Mitochondrial transcription factor B2
TFAM	Mitochondrial transcription factor A
TOM	Translocase of the outer membrane
tRNA	Transfer RNA
U	Uracil
VDAC	Voltage-dependent anion channel
WT	Wild-type
ZC3HAV1	Zinc-finger CCCH-type containing antiviral 1

INTRODUCTION

Overview

Ever since Charles Darwin published *The Origin of Species*, in 1859 (Darwin, 1859), evolution has become the grand unifying theory of biology. In particular, the study of phylogenetics has proven to be extremely insightful in decoding the diversity of life, as well as understanding the origin and evolution of current organisms.

One of the most fundamental events in the history of life is the origin of mitochondria. It was firstly proposed by Ivan Wallin, and later popularized by Lynn Margulis, as part of the endosymbiotic theory, that mitochondria initially arose from free-living bacteria that invaded eukaryotic cells (Wallin, 1992; Sagan, 1967). As a consequence, a mutually beneficial relationship was formed, where the eukaryote delivered protection and nutrients to the prokaryote and, in return, the prokaryote provided additional energy to its host by encoding the gene products essential for the energy-generating process known as oxidative phosphorylation (OXPHOS).

However, as this relationship became permanent over time, OXPHOS became indispensable to its host and the mitochondrion lost its autonomy, causing many of the mitochondrial genes to be transferred to the nuclear genome. The mammalian mitochondria has retained only a small subset of 37 genes in the form of a circular DNA molecule with a size of approximately 16.6 kb, including 13 essential subunits of the electron transport chain (ETC) (Anderson *et al*, 1981). Thus, these mitochondrial DNA (mtDNA)-encoded genes rely on nuclear encoded proteins for their transcription, processing and translation. Defects in the production or stabilization of these mtDNA-encoded subunits can lead to OXPHOS dysfunction, contributing to diverse types of human diseases, including different types of cancer, cardiomyopathies and neurodegenerative conditions (Chandra and Sing, 2011; Breuer *et al*, 2013).

Therefore, it has become of vital importance to understand and explore the regulatory mechanisms involved in controlling the production of mitochondrial gene products and their impact on mitochondrial function. The identification and study of novel proteins involved in particular mitochondrial functions will allow for the identification of new candidate genes for the molecular diagnosis of mitochondrial disorders and potential targets for the therapy of viral infections and cancer.

Structure of mitochondria

The internal structure of the mitochondria was visualized over 60 years ago using high-resolution electron-microscopy (Palade, 1952; Sjostrand, 1953). The images obtained showed mitochondria come in a wide range of sizes and shapes, ranging from punctuate structures to tubular filaments. Rather than a single organelle, mitochondria are better described as a dynamic network undergoing constant fusion and fission events while moving along cytoskeletal structures of the cell. They are capable of interacting with each other and even with other organelles like the endoplasmic reticulum (ER) (Mannella *et al*, 1998) and are therefore crucial for regulating cellular processes by acting as a communication system, both within and between cells. Consistent with this complexity in function, mitochondria also have multiple specialized compartments, some of which undergo dynamic changes in composition and structure depending on the cell type. The existence of an outer and inner membrane (OM and IM) allows the formation of two aqueous compartments, the matrix and the intermembrane space (IMS) (Figure 1).

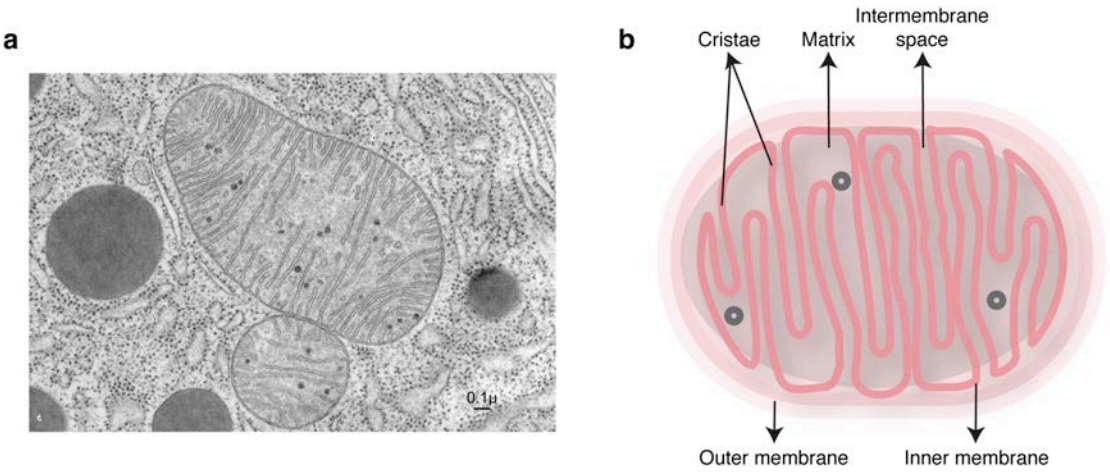

Figure 1: Mitochondria are highly organized structures. (**a**) An electron microscopy image illustrating the diversity of mitochondria by showing two very different shaped organelles. (**b**) Mitochondria are composed by an outer and inner membrane, which are separated by the intermembrane space that helps shape the matrix where the mtDNA resides. The IM is elaborately folded into structures know as cristae, which increases its surface area. The IM also harbors the components of the electron transport chain.

The OM is a relatively simple phospholipid bilayer that separates the inside of the organelle from the rest of the cell. In addition, it serves as an interacting point with other cellular organelles such as the ER. The OM contains channel structures called porins, which allow small proteins such as ATP, ADP and several ions to enter freely by diffusion. In the case of larger molecules, the OM possesses a complex of proteins called the translocase of the outer membrane (TOM), which allows their incorporation. These often include nuclear encoded proteins that are essential for mitochondrial function (Herrmann and Neupert, 2000). Due to its porosity, there is no membrane potential across the OM.

By contrast, the IM is protein rich and harbors the OXPHOS complexes (Kühlbrandt, 2015). This membrane serves as a tight diffusion barrier to all ions and molecules and these can only get across with the aid of specific membrane transport proteins, each of which is highly selective. As a result of this ion selectively, an electrochemical membrane potential builds up across the IM, which is required for the activity of its embedded ETC proteins (Yang *et al*, 2007). The IM is folded into compartmentalized structures called cristae, which maximize the surface area for ETC proteins required for energy production (Kühlbrandt, 2015).

The two mitochondrial membranes are separated from each other by the IMS, which contains redox-enzymes, cofactors and apoptosis associated factors (Webb *et al*, 2006; Koehler *et al*, 1999), while the mitochondrial matrix holds the majority of the mitochondrial proteins, including metabolic enzymes involved in the tricarboxylic acid (TCA) cycle, gene expression machinery, mitochondrial ribosome, translational regulators and protein folding complexes (Ryan and Hoogenraad, 2007).

Finally, it must be highlighted that all these mitochondrial compartments are functionally and physically connected to each other, allowing mitochondrial morphology to regulate key processes in response to metabolic alterations (Ryan and Hoogenraad, 2007).

mtDNA – the circle of life

Before the symbiosis of the proto-host cell, each one independently contained genetic information that was sufficient for their survival. However, as evolution progressed, the nuclear-cytosolic compartment took over most of the mitochondrial

functions, rendering these organelles dependent on the host genome (Anderson *et al*, 1981). It therefore remains puzzling why some genes still remain encoded by the mtDNA but some theories have been proposed to explain this. First, the proteins that remained encoded by the mtDNA are extremely hydrophobic, making it difficult for these to be translated in the cytosol, as their efficient folding and translocation into the mitochondria would be strongly affected (Popot and de Vitry, 1990). Second, the local control of mtDNA allows a rapid response of gene expression to local metabolic changes, known as co-localization for redox regulation (CORR) (Allen, 1993). Finally, there are significant differences in the genetic code used by the cytosolic and mitochondrial translation machineries; in particular, the cytosolic stop codon UGA is decoded in mitochondria as tryptophan, while the codon AUA is decoded in the cytosol as isoleucine and in mitochondria as methionine (Jacobs, 1991). Taken together, these theories highlight the unique and important nature of the remaining mtDNA-encoded proteins.

The mtDNA consists of a circular 16.6kb genome encoding 2 ribosomal RNAs (rRNAs), 22 transfer RNAs (tRNAs) and 13 open reading frames encoding subunits of the ETC complexes (Hällberg and Larsson, 2014) (Figure 2). The two mtDNA strands are differentiated by their nucleotide content, with a guanine-rich strand referred to as the heavy strand (H-strand) and a cytosine-rich strand denoted to as the light strand (L-strand). The L-strand encodes 8 tRNAs and one polypeptide, ND6, while all other mtDNA genes are encoded on the H-strand (Montoya *et al*, 1983).

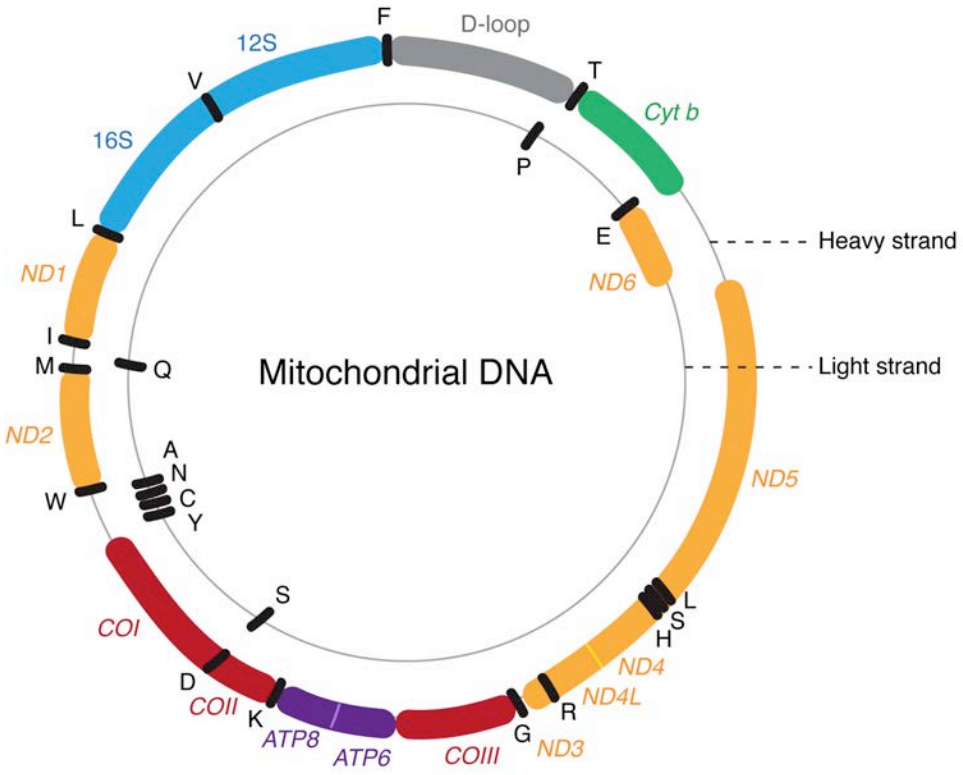

Figure 2: Human mtDNA encodes 13 proteins, 22 tRNAs and 2 rRNAs. The Gene content of mammalian mtDNA is shown with rRNAs depicted in blue, and tRNAs in black. The mRNAs encoding for the subunits of Complex I (*ND1-ND6*) are shown in yellow, Complex III (*Cyt B*) is shown in green, Complex IV (*COI-COIII*) is shown in red and Complex V (*ATP6 and 8*) is shown in purple. The genome is transcribed from two promoters: LSP (light strand promoter) initiates transcription of ND6 and the light strand tRNAs; HSP (heavy strand promoter) transcribes the two rRNAs and the remainder tRNAs and mRNAs.

Human mtDNA lacks introns and most genes are separated by only a few nucleotides, with nearly all the noncoding DNA being accumulated in the noncoding region (NCR). Here, we can find a triple-stranded region that forms a displacement loop (D-loop), which acts as a promoter for both the H and L-strands. Interestingly, the NCR is highly conserved in all of the characterized, partially deleted mtDNA in humans (Samuels, 2004). All polypeptide-encoding genes are flanked by at least one tRNA encoding gene, in what has been described as the tRNA-punctuation model (Ojala *et al*, 1981). However, genes encoding ATP6 and ATP8, as well as ND4 and ND4L have overlapping open reading frames. Furthermore, some genes lack the

termination codon, which is completed post-trancriptionally by poly(A)-addition (Ojala *et al*, 1981). To date, it still remains to be determined how these densely packed nucleoid complexes are processed and regulated in order to allow for mitochondrial transcription and translation.

Transcription and maintenance of mtDNA

Recent work using super-resolution microscopy has shown that mammalian mtDNA is packaged in small compact nucleoid structures (Brown *et al*, 2011). This process is mediated by the mitochondrial transcription factor A (TFAM), which increases the flexibility and bending of mtDNA, allowing its compaction (Hällberg and Larsson, 2011). The D-loop region contains the origin for initiation of H-strand mtDNA replication, which requires an RNA primer formed by transcription at the L-strand promoter (LSP). The replication of the lagging strand begins when the H-strand mtDNA replication is two-thirds complete and the L-strand replication origin is activated (Clayton, 1982). The mechanism of mtDNA replication remains poorly understood, and several models have been proposed (Lightowlers and Chrzanowska-Lightowlers, 2012).

mtDNA is transcribed in long polycistronic units by mitochondrial RNA polymerase (POLRMT) and can be initiated from two distinct promoters: LSP, and H-strand promoter HSP. As stated previously, the LSP encodes the messenger RNA (mRNA) ND6 and 8 tRNAs, while the HSP produces 2 rRNAs, 10 mRNAs and 14 tRNAs (Montoya *et al*, 1983) (Figure 3).

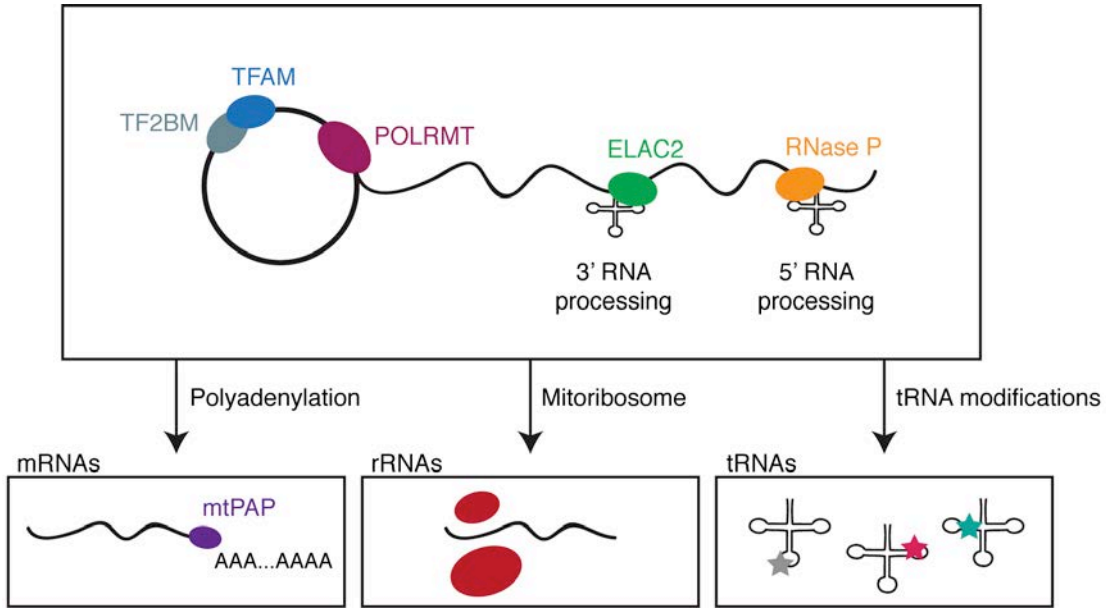

Figure 3: Regulation of the mitochondrial transcriptome. The mitochondrial genome is transcribed by POLMRT together with TFAM and TF2BM into polycistronic units which are then processed by RNAse P and ELAC2 into individual rRNAs, tRNAs and mRNAs.

In addition to POLRMT2, the transcription machinery is also composed of TFAM and the mitochondrial transcription factor B2 (TF2BM) (Litonin *et al*, 2010). Multigenic precursor strands are cleaved by RNase P and ElaC ribonuclease 2 (ELAC2) to generate the individual rRNAs, tRNAs and mRNAs that can be further modified for translation, stabilized or degraded. The stabilization and maturation of mRNAs requires polyadenylation by mitochondrial poly(A) polymerases (mtPAP), thus preventing defective mitochondrial membrane potential and oxygen consumption (Bobrowicz *et al*, 2008). Interestingly, mtPAP does not harbor a conserved RNA-binding domain nor a RNA-binding protein cofactor, suggesting that there might be additional players in this process. Removal of the poly(A) extensions can also have a variable effect on the mitochondrial transcripts, as it has been shown that they stabilize mtND1/mtND2/mtND5 while destabilizing mtCOI/mtCOII/mtCOIII and ATP6/ATP8 (Wydro *et al*, 2010; Nagaike *et al*, 2005), highlighting the complexity of how polyadenylation affects mitochondrial RNA (mtRNA) stability and translation.

Due to the polycistronic transcription, the mitochondria need to possess a robust and highly regulated RNA degradation machinery, in order to ensure optimal transmission of the transcripts without interference from non-coding RNAs. Whether

specific mitochondrial nucleases are involved in the degradation process remains unknown. Where it has been characterized, RNA decay and degradation is usually mediated by protein complexes. For instance, in *Saccharomyces cerevisiae*, Suv3 helicase cooperates with Dss1 ribonuclease, forming a complex called the mitochondrial degradosome (Margossian *et al*, 1996; Dmochowska *et al*, 1995), whereas in plants, Dss1 is replaced by the polynucleotide phosphorylase (PNPase) (Holec *et al*, 2006). Although PNPase has been proposed as a potential mitochondrial ribonuclease (Borowski *et al*, 2013; Wang *et al*, 2009), the fact that this protein localizes in the IMS makes it difficult to reconcile with a matrix role in RNA degradation. Additional nucleases have been proposed to have a role in mRNA processing. The zinc-finger CCCH-type containing antiviral 1 protein ZC3HAV1 binds to mRNA and recruits the RNA exosome to promote its degradation (Goodier *et al*, 2015; Zhu and Gao, 2008). Although it was first proposed to act specifically on RNA viruses, it was recently shown that ZC3HAV1 is also able to act on cellular mRNAs (Todorova *et al*, 2014) and its deficiency was associated with problems in the OXPHOS machinery (Arroyo *et al*, 2016). Another example is the mitochondrial protein phosphodiesterase 12 (PDE12), which has been shown to remove poly(A) extensions from mRNAs and its deficiency differentially affects specific transcripts, as well as mitochondrial translation (Rorbach *et al*, 2011). Nevertheless it still remains to be known which are the exact players involved in the mitochondrial degradation complex, highlighting the need for further studies.

Mitochondrial protein synthesis and degradation

The mitochondria contain a distinct set of ribosomes that are similar to those in the cytoplasm. These consist of the 39S large (LSU) and 28S small (SSU) subunits and two rRNA species, 12S and 16S, that are shorter than those of cytoplasmic ribosomes. This particular composition affects the ribosomal structure by making it more open and porous, with an altered sedimentation value of 55S for the complete monosome (Pietromonaco *et al*, 1991).

Mitochondrial translation is a multistep process that requires several factors for initiation, elongation, and termination (Figure 4).

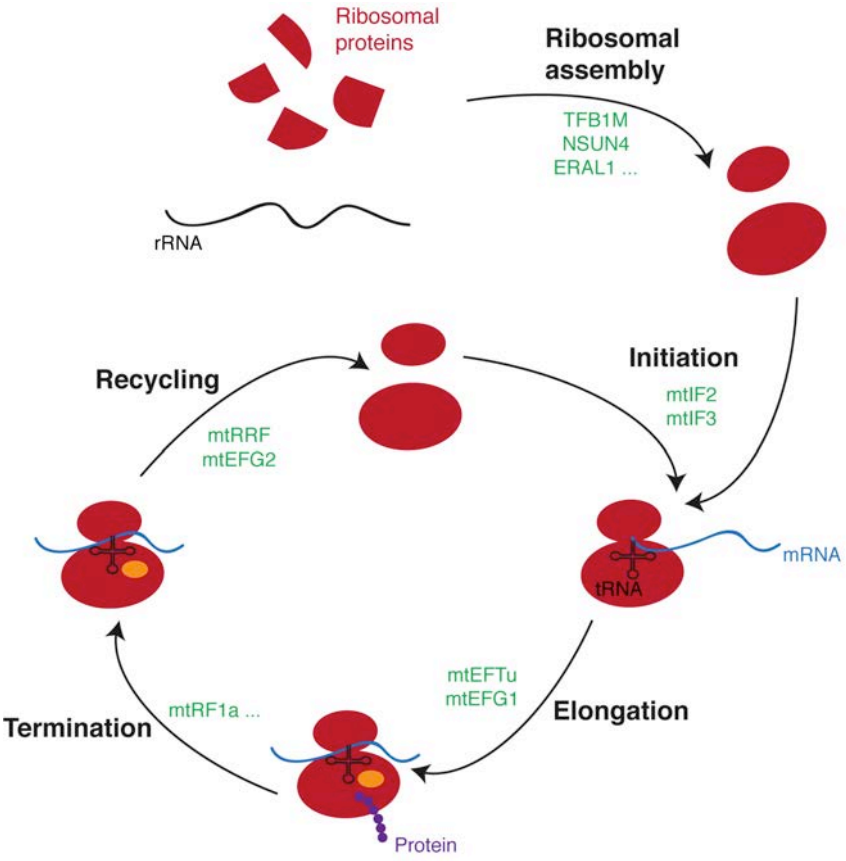

Figure 4: Biogenesis of the mammalian mitoribosomes. Mitochondrial translation involves several factors for initiation, elongation and termination that allow for the incorporation of the mRNA molecule in the mitoribosome and its translation. The anchorage of the mitoribosome in the IM facilitates the incorporation of the newly synthesized proteins into the membrane.

Mitochondria contain two initiation factors (IFs), mtIF2 and mtIF3 that are responsible for the dissociation of SSU and LSU of the mitoribosome, allowing for the incorporation of the mRNA molecule and appropriate translation. During elongation, the mitochondrial elongation factor mtEFTu delivers aminoacylated tRNAs to the ribosomes whereas a second elongation factor, mtEFG1 hydrolyzes GTP, allowing the translocation of the polypeptide sequence. The mitoribosme continues protein synthesis until a stop codon is reached and decoded and the termination of the process is mediated by the mitochondrial release factor 1a (mtRF1a) (Hällberg and Larsson, 2014). Following termination, the ribosomes are recycled by the mitochondrial ribosome recycling factor (mtRRF) and mtEFG2.

As each mitochondrial transcript is produced at the same rate, it becomes very important to regulate protein translation in order to meet the specific needs of the mitochondria. In addition to the nucleases mentioned before, several other proteins have been implicated in the stability of mitoribosomes, by promoting modification of rRNAs, such as methylation and pseudouridylation. These modifications are critical for ribosome assembly and can occur either during the transcription or immediately after, when the rRNA is assembled in the pre-ribosomal subunit (Venema and Tollervey, 1999). The mammalian TFB1M and NSUN4 have been identified as key modifying enzymes and their deficiency impairs mitochondrial translation due to a defective mitoribosome assembly (Metodiev *et al*, 2009; Cámara *et al*, 2011). The formation of mitoribosomes is also largely dependent on assembly factors, including GTPases and ATP-dependent RNA helicases, with only a few having been identified until now. The GTPase Era G-protein-like 1 (ERAL1), which is required for the maturation of the 12S rRNA, plays an important role in the assembly of the SSU and its depletion inhibits mitochondrial translation and induces oxidative stress and growth retardation (Uchiumi *et al*, 2010). Another recent study identified the DEAD-box helicase 28 (DDX28) as an interactor of the 16S rRNA and the LSU, and although its deficiency does not seem to affect mRNA stability nor rRNA processing, it dramatically impaired mitochondrial translation (Tu and Barrientos, 2015). Additional factors have also been identified, including the G-rich sequence binding factor 1 (GRSF1) and FAST kinase domains 2 (FASTKD2). Both these proteins localize in the RNA granules, where newly synthesized RNAs are stored and processed. Depletion of GRSF1 affects the assembly of the SSU and impairs mitochondrial translation (Antonicka *et al*, 2013; Jourdain *et al*, 2013), whereas FASTKD2 was shown to bind 16S rRNA and to be required for LSU assembly (Antonicka and Shoubridge, 2015). In addition to the initiation factors mentioned above, mitochondrial membrane potential and lipid composition of the IM are also known to affect mitochondrial protein synthesis (Ostrander *et al*, 2001; He and Fox, 1997). In addition, mitochondria have developed defense strategies in order to maintain cellular homeostasis. Perhaps one of the most important consists of molecular chaperones and proteases that can selectively remove damaged or excessive proteins from the organelle (Detmer and Chan, 2007). Finally, in cases where these protective mechanisms are not sufficient to ensure correct metabolic function, mitochondria can resort to a selective autophagy process called mitophagy, leading to the removal of damaged mitochondria (Kim *et al*, 2007).

Import of nuclear RNAs into the mitochondria

Given the importance of maintaining mitochondrial integrity and optimal metabolism for cellular fitness, it is not surprising that many signaling routes between the mitochondria and the nucleus have evolved.

Although mitochondria contain their own genome, most mitochondrial proteins are actually encoded in the nucleus and have to be translocated to the mitochondria (Kotiadis *et al*, 2014; Chandel, 2014). The *signal hypothesis* predicted that some proteins encode specific peptide sequences that determine their localization (Blobel and Dobberstein, 1975a; Blobel and Dobberstein, 1975b). In support of this idea, most of the nuclear encoded proteins that localize to the mitochondria possess a mitochondrial-targeting sequence (MTS), usually in the N-terminus, which addresses them to the organelle (Emanuelsson *et al*, 2000). Approaching the OM, the MTS is recognized by receptors of the TOM complex and the protein is imported into the mitochondria. The MTS is then often cleaved by the mitochondrial processing peptidase (MPP), allowing for proper protein folding (Nielsen *et al*, 1997).

However, a new paradigm is emerging whereby proteins that have an MTS can also localize to the nucleus and, in some cases, act as direct signals from mitochondria to regulate nuclear events (Monaghan and Whitmarsh, 2015). Therefore, it is of extreme importance that this communication between mitochondria and nuclei is properly regulated in order to avoid changes in metabolism and proteostasis (Kotiadis *et al*, 2014; Chandel, 2014; Whelan and Zuckerbraun, 2013).

In addition to this import mechanism, four other theories have been proposed. First, OM proteins can also be imported via a carboxy-terminal signal (Lee *et al*, 1999). A second mechanism imports hydrophobic IM proteins in a loop conformation, using a series of noncontiguous internal targeting signals (Wiedemann *et al*, 2001). Third, some small cysteine-rich IMS proteins are imported using an internal targeting sequence (Banci *et al*, 2009; Milenkovic *et al*, 2009). Lastly, some proteins are simply tailed-anchored in the OM via α-helices (Chacinska *et al*, 2009).

Finally, although the 22 tRNAs present in the human mitochondria are sufficient to decode the mitochondrial genome with wobble of the third anticodon base, nuclear tRNAs have recently been found within the mitochondria (Mercer *et al*, 2011; Rubio *et al*, 2008). The purpose and necessity of these RNAs remains unclear and underscores the complexity of the relationship between the mitochondria and nuclear encoded proteins and RNAs.

Defects in mitochondrial RNA processing in human diseases

Much of our understanding of mitochondria has come from the study of rare mitochondrial disorders. There are currently more than 150 different hereditary mitochondrial syndromes described, affecting both children and adults. Common phenotypic traits often include lactic acidosis, neurodegeneration, skeletal myopathy, blindness and deafness, among others (Vafai and Mootha, 2012).

There are several mechanisms that can lead to defective respiratory chain and mitochondrial disorders. Most directly, mutations in subunits of the respiratory chain or chaperone proteins required for proper OXPHOS function can affect ETC function (DiMauro and Schon, 2003). Mutations in proteins involved in mtDNA maintenance and protein translation can also affect the mitochondrial encoded ETC subunits and therefore lead to a defective OXPHOS function (Pancrudo *et al*, 2007). Moreover, proteins responsible for RNA processing and abundance have also been implicated in the development of mitochondrial disorders (Crosby *et al*, 2010; Haack *et al*, 2013).

However, the vast majority of human mitochondrial disorders are caused by nuclear genome defects, which is not surprising since the mtDNA encodes only 13 of the mitochondrial proteins. Advances in genomics and mitochondrial proteomics have allowed the discovery of several nuclear genes underlying mitochondrial disorders. The first of these studies identified mutations in the leucine rich pentatricopeptide repeat containing (LRPPRC) gene as a cause of Leigh Syndrome, a severe infantile disorder characterized by neurodegeneration and metabolic acidosis (Mootha *et al*, 2003). Subsequent studies have shown that LRPPRC plays a role in regulation of mitochondrial RNA, affecting the translation and stability of mitochondrial encoded cytochrome c oxidase subunits (Sasarman *et al*, 2010; Gohil *et al*, 2010). Leigh syndrome is also associated with mutations in nuclear encoded Complex I subunits (Martín *et al*, 2005), underlying the complexity and importance of a well-oiled machinery between the nuclei and the mitochondria.

Defects in mitochondrial RNA translation can also lead to several mitochondrial diseases. Frequent causes of impaired mitochondrial translation often include mtDNA rearrangements that affect mitochondrial tRNA and/or rRNA genes (Greaves *et al*, 2012; Tuppen *et al*, 2010). Some examples include mutations in the tRNA synthetases DARS2 and EARS2, both of which have been implicated in the development of leukoencephalopathy (Scheper *et al*, 2007; Steenweg *et al*, 2012).

Patients with translation elongation factor or mitochondrial ribosomal protein defects usually present at a young age and are characterized by severe multisystem disease. This lack of tissue specificity emphasizes the importance of identifying and understanding the factors regulating mitochondria translation.

Although ETC inhibition if often associated with several diseases, some observations suggest that the consequences can sometimes be beneficial. One example has to do with the use of metformin, a Complex I inhibitor. As a consequence of acting on Complex I activity, metformin also leads to the inhibition of hepatic gluconeogenesis, and has been therefore used extensively in the treatment of type-2 diabetes (Owen *et al*, 2000). Pretreatment with small-molecule inhibitors of the ETC can protect different organs from ischemia (Cahova *et al*, 2015). Finally, it has also been shown in several organisms that RNA-interference-mediated knockdown of different ETC components leads to a significant extension of lifespan (Idzorek, 1976; Copeland *et al*, 2009).

Taken together, these data point to the possibility of a therapeutic use for ETC inhibitors. Recently, a new concept of mitochondrial hormesis (mitohormesis) has arisen, defending the beneficial effects of physical exercise, reduced calorie uptake and appropriate reactive oxygen species (ROS) signaling (Ristow and Zarse, 2010). Nonetheless, it must be taken into account the need for a careful balance and evaluation of responses, given the dual effect caused by respiratory dysfunction.

The role of mitochondria in energy metabolism

Mitochondrial energy metabolism is essential for providing the cell with the fuel it needs to perform several biological processes. In eukaryotes, energy is generated by a series of interconnected and tightly regulated processes: glycolysis, which takes place in the cytosol, and TCA cycle and OXPHOS by ETC, which occur in the mitochondria (Figure 5).

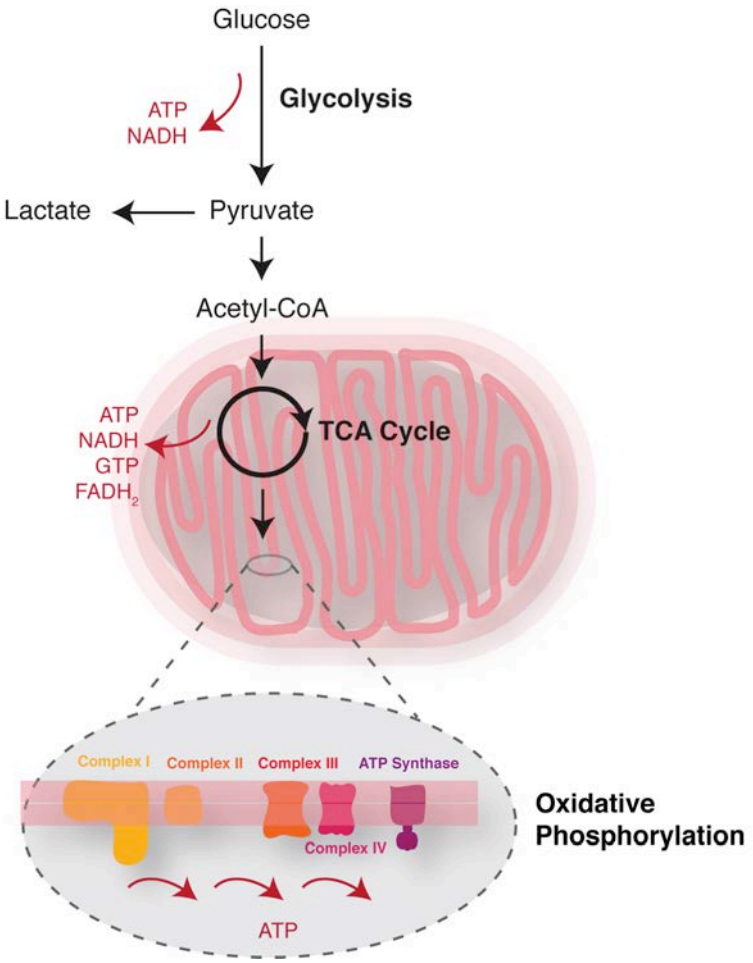

Figure 5: Cellular respiration is composed of three main processes. Energy and electrons and transferred from glucose (glycolysis) to convert NAD^+ to NADH in the TCA or citric acid cycle, which is used in the OXPHOS associated ETC to produce ATP.

Glycolysis, as the name suggests, is a process in which single molecules of glucose are split and ultimately converted into pyruvate. The fate of the pyruvate produced depends upon oxygen availability, although the process does not require oxygen. In anaerobic conditions, pyruvate cannot be completely oxidized but it can still be used for energy production by being converted into lactate, which restores the levels of NAD^+ that will fuel the next round of glycolysis. The fermented lactate is secreted out of the cell, resulting in local acidification of the cellular microenvironment. The final yield of glycolysis consists of two NADH and two ATP molecules. In contrast, when oxygen is available, the pyruvate produced can be used in the TCA cycle. Here, pyruvate is transported through the OM and IM to the matrix side, where it reacts with coenzyme A (CoA) to produce acetyl-CoA. Acetyl-CoA then

feeds into the TCA cycle, resulting in the production of three more NADH and two ATP molecules, together with two other carrier molecules: $FADH_2$ and GTP (Bratic and Trifunovic, 2010).

While pyruvate is the major fuel driving the TCA cycle, glutamine can also be used as a carbon source for this process. After entering cells via membrane transporter ASCT2, this six-carbon non-essential amino acid is hydrolyzed to glutamate and ammonia by glutaminase (GLS). Glutamate combines with cysteine and glycine to form reduced glutathione (GSH), which is involved in regulating the redox state and it also plays a major antioxidant role in the cell. In addition, glutamate can also be converted into α-ketoglutarate to feed the TCA cycle. This process is particularly useful in situations where the cell cannot properly use glucose to generate energy (Kroemer and Pouyssegur, 2008). Cancer cells have also been shown in some cases to exhibit increased glutamine uptake in order to provide the cells with the building blocks and energy necessary for high proliferation rates. In addition, this process also allows for a tight regulation of the cellular antioxidant response and control for the acidic environment triggered by lactate accumulation, characteristic of many tumors (Huang *et al*, 2013; Wise and Thompson, 2010).

Finally, the last major energy pathway involves the ETC, catalyzed by several enzymatic complexes (Complex I – Complex IV) embedded in the IM. This process is called OXPHOS and consists of the transfer of electrons from NADH and FADH2 to oxygen molecules, producing water. Free energy is conserved by coupling electron transport to the formation of a proton gradient by Complexes I, III and IV, which is then dissipated by F_1F_0-ATPase (Complex V) for ATP production. Additionally two electron carriers, coenzyme Q and cytochrome C, are also involved in the process. All complexes are composed of both nuclear and mitochondrially encoded proteins, except for Complex II, which is built exclusively by nuclear encoded factors (Bratic and Trifunovic, 2010). The net gain of OXPHOS is approximately 34 ATP molecules, making it the main respiratory process for producing cellular energy.

Fundamentals of cancer metabolism

Cancer cells have a high requirement for catabolites in order to produce ATP, generate biomass and maintain an optimal redox balance that will allow for them to

grow and proliferate at high rates. In order to answer these demands, cells need to alter their metabolism, which is often characterized by an increase in aerobic glycolysis and a reduction in OXPHOS. Although these alterations were first observed nearly a century ago, the field of cancer metabolism only became of interest for therapeutic interventions in the last decade. In fact, reprogramming of energy metabolism recently was proposed as a hallmark of cancer cells (Hanahan and Weinberg, 2011).

Otto Warburg first described in the 1920s, a tendency for increased glucose consumption in proliferating cells in comparison to non-proliferating tissues (Warburg *et al*, 1927). He hypothesized the *Warburg effect*, suggesting this specific metabolism was due to a defective mitochondrial function that could lastly result in tumor development, although it has now become clear that this is not always the case. Positron emission tomography (PET)-based imaging of the uptake of a radioactive glucose analog, ^{18}F-fluorodeoxyglucose (^{18}F-FDG) has been successfully implemented in the clinic for tumor diagnosis and staging, as well as for monitoring the response to treatment (Almuhaideb *et al*, 2011).

Similarly to glucose, glutamine is another growth-supporting fuel for the cancer cell. Besides providing carbon, it can also contribute with reduced nitrogen for the *de novo* biosynthesis of several compounds, including purine and pyrimidine nucleotides, glucosamine-6-phosphate and non-essential amino acids. Furthermore, glutamine also plays a role in the uptake of essential amino acids such as leucine, methionine and tryptophan, among others (Yanagida *et al*, 2001). Several studies have reported an increase in glutamine consumption in different cancer types (Wise *et al*, 2008; DeBerardinis and Cheng, 2010), and the use of ^{18}F-labeled glutamine has recently proven to be successful for tumor monitoring (Lieberman *et al*, 2011; Venneti *et al*, 2015).

As mentioned above, contrary to the initial hypothesis made by Warburg, it has been shown that most tumor cells possess functional mitochondria and many rely heavily on OXPHOS activity (Tan *et al*, 2015). One might wonder then why these cells switch from an oxidative metabolism to a glycolytic one. It appears that proliferating cells, surprisingly, have only a modest increase in their ATP consumption. Their greatest requirement has to do with precursor molecules and reducing equivalents in the form of NADPH, highly produced by glycolysis. In contrast, the TCA cycle is a robust producer of NADH, which works as a negative regulator of glucose metabolism. Therefore, by converting pyruvate to lactate, cancer

cells prevent the accumulation of cytosolic NADH, promoting glycolysis, which will fuel their exponential growth (Cairns *et al*, 2011). It is believed that this metabolic switch to glycolysis is what drives cancer cells to increase their glutamine uptake, in order to maintain proper mitochondrial function (Figure 6).

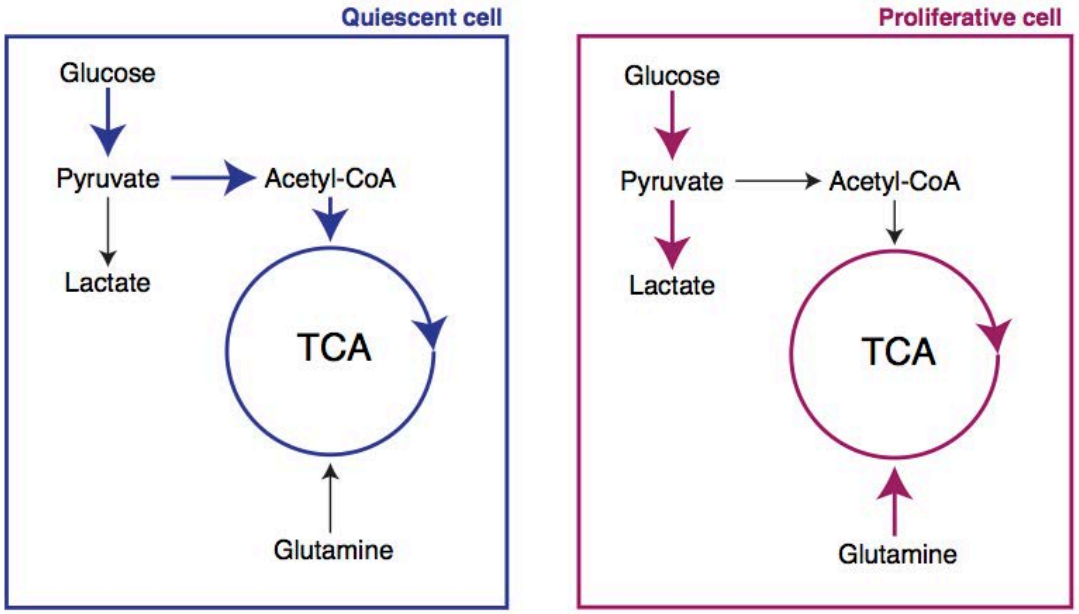

Figure 6: Metabolic differences between normal and proliferative cells. Proliferative cells often tune their metabolism towards highly elevated rates of glycolysis, followed by lactate fermentation, rather than pyruvate hydrolysis in the mitochondria. To prevent mitochondrial dysfunction, glutaminolysis is upregulated.

As a result of these observations, glutaminolysis inhibitors have become of great interest in the clinic. A wide variety of human cancer cell lines have shown sensitivity to glutamine withdrawal, including those derived from pancreatic cancer, glioblastoma and lung cancer, among others (Wu *et al*, 1978). Glutamine addicted cells undergo a drastic metabolic reprogramming, forcing the mitochondria to produce anabolic precursors from glutamine. The entry and flux of glutamine through the TCA cycle relies on a continuous production of NAD^+ through the activity of the mitochondrial ETC. As a result, inhibition of the ETC affects glutamine usage for cell growth, forcing them to depend on glycolysis. It has been shown recently that metformin induces a decrease in cellular proliferation in the presence of glucose, leading to cell death upon glucose deprivation. This suggests that cancer cells rely

exclusively on glycolysis for survival upon metformin treatment (Wheaton *et al*, 2014). Moreover, cancer cells with defects in OXPHOS or impairment in glucose usage were found to be more prone to respond to Complex I inhibition by biguanides (Birsoy *et al*, 2014). Thus, Complex I may constitute a target for adjuvant anticancer strategies, together with glutaminolysis inhibitors or anti-glycolytic drugs, allowing for a more complete control of cancer cells metabolism and thus preventing tumor growth and/or relapse.

Mitochondrial Complex I: structure and function

As stated before, the ETC consists of four major enzyme complexes that participate in the transfer of electron across the IM in order to generate energy. NADH is the electron source for Complex I, also known as NADH dehydrogenase. This is the largest of all complexes and consists of at least 44 subunits, of which 7 are encoded by the mtDNA (Sazanov, 2015; Sánchez-Caballero *et al*, 2016). Complex I is an L-shaped molecule with a peripheral arm projected into the matrix, and a membrane arm that resides in the IM. The peripheral arm consists of two functional blocks, the N (NADH binding) and the Q (ubiquinone binding) molecules, while the membrane arm consists of the P (proton pumping) molecule (Vinothkumar *et al*, 2014; Zickermann *et al*, 2015; Brandt, 2006) (Figure 7).

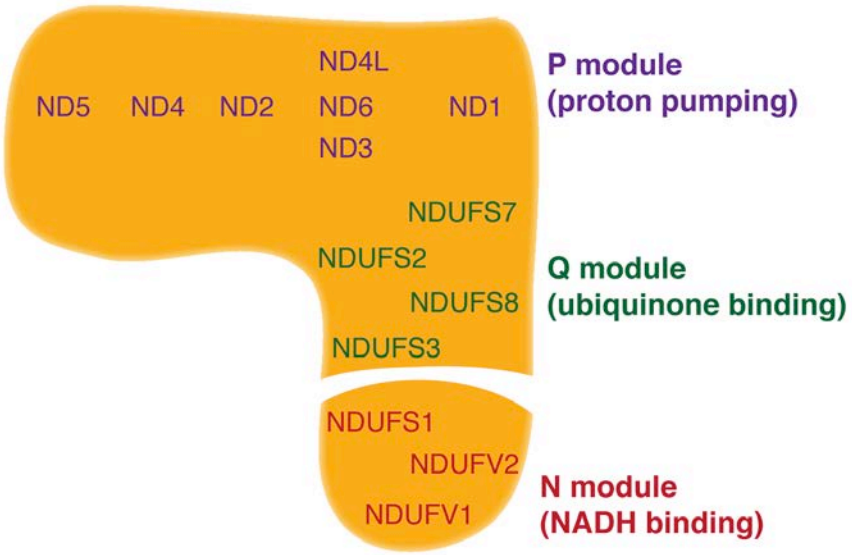

Figure 7: Schematic illustration of mammalian mitochondrial Complex I. It is an L-shaped structure containing a NADH dehydrogenase module (N module) and an electron transfer module (Q module) localized in the matrix, and a proton translocation module (P module) that resides in the IM. All of the mitochondrial-encoded subunits lie in the P module. Core subunits are indicated.

Complex I assembly is a very complex process that needs to be tightly regulated by several factors in order to assure its success and the proper functioning of the enzyme (Figure 8).

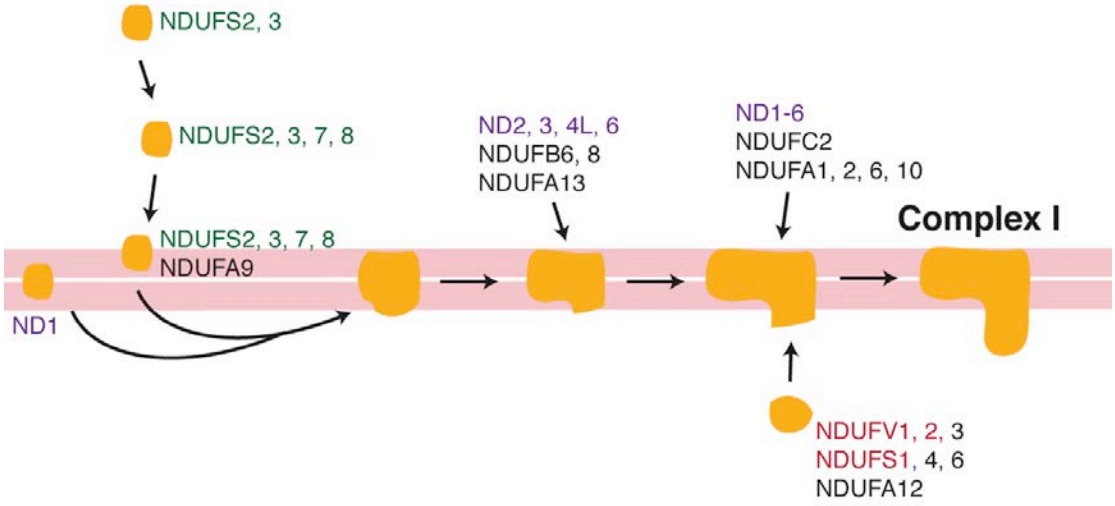

Figure 8: The assembly model of human Complex I. In the early stages, the core subunits of the Q module start merging. Later on these are combined with the most of the P module, in the IM. Finally, the N module, which was being pre-assembled independently in the matrix, is integrated with the rest of the proteins, forming a mature Complex I.

The process begins with the transcription of the nuclear and mitochondrial subunits, together with the assembly factors, followed by their translation and if needed, import into the mitochondria. Although many of these processes are common for all ETC complexes, others are quite specific and involve exact assembly factors (Ghezzi and Zeviani, 2012; Nouws *et al*, 2012). Patients with mutations on Complex I subunits or assembly factors, together with techniques such as Blue Native Polyacrylamide Gel Electrophoresis (BN-PAGE), have allowed for the identification of these assembly intermediates and revealed that the Complex I assembly process occurs in several steps (Triepels *et al*, 2001; Antonicka *et al*, 2003).

In an initial step, the core subunits NDUFS2 and NDUFS3 form a small complex, which is further enlarged by its combination with other subunits including NDUFS7, NDUFS8 and NDUFA9. This hydrophilic complex then gathers with the mitochondrial encoded ND1, forming an intermediate set that further assembles with another complex rich in mitochondrial encoded proteins. Meanwhile, the N module is pre-assembled in the matrix, involving nuclear encoded subunits involved in binding and oxidizing NADH. Finally, the N module, together with some other subunits, is added to the other modules, resulting in a mature Complex I (Mimaki *et al*, 2012).

Complex I can also form supercomplexes together with other members of the ETC, termed respirasomes, in a tightly regulated process that involves coordination between mitochondrial protein import and translation, requiring several assembly factors (Sánchez-Caballero *et al*, 2016; Lapuente-Brun *et al*, 2013; Acín-Pérez *et al*, 2008; Enríquez, 2016). These supercomplexes have been reported to modulate ROS production, regulating several processes such as hypoxia and immunity (Lenaz *et al*, 2016). Paradoxically, defects in Complex I activity, together with other ETC members, have been associated with many severe diseases (Chinnery, 2015), while also being described to extend lifespan in different organisms, in some cases in a ROS dependent manner (Yang and Hekimi, 2010a; Yang and Hekimi, 2010b; Dillin *et al*, 2002; Scialò *et al*, 2016).

ROS and mitochondria

ROS generated by mitochondria are physiologically very important, as they participate in stress signaling pathways that alert the cells of situations of oxidative damage. On the other hand, ROS production contributes to mitochondrial dysfunction in several pathologies, such as cancer, diabetes and neurodegenerative diseases (Dröge, 2002). Thus, it becomes vital to understand how mitochondria produce ROS and how these molecules affect cellular and organismal homeostasis.

Several electron transfer sites within the mitochondria have been identified as potential sources of ROS, although definitive measurements from every possible site have not been made. The ROS reactivity may vary significantly, ranging from relatively low (superoxide) to moderate (hydrogen peroxide) to high (hydroxyl radical). An excessive ROS generation or a failure in the scavenging systems can lead to mitochondrial dysfunction and affect key cellular processes (Murphy *et al*, 2011).

Most of the mitochondrial ROS are generated by the ETC. During this process, electrons can escape from flavin groups or iron-sulphur clusters and be captured by O_2 molecules, producing ROS. The ETC sites implicated in ROS generation include mainly Complexes I and III, although Complex II and IV have also been reported to play a role (Sabharwal and Schumacker, 2014). Complex V does not participate in electron transfer and to date there is no evidence that it can

contribute directly to ROS production. Nevertheless, alterations in Complex V activity may affect the mitochondrial membrane potential, which in turn can severely affect ROS levels.

In addition to the OXPHOS machinery, several other sources of mitochondrial ROS have been described (Andreyev *et al*, 2005). The cytochrome b5 reductase, localized in the OM, is involved in the oxidation of NADPH and reduction of cytochrome b5, resulting in the production if superoxide molecules (Samhan-Arias and Gutierrez-Merino, 2014). Some reports also showed ROS production in the IM, in the form of H_2O_2 by glycerol-3-phosphate dehydrogenase (Kwong and Sohal, 1998; Miwa *et al*, 2004). As with ETC enzymes, several TCA proteins with flavin-containing prosthetic groups also contribute to the generation of ROS (Quinlan *et al*, 2014).

Different subcellular compartments can be affected by mitochondrial ROS, underlying the importance of specialized antioxidant machineries that allow an independent control of redox homeostasis within each compartment. Superoxide dismutases, present in the cytosol, IMS and matrix, redistribute electrons between two superoxide molecules to form H_2O_2, which is then metabolized by different enzymes, including glutathione. Glutathione peroxidase reduces H_2O_2 to water while it oxidizes GSH to GSSG. The GSH/GSSG ratio is of extreme importance to maintain an optimal redox state within the cell and it can be used as an indicator of oxidative stress (Morgan *et al*, 2013) (Figure 9).

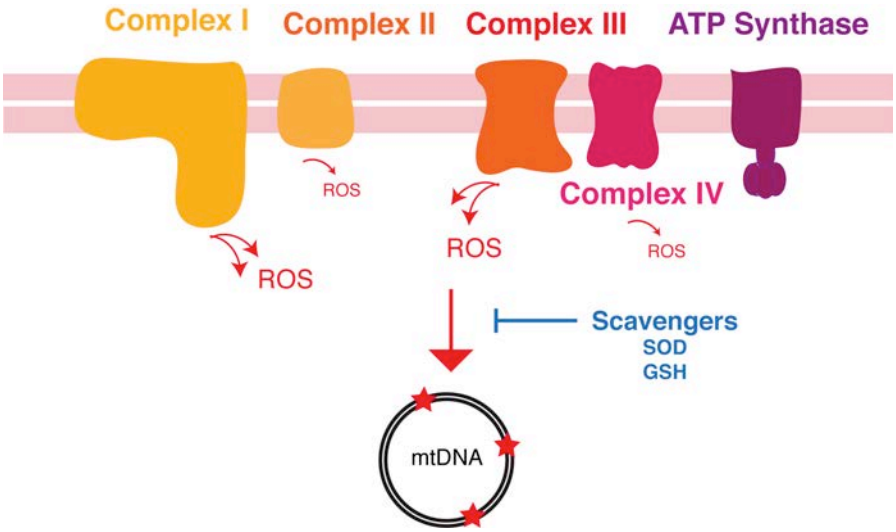

Figure 9: Generation of mitochondrial ROS. The mitochondrial electron transport chain is the major producer of reactive oxygen species, particularly by Complexes I and III. In order to avoid mtDNA damage and cellular dysfunction, ROS must be removed, thus mitochondria has developed scavengers such as SOD and GSH to help prevent excessive oxidative stress.

Although ROS production is thought to be deleterious for the cell, by promoting mtDNA damage and mitochondrial dysfunction, recent evidence has associated increased oxidative stress with lifespan extension in several organisms (Dillin *et al*, 2002; Van Raamsdonk and Hekimi, 2009; Mesquita *et al*, 2010), forcing the scientific community to reevaluate the role of ROS in the aging process (Hekimi *et al*, 2011; López-Otín *et al*, 2013).

Mitochondrial oxidative stress in aging

The exact processes that underlie the aging process are still poorly understood. Overall, aging can be roughly defined as the progressive decline in viability and the increase in vulnerability associated elements, which will ultimately lead to a reduced physical performance and increased risk of disease (Comfort, 1964). Several aging theories have been proposed, including the mitochondrial free radical theory of aging (MFRTA) (Harman, 1956). According to this model, cells

accumulate mitochondrial free radicals, produced during normal metabolism, which promote oxidative damage and thus promoting aging. This theory is based on several observations: (a) mitochondrial ROS levels increase with age due to deterioration in mitochondrial function; (b) important ROS scavengers degenerate with age; (c) mtDNA mutations increase during aging; (d) affecting ETC subunits and therefore OXPHOS function, which also translates in an increase in ROS production (Fraga *et al*, 1990; Stadtman, 1992; Marnett *et al*, 1985). Taken together, these evidences point to a central role of mitochondria in the aging process.

In recent years, however, several reports have challenged the pervasive MFRTA model. One concern has to do with the absence of a clear correlation between efficacy of antioxidant defenses and longevity. Assuming ROS cause cellular damage, one would expect that lowering ROS levels by increasing antioxidant defenses should slow the aging process and therefore result in lifespan extension. Conversely, the manipulation of antioxidant defense enzymes shows no clear correlation between oxidative damage and longevity (Mockett *et al*, 2003; Orr *et al*, 2003; Zhang *et al*, 2009; Doonan *et al*, 2008). Furthermore, some studies have suggested that inhibiting antioxidant genes may lead to an extension in lifespan (Van Raamsdonk and Hekimi, 2009; Ristow and Schmeisser, 2011).

Another controversial point is that specific lifespan in different animals does not directly correlate with ROS production. One of the more curious cases is the naked-mole rat, a long-lived rodent with a maximum lifespan of approximately 25-30 years. Contrary to what would be expected, these rodents have higher mitochondrial ROS compared with mice, which show a maximal lifespan of only 3-4 years (Andziak *et al*, 2006). These findings are consistent with other studies that show that increasing ROS production may lead to lifespan extension in worms, flies and mice (Yang and Hekimi, 2010b; Copeland *et al*, 2009; Csiszar *et al*, 2008). Finally, these observations have been supported by results showing that inhibition of different ETC components leads to an increase in longevity in several organisms (Hamilton *et al*, 2005; Copeland *et al*, 2009; Dillin *et al*, 2002). In order to reconcile these results with what the MFRTA postulates, it has been proposed that ROS may act as signaling molecules, thereby activating protective and adaptive programs (Ristow and Schmeisser, 2011; Zarse *et al*, 2012).

In addition to the MFRTA, another important model in the aging field is the Disposable Soma theory. This theory suggests that trade-offs result from splitting finite resources between growth, maintenance and reproduction (Kirkwood, 1977).

Numerous studies have supported the existence of a compromise between lifespan and fertility, most of which has been done in *Drosophila melanogaster*. One example is the experiment carried out by Partridge and collaborators, which showed that fly strains with longer lifespans showed a decrease in fecundity (Partridge *et al*, 1999). It has been proposed that the observed trade-offs between early- and late-life reproductions may be mediated by germ stem cells (GSCs) maintenance (Kaczmarczyk and Koop, 2011). A declining rate of GSC division or accelerated loss through differentiation appears to contribute to aging-induced sterility. Moreover, several studies have shown that an accumulation of ROS prompts differentiation of a variety of stem populations (Ong *et al*, 2016; Kong *et al*, 2016; Cao *et al*, 2016; Owusu-Ansah and Banerjee, 2009; Khacho *et al*, 2016). Defects in mitochondrial function have been reported to lead to a decrease in fecundity (Chang *et al*, 2015) and several mitochondrial genes have been implicated in the GSCs maintenance or differentiation in both male (Yu *et al*, 2016) and female (Teixeira *et al*, 2015) *Drosophila*.

Important future challenges include the discovery and characterization of novel proteins involved in the regulation of mitochondrial function that could have a potential impact on therapeutic strategies to delay the onset of age-related diseases and aging itself. As Bernard Strehler once said, “Aging and death do seem to be what Nature has planned for us. But what if we have other plans?”

METHODS

Generation of expression constructs

Human EXD2 was amplified from U2OS cell cDNA, sequenced and cloned into pENTR/D-TOPO (Invitrogen). EXD2 was subcloned using LR clonase into the retroviral vector pLPC-C-SF-TAP (SF=Strep-FLAG) generated by subcloning the C-SF-TAP cassette (a kind gift from Christian J. Gloeckner (Gloeckner *et al*, 2007)) into the pLPC-N-Myc plasmid (a kind gift from Titia de Lange, Addgene plasmid #12540). EXD2 mutants were generated using the QuikChange Lightning Site-Directed Mutagenesis Kit (Agilent Technologies 210518-5) according to the manufacturers instructions. Briefly, the PCR mixture was prepared with 5µl of 10x reaction buffer, 100ng of pLPC-EXD2-SF-TAP, 125ng sense primer 125ng, antisense primer, 1µl of dNTP mix, 1.5µl QuikSolution reagent, ddH_2O to a final volume of 50µl and 1µl of QuikChange Lightning Enzyme. All primers used are shown in Table 1. The supercoiled parental dsDNA was digested by 2µl of DpnI restriction enzyme (Stratagene) for 5min at 37°C, and X-Gold Ultracompetent Cells (45µl) were transformed with the DNA (5µl) by heat-shock. 500µl of LB-media was added followed by incubation at 37°C for 1h, after which the reaction was spread on agar with kanamycin and incubated at 37°C O/N. Clones were purified using the PureLink® Quick Plasmid Miniprep Kit (Invitrogen) and the sequence of constructs confirmed. Large-scale plasmid purification was performed using the PureYield™ Plasmid Maxiprep System (Promega).

Human cell culture

Human cell lines (U2OS, HEK293T, AD293, MDA-MB-231 and RPE2) were cultured in Dulbecco's modified Eagle Medium (DMEM, Invitrogen 41966) supplemented with 10% (v/v) fetal bovine serum (FBS, Sigma F7524-500ML) and 100U/ml penicillin/streptomycin (Reactiva 01030311B000) in 5% CO_2. Cells were periodically tested for mycoplasma using PCR and found negative (Primers shown in Table 1).

Generation of retrovirus/lentivirus and stable cell lines

For viral production, HEK293T cells were seeded in 10cm plates 24h prior to transfection with polyethyleneimide (PEI). For lentivirus, a mixture of 10μg lentivirus-shRNA, 2μg REV, 6μg RSV-RRE and 2μg VSV-G plasmids with 78μl PEI and 900μl 150mM NaCl was added to the cell culture media and for retrovirus, a mixture of 10μg retroviral vector DNA, 9μg GAG-Pol and 1μg VSV-G plasmids with 78μL PEI and 900μL 150mM NaCl was added to the cell culture media. In both cases, 16h later, cells were washed in PBS and the media replaced. 48h later the viral supernatant was removed, cleared with a 0.45μM filter, and incubated with target cells (2x). 3 days after infection, cells were selected with Puromycin (Sigma P8833-25MG) for 5 days and maintained subsequently in the normal growth medium. Lentivirus shRNA constructs were purchased from the Sigma MISSION lentiviral library against *EXD2* (*shEXD2#2*: TRCN0000051631 (NM_018199.1-155s1c1), *shEXD2#1*: TRCN0000327822 (NM_018199.2-1001s21c1) and *shCont*: SHC016 was used as control.

Generation of EXD2 knockout cells with CRISPR/CAS9

Forward and reverse oligonucleotides containing the guide sequence were annealed and cloned into the pX330 plasmid (Cong *et al*, 2013) that was subsequently transfected into U2OS and MDA-MB-231 cells using lipofectamine (Lipofectamine® 2000 Transfection Reagen, ThermoFisher). GFP-positive cells were sorted 24h after transfection (BD FACSAria III SORP) and grown as single clones. Screening for EXD2-KO cells was carried out by Western blotting. Two clones of both U2OS and MDA-MB-231 showing complete loss of EXD2 protein were selected for further phenotypic analysis.

Isolation of DNA, RNA and cDNA preparation

For DNA isolation of human cancer cell lines, 1,000,000 cells were plated on 10cm plates and collected 24h later in 515µl of lysis buffer (75mM NaCl, 50mM EDTA, 0.02% SDS, 0.4mg/ml Proteinase-K). Lysate was transferred to 1.5ml Eppendorf tubes and incubated at 50°C for 2h. 1 volume of isopropanol was added and mixed and incubated at 4°C O/N. Tubes were centrifuged at 8,500x*g* for 30min at 4°C and pellets washed with 70% EtOH and air-dried. DNA was resuspended in TE and diluted to 100ng/ml for qPCR. Drosophila DNA was obtained from adult flies that were snap frozen in liquid nitrogen and the abdomens homogenized with a pestle in grinding buffer (0.2M sucrose, 0.1M Tris pH 9.2, 50mM EDTA and 0.5% SDS) and incubated at 65°C for 10min. KAc was added to a final concentration of 5M and the samples were incubated on ice for 20min. DNA was precipitated with Phenol/Chloroform/Ethanol. Total RNA was isolated according to manufacturers instructions (PureLink RNA mini kit, Ambion). 1µg of total RNA was used as a template for cDNA synthesis using a High Capacity RNA-to-cDNA Kit (ABI).

Real Time qPCR

Real-time quantitative PCR was performed using the comparative CT method and a Step-One-Plus real-time PCR Applied Biosystems Instrument. Amplification was performed using Power SYBR Green PCR Master Mix (Applied Biosystems, 4309155) and all assays were performed in triplicate. Primers (Sigma) used are provided in Table 1. Analysis of EXD2 mRNA levels was done using Taqman probes from Applied Biosystems (*EXD2* Hs00217045_m1, *ACTB* 4352935E) together with Taqman master mix (AB). To assess mitochondrial mtRNA-levels, 1ug of RNA was used for cDNA synthesis according to the manufactures instruction (Applied Biosystems, 4387406). For analyzing mitochondrial mRNAs, possible DNA-contamination was controlled by DNase treatment according to manufactures instruction (ThermoFisher, EN0525) and cDNA-synthesis reaction without reverse transcriptase followed by qPCR.

Flow cytometry based assays for mitochondrial function

To measure mitochondrial membrane potential, 100,000 U2OS cells were seeded on 24-well plate in triplicate, 24h prior to analysis. The next day, cells were typsinized and 200,000 cells were suspended in 1ml of fresh medium. Cell suspension was stained with 2.5μg/ml JC-1 (Sigma, T4069) for 20min at RT in the dark. Cells were washed 2X for 5min in PBS, resuspended in 0.3ml of PBS and immediately analyzed by flow cytometry using channels FL1 and FL2. The ratio FL1/FL2 (aggregates/monomeric) was measured to determine the membrane potential. For the analysis of mitochondrial mass, 150,000 cells were seeded in 6-well plates in duplicate 24h prior to analysis. Cells were incubated for 30min with 250nM Mitotracker red probe in normal growth medium at 37°C. Cells were trypsinized and washed with warm PBS once and analyzed by flow cytometry immediately. To detect intracellular and mitochondrial ROS production, 150,000 cells were seeded in 6-well plates in duplicate 24h prior to analysis. Cells were incubated at 37°C for 30min in 5μM MitoSox (Molecular Probes M36008) and then trypsinized and washed with warm PBS once and analyzed immediately by flow cytometry.

Immunofluorescence

For immunofluorescence cells were fixed with 4% formaldehyde for 10min at RT. After two washes with PBS, cells were permeabilized with PBS containing 2% Triton X-100 for 10min at RT. Cell were washed twice with PBS and incubated with first antibody (1:500) in PBS-T containing 10% FBS for 1 hour at room temperature. After two washes with PBS-T, cells were incubated with secondary antibody (1:500) in PBS-T containing 10% FBS and DAPI for 1h at RT. Slides were rinsed in PBS-T, washed twice for 5min in PBS-T and mounted with Vectashield (Vector Laboratories, H-1000). Adult ovaries from *Drosophila* were dissected in Schneider medium and fixed in 4% formaldehyde in PBS for 20min at room temperature. After washing with PBS, they were permeabilized with 1% Triton X-100 in PBS for 2h and then incubated in PBST (1% (w/v) BSA, 0.2% Triton X-100, PBS) for 1h. Ovaries were then incubated with primary antibodies diluted in PBS-T O/N at 4°C. The next day, they were washed with PBS, incubated in the dark with secondary antibodies diluted

in PBST for 3h at room temperature and further stained with rhodamine-phalloidin (BT#00027) and Hoechst (Sigma) for 20min. After final washes with PBS, ovaries were mounted in Vectashield (Vector Laboratories, H-1000) Images were acquired with a Leica SPE confocal microscope and cropped in ImageJ. Depth (z) thresholds were set accordingly in order to apprehend the entire architecture. In some cases, brightness and constrast were adjusted in ImageJ (v 1.49b), any changes were applied to all images equally for direct comparison. Antibodies used are presented in Table 2.

Protein lysates, fractionation and Western blotting

Cells were rinsed with PBS and collected in lysis buffer (50mM HEPES, 16mM NaCl, 1% NP-40, 0.5% DOC, 0.1% SDS, 1x protease inhibitor cocktail (Roche 04693132001) and phosphatase inhibitor cocktail (Sigma P5726). Samples were sonicated (15s-15s) for 30min, spun down at 4°C for 20min at 12,000x*g* and quantified with the DC Protein assay (Biorad, 500-0114). 50µg of total protein was boiled 10min with loading dye (50mM Tris-Cl (pH 6.8), 0.3% SDS, 0.1% bromophenol blue, 10% glycerol, 0.4% b-mercaptoethanol) and separated by SDS-PAGE followed by electrophoretic transfer to PVDF membrane (Millipore). Membranes were blocked for 20min in PBS-T with 5% dry milk and primary antibody (in PBS-T with 5% dry milk) was added for either 1 hour at RT or O/N at 4°C. Membranes were washed 3X in PBS-T and incubated with secondary antibody (in PBS-T with 5% dry milk) 1h at RT. After 3X PBS-T washes, ECL-reagent (Amersham, RPN2132) and X-ray film (Fujifilm, 47410 19236) were used to detect signal. Antibodies used are listed in Table 2. Separation of cellular compartments was performed according to manufacturers instructions with Standard Cell Fractionation Kit (ab109719). Further HCl treatment of the nuclear fractions was used for chromatin extraction. Alternative chromatin fractionation (Supplementary Figure 1) was performed in accordance with a previous publication (Broderick, 2016). U2OS cells were resuspended in buffer A (10mM HEPES-KOH pH=7.9, 10mM KCl, 1.5mM $MgCl_2$, 340mM sucrose, 10% glycerol, 1mM DTT, 1x protease inhibitor cocktail and phosphatase inhibitor cocktail) and Triton-X100 was added to a final concentration of 0.1%. After incubation on ice for 5min, samples were centrifuged at 1,300x*g* for 4min. Pelleted nuclei were washed

with buffer A, resuspended in buffer B (3mM EDTA, 0.2mM EGTA, 1mM DTT, 1x protease inhibitor cocktail and phosphatase inhibitor cocktail) and lysed for 20min on ice. After centrifugation at 1,700x*g* for 5min, the supernatant (nuclear soluble fraction) was collected, and the pellet (chromatin fraction) was washed with buffer B, resuspended in urea buffer (9M urea, 50mM Tris-HCl pH=7.3) and sonicated.

Cross-linking and immunoprecipitation (ChIP)

HEK293 cells were transfected with *EXD2-WT*, *EXD2-NUC*, *EXD2-C1* and *EXD2-C2* cloned into a SF-TAP vector. Cross-linking was carried out in 1% formaldehyde for 10min at RT. The reaction was stopped by adding 125mM of glycine for 5min on ice. Cells were then collected on ice and centrifuged at 1,000x*g* for 5min at 4°C, pellets were washed with PBS and mitochondria were purified in agreement to a previous protocol (Dimauro *et al*, 2012). Mitochondria were then incubated with pre-washed anti-FLAG M2 magnetic beads at 4°C O/N and bound complexes were washed once with wash buffer (30mM TrisHcL, PH=7.4, 150mM NaCl, 0.1% NP-40) and twice with TBS buffer (30mM TrisHcL, PH=7.4, 150mM NaCl). The proteins were eluted in TBS buffer containing 100µg/ml 3XFLAG peptide (Sigma) at 4°C for 6h and analyzed by Western Blot. All buffers included fresh 1x protease inhibitor cocktail and phosphatase inhibitor cocktail.

Transmission electron microscopy (TEM)

HEK293T-cells stably overexpressing EXD2-Strep-FLAG or empty Strep-FLAG vector were grown to 80% confluency, washed 3X in PBS and fixed in 2.5% glutaraldehyde for 1h. Cells were detached by scraping and pelleted (4°C, 2,500rpm for 10min). Pellets were washed in 0.1M PB 4X for 10min, stained with 1% OsO_4 for 1h and washed again for 10min in 0.1M PB. Cells were dehydrated at 4 °C (series of acetone concentrations: 50, 70, 90, 96, 100 %) prior to embedding. Sections were cut with a UCT ultramicrotome (Leica Microsystems) and incubated with blocking buffer (5% and 1% bovine serum albumin (BSA) in 0.01M PBS solutions for 10 and 1min,

respectively). Grids were incubated 30min at room temperature with polyclonal FLAG antibody (Sigma) diluted 1 to 10 in blocking buffer (1% BSA in 0.01 M PBS). After four washes (0.25% Tween 20 in 0.01M PBS for 4min and 1% BSA in 0.01M PBS for 1min), sections were incubated with IgM anti-rabbit coupled colloidal gold particles (Jackson, West Grove, USA) diluted in blocking buffer for 15min, rinsed with water, rinsed in 0.01M PBS, fixed in 1% GA in 0.01M PBS, and rinsed abundantly in ddH_2O. Sections were stained with 1% potassium permanganate and 1% UA in water for 15min. Controls for non-specific binding of the colloidal gold-conjugated antibody were performed by omitting the primary antibody. Electron micrographs were obtained with a Jeol JEM 1010 MT electron microscope (Japan) operating at 80 kV in the Electron Microscopy core unit of the Parc Cientific de Barcelona.

Metabolomic analysis of human cell lines

A combination of LC-MS and GC-MS analysis performed by Metabolon (www.metabolon.com) (Evans *et al*, 2009) was used for the detection of a total of 253 metabolites in cell extracts. Analysis was performed using 5 replicates (cells and media) of control U2OS cells selected with a stable shRNA or cells expressing shRNA (*shEXD2#1*) against *EXD2*. Cells were collected, snap frozen and metabolites were extracted using a proprietary series of organic and aqueous extractions and divided into two fractions for analysis using liquid chromatography/mass spectrometry (LC/MS, LC/MS2) and gas chromatography/mass spectrometry (GC/MS). LC/MS was based on a Waters ACQUITY UPLC and a Thermo-Finnigan LTQ mass spectrometer, which consisted of an electrospray ionization (ESI) source and linear ion-trap (LIT) mass analyzer. Samples for GC/MS were re-dried under vacuum desiccation for a minimum of 24h prior and derivatized under dried nitrogen using bistrimethyl-silyl-triflouroacetamide (BSTFA). The GC column was 5% phenyl and the temperature ramp from 40°C to 300°C in a 16min period. Samples were analyzed on a Thermo-Finnigan Trace DSQ fast-scanning single-quadrupole mass spectrometer using electron impact ionization. Raw data was median-centered, and metabolite levels were compared between *shCont* and *shEXD2#1* groups using the t-test. False discovery rate was controlled using the Benjamini & Hochberg procedure (p-adjusted<0.1 and FC above 1.3 in

absolute value was used for statistical significance). Data analysis was performed using R version 3.2.0. MetPa (Xia and Wishart, 2010) was used to perform pathway enrichment and topological analysis.

For ^{13}C stable isotope tracer analysis, $6xE^6$ U2OS cells stably expressing the indicated shRNA constructs were seeded on 15cm tissue culture plates in triplicate. The following day, cells were rinsed 2X in PBS and 20ml media (DMEM w/o glucose, w/o glutamine, 10% FBS, 1x Penstrep) containing 5mM glucose (unlabeled or [U^{13}C6]-D-Glucose, Cambridge Isotope Laboratories, CLM-1396-1) or 2mM glutamine (unlabeled or [U-^{13}C5]-Glutamine, Cambridge Isotope Laboratories, CLM-1822-H-0.1) was added to the cells for 6h. Cells were collected by trypsinization and $10xE^6$ cells were pelleted and snap-frozen, after which the metabolites were extracted into solvent by adding 2mL of ice cold chloroform/methanol (2:1 v/v). The suspension was bath-sonicated for 3min, and 2mL of cold water was added and then, 1mL of chloroform/methanol (2:1 v/v) was added to the samples followed by bath-sonication for 3min. Cell lysates were centrifuged (5,000x*g* for 15min at 4°C) and the aqueous phase transferred into a new tube. The sample was frozen until analysis using Positional Enrichment by Proton Analysis (PEPA). PEPA detects the position of carbon label in isotopically enriched metabolites and quantifies fractional enrichment by indirect determination of ^{13}C-satellite peaks using 1D-^{1}H-NMR spectra.

Cell proliferation/survival assays

For colony formation assays, *c*ells were seeded at a density of 1,000 cells per well in 6cm plates and allowed to attach overnight. After completion of drug treatments (10 days), cells were stained with 0.1% crystal violet in 20% methanol. The number of colonies was analyzed with ImageJ. Cells were treated with the indicated doses of CPT-11 (Sigma, I1406) and MMC (Sigma, M4287).

Cell migration assay

Cells were seeded at high density in 12-well plates and incubated for 1 to 2 days until they reached a confluent monolayer. Wounding was performed by scraping the monolayer with a pipette tip and cells were monitored overnight. For kinetic analysis, kymographs were generated to four individual fields of each well and average speed was calculated.

Injection of MDA-MB-231 cells into mice

For orthopedic injections, 1 million cells were resuspended in PBS and mixed with matrigel (1:1). Eight-week-old female nude mice were anesthetized with ketamine (100mg/kg body weight) and xylazine (10mg/kg body weight). Immediately after injection of the cells, mice were imaged for luciferase activity and continued to be monitored weekly using IVIS imaging. A maximum tumor volume of 1,000mm^3 dictated the end of the experiment.

Seahorse bioanalyzer analysis

Cellular respiration was measured using a Seahorse XF24 bioanalyzer (Seahorse Biosciences). U2OS or MDA-MB-231 cells were seeded at 50,000-75,000 cells/well respectively on XF24 V7 PS cell culture microplates (Seahorse Biosciences, 100777-004) and cultured for 16h prior to the analysis. The analysis was performed according to the manufacturer's instructions in DMEM (Seahorse Bioscience 102353-100) supplemented with 5.5mM D-glucose and 2mM L-glutamine for the OCR experiments. For OCR measurement, the following reagents were added: Oligomycin (1μM), FCCP (0.4μM), and Rotenone (1μM) + Antimycin A (1μM). For the ECAR analysis the following reagents were added: Glucose (10mM), Oligomycin (1μm) and 2-DG (50mM). For the OCR analysis of individual complexes, digitonin (25μg/mL) was added to the media to allow cells to permeabilize for

approximately 1h, followed by sequential injections of malate (2.5mM) + pyruvate (5mM), rotenone (1μM), succinate (10mM) and antimycin (5μM).

Blue Native Page electrophoresis

Blue native PAGE (BN-PAGE) analysis was done according to a previously published protocol (Wittig, 2006). Briefly, 200μg mitochondria were isolated from U2OS cells, solubilized with 8g/g digitonin and loaded into a gradient gel. Coomassie staining allowed for the identification of mitochondrial complexes.

BioID analysis of proximity interactions

EXD2, EXD2-C2 or TLK2 were amplified with primers containing 5' AscI or 3' NotI restriction sites (see Table 1) using KOD Hot Start DNA Polymerase (Millipore) and cycling conditions recommended from the manufacturer (Polymerase activation at 95°C for 2min, denaturation at 95°C for 20sec, annealing at 55°C for 10sec and extension at 70°C for 50sec, repeated for 40 cycles). PCR products were purified using the PureLink Quick Gel Extraction Kit (Invitrogen) and cloned into pCR2.1-TOPO vector (Invitrogen). Top10 competent *E. coli* cells (Invitrogen) were transformed with pCR2.1-TOPO-EXD2, -EXD2-C2 or -TLK2 and colonies were selected in carbenicillin. Constructs were verified by restriction digestion and sequencing (Macrogen) with primers for the TOPO vector (T7 Promoter-F and M13-R). Afterwards, EXD2, EXD2-C2 or TLK2 were cut out from the pCR2.1-TOPO vector by restriction digestion with AscI (NEB) and NotI-HF (NEB), purified using the PureLink Quick Gel Extraction Kit (Invitrogen) and ligated into pcDNA5/FRT/TO-C-FLAG-hBirA* (EXD2) or pcDNA5/FRT/TO-FLAG-hBirA* (TLK2) (kind gifts from Dr. Brian Raught) using Quick Ligation Kit (BioLabs). Top10 competent *E. coli* cells (Invitrogen) were transformed with pcDNA5/FRT/TO-C-Flag-hBirA*- Exd2 Wt, pcDNA5/FRT/TO-C-Flag-hBirA*- Exd2 C2 or pcDNA5/FRT/TO-Flag-hBirA*- TLK2 vector and carbenicillin selected. The constructs were confirmed by restriction digestion with AscI (NEB) and NotI-HF (NEB) and sequencing (Macrogen). AD293

cells were seeded and transfected the next day with either pcDNA5/FRT/TO-C-FLAG-hBirA*-EXD2, pcDNA5/FRT/TO-C-FLAG-hBirA*-EXD2-C2, pcDNA5/FRT/TO-FLAG-hBirA*-TLK2 or pcDNA5/FRT/TO-C-FLAG-hBirA* using *Polyethylenimine* (PEI, Sigma) +/- 50μM biotin (IBIAN Biotechnology 2-1016-002). For mass spectrometry, 5x15cm plates per condition were harvested 24h post-transfection by scraping cells into PBS, washing 2X in PBS and snap freezing on dry ice. Cell pellets were lysed in 5ml modified RIPA buffer (1%TX-100, 50mM Tris-HCl pH 7.5, 150mM NaCl, 1mM EDTA, 1mM EGTA, 0.1%SDS, 0.5%Sodium deoxycholate and protease inhibitors) on ice, treated with 250U benzonase (EMD Millipore) and biotinylated proteins were isolated using streptavidin-sepharose beads (GE). Proteins were washed in Ammonium bicarbonate and digested with trypsin. Mass spectrometry was performed as previously described (Gupta *et al*, 2015).

Analysis of mitochondrial translation

To analyze the rate of mitochondrial translation, experiments were performed essentially as described (Sasarman and Shoubridge, 2012) with minor modifications. 400,000 cells were plated on 6cm plates the day prior to the experiment. Media was replaced with 2ml DMEM lacking methionine or cysteine (Life Technologies) with 10% dialyzed FBS (Hyclone) for 20min. 100ml of 6mg/ml sterile filtered emetine (Sigma) in PBS was added to the media for 10min followed by the addition of 400 mCi of S35 Easy tag (Perkin Elmer) for 1h, unless otherwise indicated. For some experiments, chloramphenicol (Sigma) was added at 40mg/ml or NAC (Sigma) was added at 5mM. Labeling media was removed and cells washed 2X in PBS followed by a 10min incubation in DMEM with 10% FBS with pen/strep. Cells were washed 3X in PBS and scraped into 1ml PBS. Following gentle centrifugation at 1,000x*g*, cell pellets were resuspended in RIPA buffer (50mM Tris–HCl pH=7.5, 150mM NaCl, 1% NP-40, 1mM $MgCl_2$, 1X EDTA-free protease inhibitor cocktail), nuclei pelleted by centrifugation at 2,000x*g* for 10min and the protein concentration determined by a modified BCA assay (Biorad). 20-40μg of lysate was run on a 14% SDS-PAGE gel and transferred to PVDF membrane. Dried membranes were exposed to a Storage Phosphor Screen (Molecular Dynamics) for 3 to 8 days and imaged using a Typhoon

8600 Variable Mode Imager (Molecular Dynamics). Contrast was adjusted and band intensity was quantified using ImageJ.

Protein purification and enzymatic assays

EXD2 61-470 was used for protein expression due to improved solubility and yield. It was PCR amplified and cloned into pet28a with an N-terminal His-SUMO tag using BsmBI and XbaI and protein was expressed in Bl21(DE3)pLysSRARE by the addition of 1mM IPTG at 25°C for 3h. Soluble proteins were purified using Nickel affinity resin in 50mM Tris pH=7.5, 500mM NaCl, 10% glycerol and eluted with increasing imidazole concentrations (up to 300mM). To confirm activity was that of EXD2 rather than potential contaminants, mutations D108A and E110A (*NUC*) were generated in the active site by site directed mutagenesis. This protein was then purified using nickel affinity resin following the same procedure as the wild type protein. Protein was further purified using ion exchange chromatography with a Q-hitrap column in 50mM Tris pH=7.5, 10% glycerol and proteins were eluted with a NaCl gradient and fractions were tested with ssDNA template to confirm activity correlated with the EXD2 protein.

For enzymatic activity assays, 60 ng-1 µg protein was incubated with 20nM 5' FAM labelled DNA/RNA in 50mM Tris pH=7.5, 100mM NaCl, 10mM $MnCl_2$, 0.5µg/ml BSA and 10% glycerol. Reactions were incubated at 37°C for 30min before DNA was denatured by boiling in 35% formamide. DNA was separated on an 18% polyacrylamide urea TBE gel at 21W for 2h. Products were visualized using a Fujifilm FLA-5100 image reader or Typhoon 9410 Variable Mode Imager (Amersham Biosciences). To generate double-stranded (ds) substrates oligos indicated in figure legends were annealed in 20mM Tris pH=7.5, 50mM NaCl, 0.5mM EDTA to make dsDNA and RNA/DNA hybrid substrates.

2D-agarose gel electrophoresis of mitochondrial replication intermediates

2D agarose gel electrophoresis was carried out as described previously (Reyes *et al*, 2009). Briefly, total DNA was extracted from approx. $4x10^6$ cells using Phenol chloroform and proteinase K. 30µg total DNA was digested with HinCII (NEB) and DNA was then separated in the first dimension on a 0.4% TBE agarose gel without ethidium bromide (EtBr) for 18h at 1.1 V/cm. The lane was then cut from the gel and rotated through 90° and the DNA was further separated in a 1% TBE agarose gel containing 500ng/ml EtBr for 6h at 260mA, 4°C. The gel was Southern blotted and DNA was identified using a radioactive probe made using Ready-To-Go™ dCTP DNA labelling beads (GE healthcare). The probe was specific to region 16341-151 and was generated by PCR (primer sequence in Table 1) (Yasukawa, 2005). Labelled membranes were exposed to a phosphor screen that was scanned using a Fujifilm FLA-5100 image reader.

Drosophila stocks and maintenance

Drosophila melanogaster with a transposon insertion mapped to *CG6744/dEXD2* (y^1 w^{67c23}; P{EPgy2}$CG6744^{EY03872}$; stock #16578) were obtained from the Bloomington Drosophila Stock Center at Indiana University (http://flystocks.bio.indiana.edu/) and reduced transcript level was confirmed by qRT-PCR as described. Flies were maintained at 25°C on a 12 h:12 h light:dark cycle at constant humidity. Flies were back-crossed to our control *yellow white* files for 14 generations.

Drosophila food preparation

For lifespan analysis, different fly-food formulations were prepared. Normal food (100 g yeast, 100 g sugar, 20 g agar, 30 ml nipagen and 3 ml propionic acid per liter of food); Caloric Restriction food (100 g yeast, 50 g sugar, 20 g agar, 30 ml

nipagen and 3 ml propionic acid per liter of food); Antioxidant food (100 g yeast, 100 g sugar, 20 g agar, 30 ml nipagen, 3 ml propionic acid and 10 mg/ml NAC per liter of food); Paraquat food (100 g yeast, 100 g sugar, 20 g agar, 30 ml nipagen, 3 ml propionic acid and 5mM paraquat). To prepare each diet, yeast, sucrose and agar were first dissolved in water and boiled for 10 min. After cooling, propionic acid and nipagen were added, and the food was distributed into the glass vials and allowed to solidify. Finally, NAC or paraquat were added to the specific diets.

Analysis of *Drosophila* lifespan, fecundity and development

To assess lifespan, newly hatched flies from each genotype were allowed to mate for 48h, after which females and males were separated and grouped into 30 flies per vial. Food vials were changed every 3 days and deaths were scored until all flies were dead. To determine fecundity, age- and diet-specific flies from each genotype were allowed to mate for 4h and fecundity was estimated from 6 independent egg-counts. The mean number eggs/fly was calculated. For the analysis of development, 0-4h embryos were collected on grape-juice agar plates. To assess pupariation, 40 newly hatched larvae were transferred to specific-food vials. Once the L3 stage was reached, larvae were monitored and new pupae were counted every 2 hours. For size measurements, 0-4h embryos and pupae were mounted for imaging and processed with ImageJ (v 1.49b).

Hypoxia treatment

Thirty males and thirty females of each genotype were used for each hypoxia recovery experiment. Flies were 3-day-old adults. Flies were exposed to 0.6% O_2 for 30min at 25°C and then put at normal oxygen conditions and observed for the time to recover from paralysis, indicated by the ability to climb the vial > 2cm. Experiments were repeated three times.

Climbing activity

Locomotor activity of young and old flies was assessed using the climbing assay previously reported (Bahadorani and Hiliker, 2008) with slight modifications. In brief, 20 flies/trial were placed in the bottom of a measuring cylinder and given 30sec to climb up. At the end of each trial, the number of flies that climbed up to a vertical distance ≥ 10cm was recorded. Each trial was repeated twice.

Glycogen measurement

Glycogen content was determined using a modified method previously described (Chan and Exton, 1976). Briefly, young and old flies were rapidly frozen in liquid nitrogen and homogenized in a 30% KOH solution. The samples were then boiled at 100°C for 15min and glycogen was precipitated with cold 66% ethanol overnight. Finally, the pellet was digested with α-amyloglucosidase and the glycogen content was measured using by spectrophotometry.

Statistical analysis

Statistical analysis was performed using Prism 7 and R. A two-tailed t-test was performed when comparing two groups with normal distribution. An ANOVA test was used when comparing more than two groups, followed by a Dunnett multiple comparison post-test. Survival and cumulative hazard functions were estimated by proportional-hazard Cox models. Hazard Ratios (HR) and their corresponding 95% confidence intervals were computed as a measure of association (results are shown in Supplementary Table 4).

Table 1: Primers (5'-3') used in this study. All primers were ordered from Sigma. Mutagenesis primers were designed using the ABI online primer design tool.

Gene/target	Purpose	Forward (5'-3')	Reverse (5'-3')
EXD2	Amplify endogenous gene	CACCATGTCTAGACAGAACTTAGTG	CAGACAGCTGGATGGGAAGATC
EXD2-D>A	Mutagenesis of the exonuclease catalytic residues (*EXD2-NUC*)	GATTTTCCAGTACTTGGAATTGCCTGTGAGTGGGTAAATTTGGAAG	CTTCCAAATTTACCCACTCACAGGCAATTCCAAGTACTGGAAAATC
EXD2-E>A	Mutagenesis of the exonuclease catalytic residues (*EXD2-NUC*)	GATTTTCCAGTACTTGGAATTGCCTGTGCGTGGGTAAATTTGGAAG	CTTCCAAATTTACCCACCCACAGGCAATTCCAAGTACTGGAAAATC
EXD2-CXXC1	Mutagenesis of the first CXXC motif (*EXD2-C1*)	TGGTTAAAGAGAACCTCTGTGTAGTGTCTGGCAAG	CTTGCCAGACACTACACAGAGGTTCTCTTTAACCA
EXD2-CXXC2	Mutagenesis of the second CXXC motif (EXD2-*C2*)	ATGTGCTGCTGCTCTCCACCTCCTCCCATGCCATTTCCA	TGGAAATGGCATGGGAGGAGGTGGAGAGCAGCAGCACAT
EXD2Δ1-62	Deletion of the MTS (ΔMTS)	ATGCGGATCCTTAAAGCAAAGGTGG	ATGGAGTGGGATCAAATCGAGCCCTT
EXD2-MTS (1-62)		CCACCTTTGCTTTAAGGATCCG	GCAAGGGCTCGATTTGATCCCACTCT
EXD2-G1	Guide RNA for CRISPR/CAS9 targeting	CACCGACTCGTTTTACTCCTTCGG	AAACCCGAAGGAGTAAAACGAGTC
EXD2-G2	Guide RNA for CRISPR/CAS9 targeting	CACCGTTGTGGTCCTTATCTCGAT	AAACATCGAGATGAAGGACCACAAC
EXD2-G3	Guide RNA for CRISPR/CAS9 targeting	CACCGAATCACGTTCTTCCGAATGT	AAACACATTCGGAAGAACGTGATTC
EXD2-Asc1/NotI	Amplify EXD2 for BirA fusion cloning	AAAAAAGGCGCGCCTATGTCTAGACAGAACTTAG	AAAAAAGCGGCCGCAGACAGCTGGATGGGA
TLK2-Asc1/NotI	Amplify TLK2 for BirA fusion cloning	AAAAAAGGCGCGCCTATGGAAGAATTGCATAGCC	AAAAAAGCGGCCGCTTAATTAGAAGAACTGTT
H1-forward and reverse	For generating 2D-AGE probe	TTACAGTCAAATCCCTTCTCGTCC	GGATGAGGCAGGAATCAAAGACAG
EXD2-61-470 BsmBI-XbaI	Cloning EXD2 for bacterial expression	CGCGCGTCTCGAGGTCTGCACTCCAGTGCCCCCAGATCC	CGCGTCTAGATCA GTCATAGTAGTTGGAAATGGCATGGCA
EXD2-61-470 DXA-AXA	For mutagenesis to make EXD2-61-470-NUC	CCA GTA CTT GGA ATT **GCC** TGT G**C**G TGG GTA AAT TTG	GTACTGGAAAATCTTCTAATTCACTTCTAAGC

GAPDH	Real time PCR	TAAATTCGACTCGACTCACGGT	CTCCACCACATACTCGGCTC
COX II	Real time PCR	GTTGACGGTACACCTGGACG	GCCCCACAGATTTCTGAACA
RNA pol II	Real time PCR	AGGGCGGCGAGGACATGGAT	CGACGGCTGGTAGTGACCG
dEXD2	Real time PCR	AATGAACTGAAGAATCACTGCCA	CACATAGACCCCGATGGGA
Sir2	Real time PCR	CGGCCTCGTGCACCAAGTGT	CACTGCGGGCACACCGGAAT
EcR	Real time PCR	CGAACAAAAGACCGCGACTT	GCCTGGACTAGGAGTGGACAT
dILP2	Real time PCR	CGACAGCGATCTGGACGCC	AGGGCACTTCGCAGCGGTT
dILP3	Real time PCR	GGCCGCAAACTGCCCGAAA	ACGGGGTCCAAAGTTCTCTTGGT
dILP5	Real time PCR	AGCAGCAGTTCCAGCAAGGCA	GTTTGCGGCCTGGGCGGATA
InR	Real time PCR	ACAAAATGTAAAACCTTGCAAATCC	GCAGGAAGCCCTCGATGA
Myco	Mycoplasma testing	TGCACCATCTGTCACTCTGTTAACCTC	ACTCCTACGGGAGGCAGCAGTA

Table 2: Antibodies used in this study.

Antibody	Species	Company	Dilution
FLAG	Mouse	Sigma (F3165)	IF 1:500
EXD2	Rabbit	Sigma (HPA005848-100ul)	WB 1:500, IF 1:250
TOM20	Mouse	Santa Cruz (sc-17764)	IF 1:250
H3	Rabbit	Abcam (ab18521)	WB 1:500
ATP5A	Mouse	Abcam (ab14748)	WB: 1:1000, IF 1:500
NDUFA9	Mouse	Invitrogen (459100)	WB 1:1000
VDAC	Rabbit	Abcam (ab15895)	WB 1:500
Cytochrome C	Rabbit	Santa Cruz (sc-7159)	IF 1:500
GFP	Rabbit	Abcam (ab6556)	WB 1:1000, IF 1:500
OXPHOS Cocktail	Mouse	Abcam (ab110413)	WB 1:1000
GAPDH	Mouse	Millipore (MAB374)	WB 1:1000
Lamin	Rabbit	Santa Cruz (sc-20680)	WB 1:250
Hts (1B1)	Mouse	DSHB (528070)	IF 1:250
RPA2	Rabbit	Bethyl (A300-244A)	IF 1:250
FLAG	Rabbit	Sigma (F7425)	EM 1:200, IF 1:500
Alexa Fluor 488	Goat (anti-mouse)	Molecular Probes (A11001)	IF 1:500
Alexa Fluor 594	Goat (anti-mouse)	Molecular Probes (A11005)	IF 1:500
Alexa Fluor 488	Goat (anti-rabbit)	Molecular Probes (A11008)	IF 1:500
Alexa Fluor 594	Goat (anti-rabbit)	Molecular Probes (A11012)	IF 1:500
Anti-rabbit HRP	Goat (anti-rabbit)	Cultek (32490	WB 1:30000
Anti-mouse HRP	Goat (anti-mouse)	Thermo Scientific (31430)	WB 1:30000

Table 3: DNA sequences used to generate substrates for the biochemical characterization of EXD2

Template	Sequence 5' – 3'	modification
A	AGTCGCATAGTGTAGTCGGTCTTGTTCGGTCATAGCTCATCGTGG	5' Fam
A-RC	CCACGATGAGCTATGACCGAACAAGACCGACTACACTATGCGACT	unmodified
A-RNA	AGUCGCAUAGUGUAGUCGGUCUUGUUCGGUCAUAGCUCAUCGUGG	5' Fam
B	CATATCCGTGTCGCCCCTTATTCCGATAGTGACTACA	5' Fam
B-RC	TGTAGTCACTATCGGAATAAGGGGCGACACGGATATG	Un modified

OBJECTIVES

Objectives

The objective of this work is to characterize the role of EXD2 in mitochondrial homeostasis by evaluating its function in cell metabolism, cancer and development.

Detailed objectives:

1 – Define the subcellular localization of EXD2

2 – Characterize the effect of EXD2 depletion on mitochondrial homeostasis

3 – Identify EXD2 interacting proteins

4 – Establish the enzymatic activity and substrate-specificity of EXD2

5 – Characterize the role of EXD2 *in vivo*, using *Drosophila melanogaster*

6 – Determine the effect of EXD2 deficiency on breast cancer growth

RESULTS

Chapter 1

EXD2 is a novel regulator of mitochondrial translation and oxidative metabolism

Contributors: Joana Silva, Suvi Aivio, Philip A. Knobel, Laura J. Bailey, Maria Vinaixa, Pablo Perez-Ferreros, Etienne Coyaud, Alexis A. Jourdain, Brian Raught, Aidan J. Doherty, Oscar Yanes and Travis H. Stracker

EXD2 is an evolutionarily conserved exonuclease

Exonuclease 3'-5' domain containing 2 (EXD2) is an evolutionarily conserved gene that is present in a large percentage of the eukaryotic lineage, suggesting it could play essential roles in cellular physiology. EXD2 encodes a 3'-5' exonuclease domain similar to that of the WRN protein, mutated in Werner's progeria, which predisposes patients to cancer and premature aging, among other pathologies (Kudlow *et al*, 2007) (Figure 10a). However, most of the genetic instability found in Werner's syndrome patients has been attributed to a defective helicase activity, whereas the function of the exonuclease domain remains unclear. In addition to the exonuclease domain of EXD2, we identified a highly conserved domain near the C-terminus with homology to some HNH endonucleases that contain tandem CxxC motifs (Figure 10b). Alternative structural predictions suggest this region may also be related to multiheme cytochromes that bind heme through cysteine and histidine residues, suggesting EXD2 could be important for oxygen sensing and other metabolic functions, such as antioxidant defense or electron transport (Figure 10c).

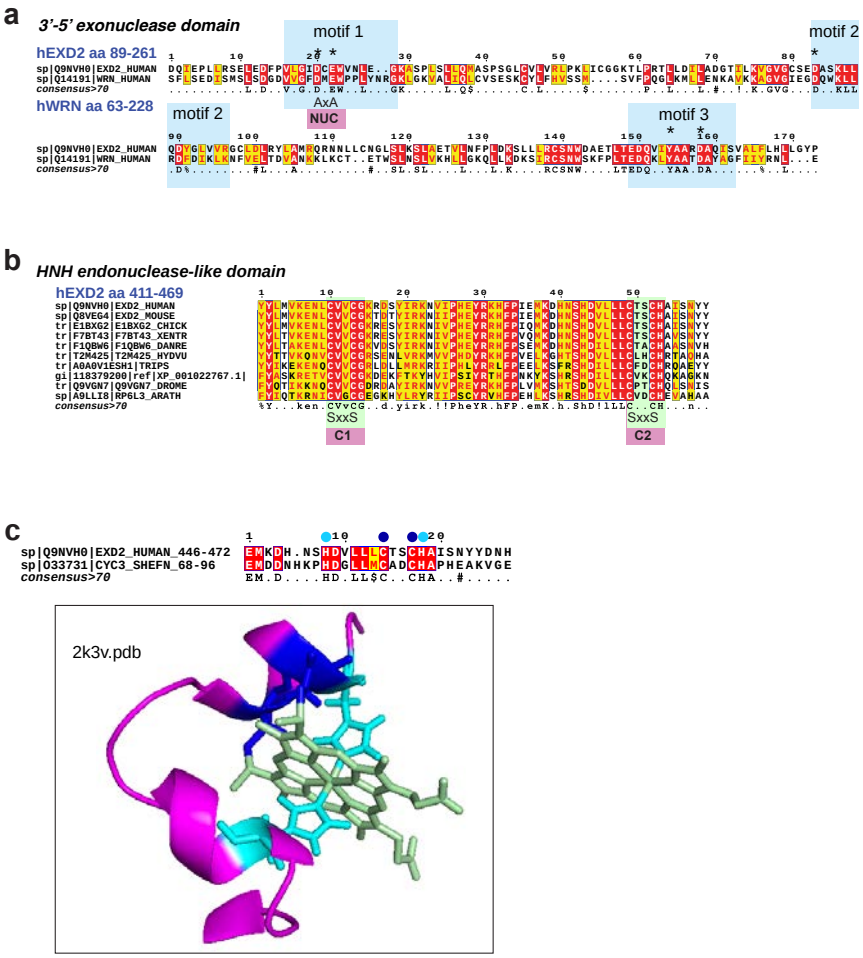

Figure 10: EXD2 is a conserved exonuclease. (**a**) Sequence alignments of the 3'-5' exonuclease domains of human EXD2 (aa 89-261) and WRN (aa 60-228). The 3 conserved exonuclease signature motifs of DNAQ family members are highlighted in blue. Critical metal binding residues are indicated with and asterisk. The NxE to AxA mutations made to generate the nuclease dead (*EXD2-NUC*) allele are shown in pink. (**b**) Alignment of the HNH endonuclease-like domain of EXD2 (human aa 411-469) proteins from the indicated species. The CxxC motifs are highlighted in green and the sites of the CxxC to SxxS mutations in the *C1* and *C2* alleles are indicated in pink. (**c**) Sequence alignment showing similarity between EXD2 and a Tetraheme cytochrome (CYC3) heme-binding domain. Iron contacting histidines are shown in light blue and heme binding cysteines in dark blue. The structure of CYC3 is shown with H and C residues annotated with the same colors as the alignment. Structure graphic of the homologous region to CYC3 was prepared in MacPyMOL using the 2k3v.pdb file.

EXD2 is a mitochondrial protein

Given the role of WRN, and many other nucleases, in DNA replication and repair, we examined the localization of EXD2 in mock treated cells and cells exposed

to the topoisomerase I inhibitor camptothecin (CPT) that induces DNA damage primarily during S-phase. Using confocal microscopy, endogenous EXD2 was predominantly detectable in the cytoplasm, regardless of CPT treatment (Figure 11a). As the pattern of EXD2 localization was reminiscent of the mitochondrial network, we then performed co-localization experiments with TOM20, a well-known mitochondrial protein, and confirmed substantial mitochondrial localization (Figure 11a). To further confirm this, we performed subcellular fractionation, in both mock and CPT treated cells. The separation of cytosolic, mitochondrial, nuclear and chromatin fractions confirmed that endogenous EXD2 was primarily mitochondrial, regardless of whether cells experienced DNA damage (Figure 11b). Keeping in mind the exonuclease domain of *EXD2*, we next tried to assess whether this protein localized close to the mtDNA, possibly playing a role in replication or repair. In order to address this we performed a modified chromatin immunoprecipitation (ChIP) procedure, with cells overexpressing wild-type protein (*EXD2-WT*), a mutant for the nuclease domain (*EXD2-NUC*), and two different mutants for the C-terminal domain (*EXD2-C1* and *EXD2-C2*), fused with a FLAG-tag protein. We found that EXD2 co-precipitates with mtDNA, suggesting a potential physical interaction (Figure 11c). This interaction becomes slightly reduced in *EXD2-NUC* cells and is almost absent in both *EXD2-C1* and *EXD2-C2* cells, suggesting these residues located in the C-terminus of the gene appear to be essential for this interaction. We also used, as a positive control, cells overexpressing *POLG2* a well-described mtDNA-replication protein.

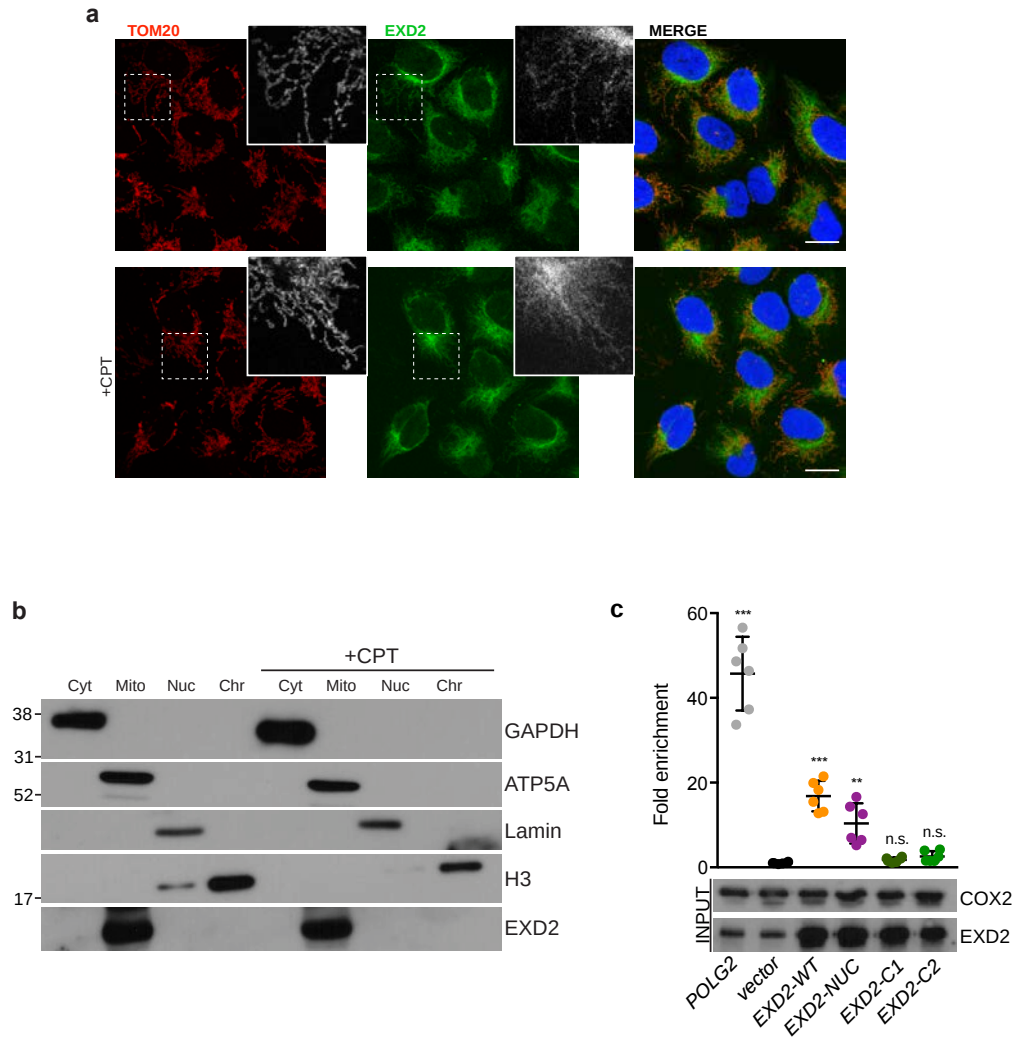

Figure 11: EXD2 is a mitochondrial protein. (**a**) Immunofluorescence analysis of endogenous human EXD2 in U2OS cells revealed extensive co-localization with the mitochondrial TOM20 protein. Localization of EXD2 was unaltered by treatment with 1uM CPT to induce DNA damage (lower panels). (**b**) Subcellular fractionation of EXD2 in the presence or absence of 1uM CPT treatment indicated exclusively mitochondrial localization. (**c**) A modified ChIP assay indicated that EXD2 localized in the proximity of the mtDNA. The mtDNA enrichment was reduced in the *EXD2-NUC* and completely abolished in both *C1* and *C2* mutants. The mitochondrial DNA polymerase subunit POLG2 was used as a positive control. Mean compiled from 2 independent experiments performed in triplicate (n=6) and the standard deviation are shown. Statistical analysis was performed using one-way ANOVA together with Dunnett's test (***$p < 0.001$, **$p < 0.01$, n.s. = non-significant, analysis of variance compared with the vector).

The MTS is necessary and sufficient for EXD2's mitochondria localization

Comparative sequence analysis identified a putative, mitochondrial targeting sequence (MTS) in the N-terminus of EXD2 that is conserved amongst many of the EXD2 homologues that have been identified to date (Figure 12a). To determine if this was a functional MTS, we overexpressed a GFP tagged full length EXD2 (*EXD2-GFP*), a truncation allele lacking the putative MTS (*ΔMTS-GFP*), and we also created a GFP fusion-protein consisting only of the MTS (*MTS-GFP*). The results showed that the full length *EXD2-GFP* was efficiently transported to the mitochondria (Figure 12b upper panel), whereas deletion of the MTS in the *ΔMTS-GFP* led to a diffuse nuclear and cytoplasmic localization consistent with protein degradation (Figure 12b middle panel). Finally, the MTS alone was sufficient to transport GFP to the mitochondria (Figure 12b bottom panel). These results confirmed that the N-terminus of EXD2 contains a *bona fide* MTS that is both necessary and sufficient for its mitochondrial localization.

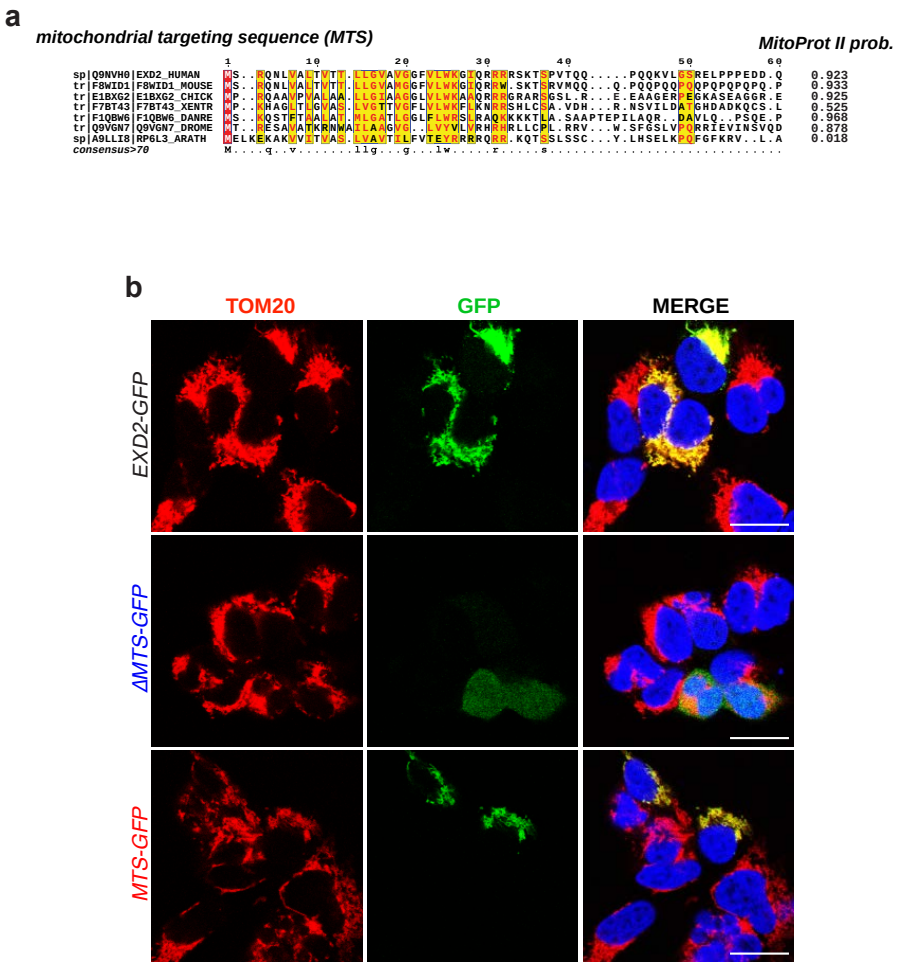

Figure 12: The MTS is both necessary and sufficient for mitochondria localization (**a**) Sequence alignment of the MTS of EXD2 proteins from the indicated species and their predicted mitochondrial targeting probability (MitoProt II). (**b**) The N-terminus of EXD2 contains a MTS that localizes GFP to the mitochondria (upper panel); Deletion of the MTS leads to protein degradation and diffuse localization (middle panel); Fusion of the MTS to GFP is sufficient to localize GFP to the mitochondria (bottom panel).

Depletion of EXD2 is not toxic to cancer cell lines

To address the potential functions of EXD2, we depleted different cancer cell lines of the endogenous proteins using two approaches: we created stable knock down cells using two independent non-overlapping short hairpin RNAs (*shEXD2#1* and *shEXD2#2*), each one resulting in a significant reduction in expression (Figure 13a); and we generated cell lines lacking EXD2 using CRISPR/CAS9 mediated deletion and complemented them with the wild type cDNA (*EXD2-WT*) or mutants in

the exonuclease (*EXD2-NUC*) or HNH domains (*EXD2-C1* and *EXD2-C2*) (Figure 13b).

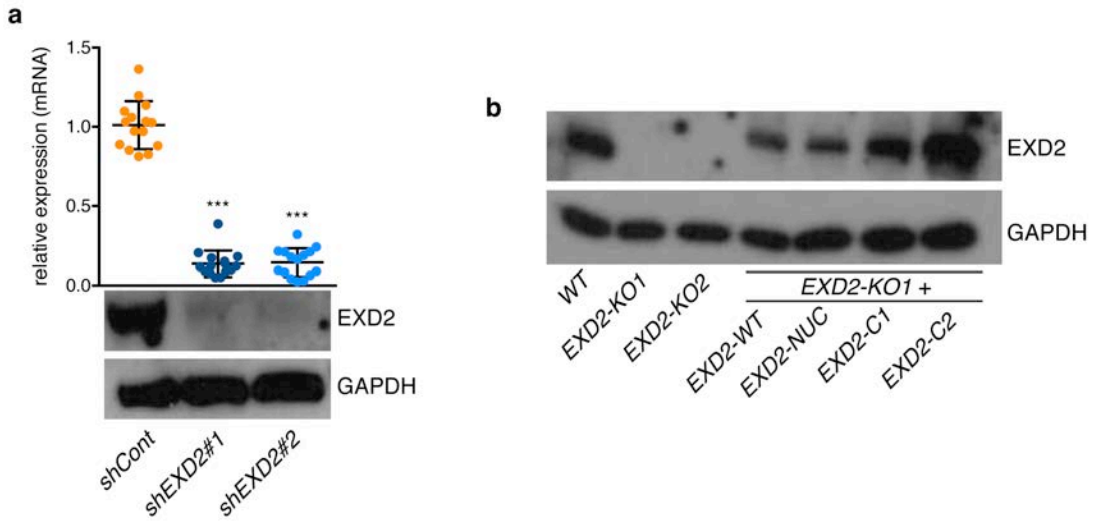

Figure 13: Generation of EXD2 deficient cells. (**a**) Depletion of EXD2 in U2OS cells by stable shRNA expression with 2 independent vectors (*shEXD2#1* and *shEXD2#2*) reduces mtRNA and protein levels. Mean compiled from 2 independent experiments performed in triplicate (n=6) and the standard deviations are shown. Statistical analysis was performed using one-way ANOVA together with Dunnett's test (****p* < 0.001, analysis of variance compared with the WT). (**b**) Generation of cells lacking EXD2 using CRISPR/CAS9 targetting and complemented with EXD2 or indicated mutant forms. A representative western blot of U2OS cells showing relative levels of EXD2 is presented.

EXD2 is not a DNA damage response factor

It was previously reported that cells lacking EXD2 were more sensitive to different alkylating agents, including mitomycin C (MMC) and CPT (Smogorzewska *et al*, 2010) and a recent publication has proposed EXD2 as a key player in homologous recombination by facilitating DNA end resection (Broderick *et al*, 2016). In order to determine if EXD2 could play a role in the DNA damage response (DDR), or influence sensitivity to damage, the colony formation assay was employed to measure the sensitivity of the *EXD2-KO* clones to different DNA damaging agents. The results showed no significant differences in the survival of the different cell lines exposed to different doses of CPT and MMC (Figure 14).

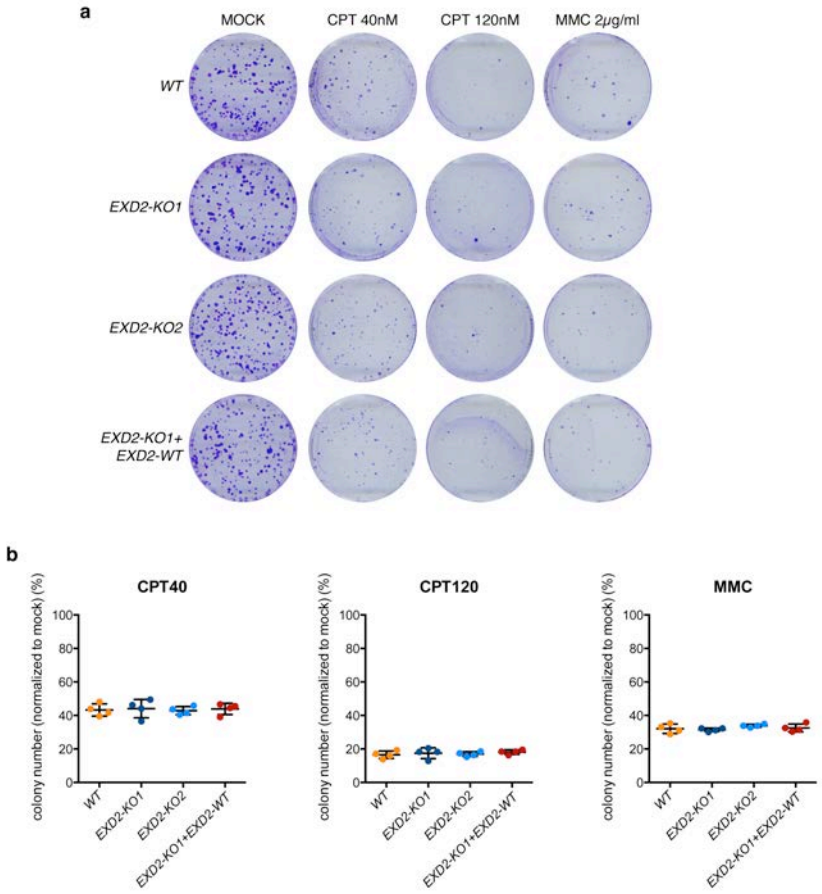

Figure 14: EXD2 depletion does not affect DNA-damage sensitivity. (**a**) U2OS cells were treated with different doses of CPT and MMC and cellular sensitivities were assayed by clonogenic survival assay. (**b**) The surviving fractions (normalized to mock-treated cultures) are plotted for the different treatments. Mean compiled from 2 independent experiments performed in duplicate (n=4) and the standard deviations are shown. Statistical analysis was performed using one-way ANOVA together with Dunnett's test.

To further explore a potential role in DNA repair, we used mock and CPT treated *EXD2-KO* cells and assessed their ability to form replication protein A (RPA) foci, a protein known to accumulate at sites of ssDNA generated by resection and to trigger the DDR. We could not detect any differences in the RPA signal intensity between the *EXD2-KO* cells and the *EXD2-WT* cells, regardless of whether cells experienced DNA damage (Figures 15a and 15b). Together, these results suggested that EXD2 does not seem to have a direct effect on resection or sensitivity to these types of DNA damage.

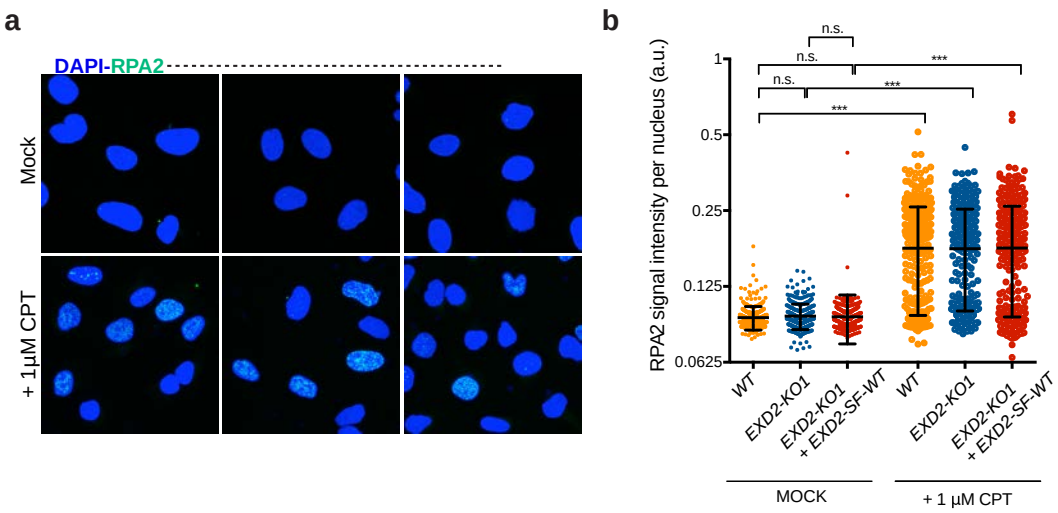

Figure 15: EXD2 depletion does not affect RPA foci formation. (**a**) U2OS cells were immunostained with RPA2 with and without treatment of CPT. (**b**) Quantification of the RPA signal intensity per nucleus. A minimum of 390 cells was quantified for each condition. Statistical analysis was performed using one-way ANOVA together with Dunnett's test (****p* < 0.001, n.s. = non-significant).

EXD2 deficiency impairs glucose usage

Considering that EXD2 appears to localize exclusively in the mitochondria, we were next interested in exploring a possible role for this protein in metabolism. By using a combination of LC/MS and GC/MS (Evans *et al*, 2009), we were able to analyze global metabolite levels in *shCont* and *shEXD2#1* cells. Depletion of EXD2 led to significant changes in the levels of several metabolites and pathway analysis revealed that the most affected categories were glutathione and the metabolism of a number of particular amino acids and sugars (Figures 16a and 16b and Supplementary Table 1). To better understand the origin of these defects, we incubated cells to culture medium containing either labeled glucose ([U-^{13}C]-Glc) or labeled glutamine ([U-^{13}C]-Gln) and measured the incorporation of the isotopes in the different metabolic intermediates using the NMR based PEPA technique developed by our collaborators (see Methods). While the control cells were able to incorporate both glucose and glutamine in many metabolic intermediates, most of these metabolites were being generated exclusively from glutamine following the depletion of EXD2, as we found significant defects in the incorporation of glucose-derived carbon into many important

metabolites, while glutamine usage was relatively unaffected in many cases (Figures 16c and 16d and Supplementary Table 2). Consistent with the data obtained before, the affected metabolites included glutathione, which plays an important role in the antioxidant response and has been described as a potential indicator of oxidative stress (Diaz-Vivancos *et al*, 2015; Escribano *et al*, 2015). These data indicated that EXD2 is required for glucose oxidation through the TCA cycle and glutathione synthesis, suggesting that cells lacking EXD2 may have alterations in ROS levels or antioxidant capacity and could rely on glutamine for the generation of key metabolites.

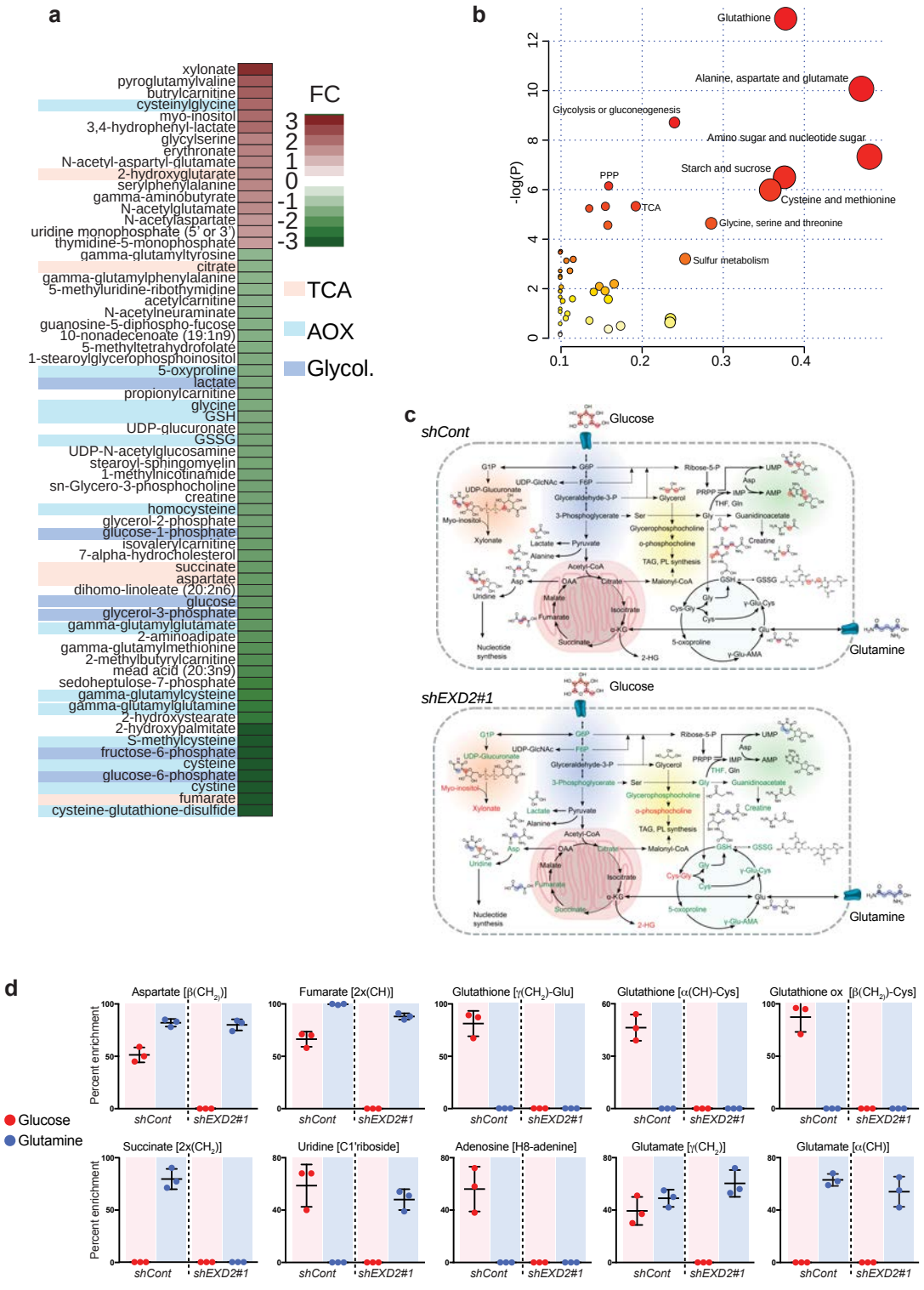

Figure 16: EXD2 is required for normal cellular metabolism. (**a**) Analysis of metabolite levels in cells with reduced EXD2 levels. A heatmap representation of metabolite fold changes (FC) that are significantly altered by the shRNA-mediated depletion of EXD2 (EXD2-22) compared to control shRNA expressing cells are shown. Values represent the mean of 5 independent samples. Depicted metabolites have a fold change > 1.3 and p-adjusted value < 0.1. Full results and statistics are provided in Supplemental Table 1. (**b**) Pathway enrichment analysis of metabolite differences from combined MS-

data and ^{1}H-NMR metabolite profiling. The x-axis represents Pathway Impact calculated from topological analysis based on the centrality measures of individual metabolites in a given metabolic network and the y-axis represents FDR p-values from a hypergeometric test. Overrepresented pathways with higher impact are highlighted. (**c**) Metabolic summary chart showing active pathways in U2OS cell lines as revealed by ^{1}H-NMR metabolite profiling. Metabolic structures are depicted with red and blue dots indicating fates of [U-^{13}C]glucose or [U-^{13}C]glutamine respectively. Additional data is provided in Supplementary Tables 1 and 2. (**d**) ^{1}H-NMR metabolite profiling predicted significant fractional enrichments. Red and blue dots represent individual F values calculated using [U-^{13}C]glucose or [U-^{13}C]glutamine, respectively. Results depicted are the average and standard deviation of 3 replicates with individual values shown.

EXD2 deficiency leads to increased ROS and glutamine dependence

Considering that glutathione production was particularly impaired in *EXD2-KO* cells, and given that mitochondria are considered the major source of ROS, we decided to evaluate if these were also affected. Using mitoSOX staining, we observed that two independent KO CRSIPR clones (*EXD2-KO1* and *EXD2-KO2*) had higher levels of mitochondrial ROS that could be rescued by the expression of *EXD2-WT* but not with the different mutants *EXD2-NUC* or *EXD2-C2* (Figure 17a). Treatment of the cells with N-acetyl cysteine (NAC) resulted in a decrease of mitoSOX positive cells, while treatment with the mitochondrial membrane depolarizing agent paraquat (PQT) led to high levels of ROS in all cases as expected (Figure 17a). Mitochondria utilize the ETC to enzymatically produce a membrane potential that allows for the generation of a proton gradient in the inner membrane and for ATP to be generated (Marchi *et al*, 2012; Poburko *et al*, 2011; Dzbek and Korzeniewski, 2008). To examine the effect of EXD2 on mitochondrial membrane polarization, we performed JC-1 staining in our cell lines. Results showed a decrease in the mitochondrial membrane potential in the *EXD2-KO* cells, indicating a possible dysregulation of this organelle (Figure 17b). Once again, this phenotype could be rescued by reintroducing *EXD2-WT*, but not any of the mutant forms *EXD2-NUC* or *EXD2-C2*. We hypothesized that increase ROS levels could lead to oxidative damage and accelerated turnover or impaired replication of mtDNA. qPCR analysis revealed a significant reduction in mtDNA levels in two independent *EXD2-KO* clones that could be complemented by EXD2-WT and to some extent by *EXD2-NUC*, but not by *EXD2-C1* or *EXD2-C2* mutants (Figure

17c). However, this mtDNA reduction was independent of changes in mitochondrial mass (Figure 17d) or mtDNA replication (Figure 17e), and could be largely rescued in cells treated with NAC (Figure 17c). Although we could not observe differences in the growth of EXD2 deficient cell lines compared with the WT in rich medium containing both glucose and glutamine (Figure 17f), we noticed significant differences when growing cells in glutamine free media (Figure 17g). Glutamine independent growth could be restored by the expression of *EXD2-WT*, but not *EXD2* mutants in the nuclease or HNH-like domains (Figure 17g). The addition of the antioxidant NAC did not rescue growth, indicating that growth defects were not secondary to increased ROS production or sensitivity to hyperoxic culture conditions (Figures 17h and 17i). Thus, EXD2 appears to be important for the maintenance of mtDNA levels possibly through the suppression of ROS levels and its deficiency confers glutamine dependence for cell growth in normal culture conditions.

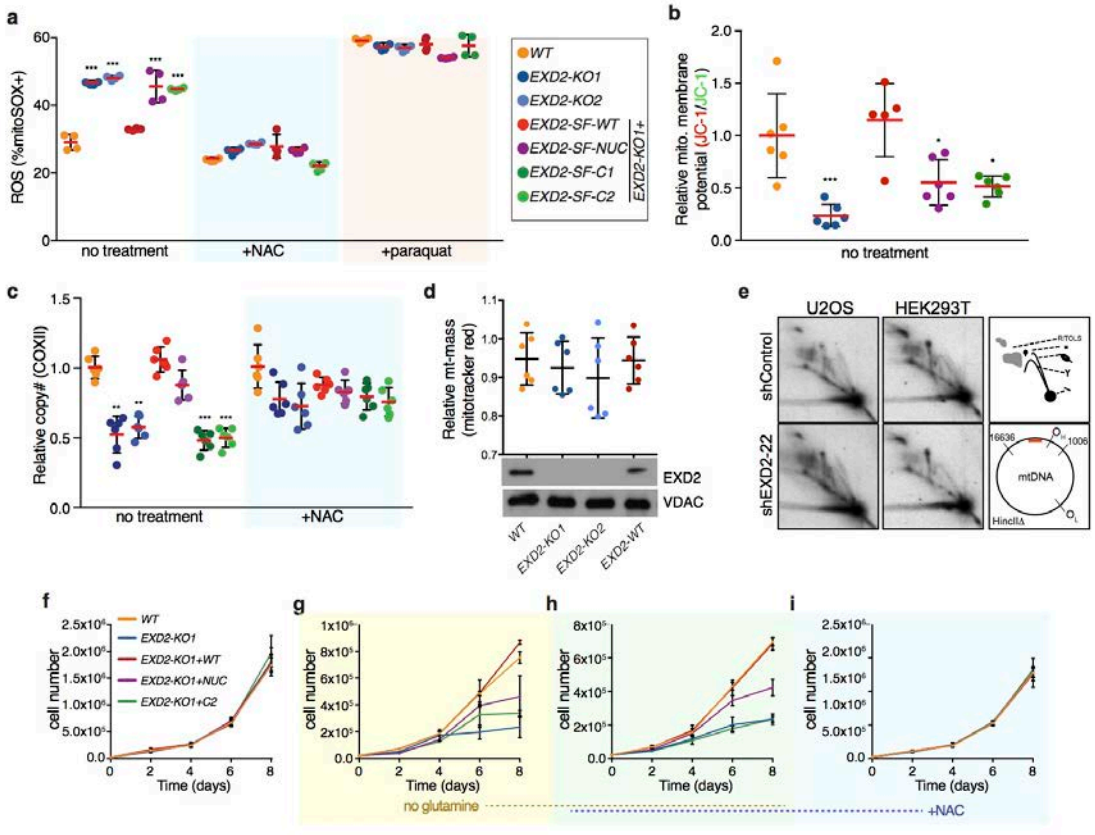

Figure 17: EXD2 depletion causes increased ROS and confers glutamine dependence. (**a**) EXD2 deficiency leads to increased levels of mitochondrial ROS. ROS levels were measured using MitoSOX red dye and flow cytometry. As a control, cells were treated in parallel with N-acetyl cysteine (NAC; 5 mM) to reduce ROS or paraquat (PQT; 0.4 mM) to increase ROS. Results are compiled from 2 experiments performed in duplicate with the individual values, mean (red bar) and standard deviation

shown. (**b**) EXD2 deficiency leads to reduced mitochondrial membrane potential. Cells were stained with JC-1 dye and analyzed by flow cytometry. The ratio of red to green fluorescence is plotted with the individual values, mean (red bar) and standard deviation shown. Results shown are from duplicate experiments performed in triplicate. (**c**) EXD2 deficiency leads to decreased levels of mtDNA. mtDNA levels were analyzed using qRT-PCR to *COXII* and normalized to genomic DNA (*ACTB*). Cells in parallel were treated with NAC at 5 mM to reduce ROS levels. Results presented are compiled from 2 experiments performed in triplicate with the individual values, mean (red bar) and standard deviation shown. (**d**) EXD2 does not reduce mitochondrial mass as measured by mitotracker red staining and VDAC protein levels. 2 independent experiments performed in triplicate are plotted and the individual values, mean (red bar) and standard deviation shown. (**e**) 2D-AGE analysis of mitochondrial replication intermediates did not reveal differences between U2OS or HEK293T cells stably expressing *shCont* or *shEXD2#1*. Schematic of replication intermediates (top right panel) and the location of the probe and restriction sites (bottom right panel) are shown. (**f-i**) Analysis of the growth rates of U2OS cells in normal rich media or media lacking glutamine as indicated. While EXD2 deficient cells do not show growth defects in rich media (**f**), the loss of glutamine severely impaired growth (**g**). The addition of NAC (5 mM) did not affect the outcome of glutamine depletion (**h**) but slightly reduced growth in all cell lines (**i**). Plots are the mean of 2 independent experiments performed in triplicate (n=6 per point) and standard deviation is shown. For all data in this figure, statistical analysis was performed using one-way ANOVA together with Dunnett's test (***$p < 0.001$, *$p < 0.05$, analysis of variance compared with the *WT*)

EXD2 is required for oxidative metabolism and ATP production

Mitochondrial ROS is generated predominantly by Complexes I and III of the ETC, suggesting that the increased ROS observed in the *EXD2-KO* cells could reflect defects in the regulation or activity of the ETC. To address this, we measured oxygen consumption rates (OCR) using a Seahorse XF24 bioanalyzer. Compared to the parental cell line or *EXD2-WT* complemented cells, *EXD2-KO* cells exhibited reduced basal and ATP-linked OCR that could not be rescued by any of the mutants *EXD2-NUC* or *EXD2-C2* (Figures 18a and 18b). Furthermore, this reduction in OCR appears to be due to a defective mitochondrial respiration as the addition of FCCP to the cells was not able to stimulate the respiratory chain to operate at maximum capacity to the same extent in the *EXD2-KO* cells (Figure 18b). In addition, we were also able to detect a growth in the extracellular acidification rates (ECAR) in the *EXD2-KO* and mutant cells after adding glucose to the cells, indicating an increase in aerobic glycolysis and lactate production that often accompany defective ETC activity (Figures 18c and 18d). The addition of NAC to the cells rescued the overall OCR but

did not strongly enhance the levels of ATP-linked OCR, suggesting that defects in the ETC are likely the primary defect leading to increased ROS (Figure 18e). However, the increased ECAR was reduced upon addition of NAC, indicating that it was secondary to ROS production (Figure 18f). Furthermore, we noticed that the differences seen in OCR are probably due to an impairment of glucose usage in the *EXD2-KO* cells, that cannot be rescued in the mutants *EXD2-NUC* and *EXD2-C2* (Figures 18g and 18h), confirming our hypothesis that EXD2 depletion probably prevents the cells from using glucose as a fuel for an effective OXPHOS, thus rendering the cells dependent on glutamine. Finally, to further confirm a role for EXD2 in ATP production, we analyzed levels using mass spectrometry. *EXD2-KO* cells had reduced levels of both ADP and ATP that were rescued to levels similar to *WT* by *EXD2-WT* expression (Figure 18i). We conclude that EXD2 is required for normal respiration and its absence leads to impaired ATP production and altered glycolysis, consistent with the induction of a Warburg like effect, likely resulting from ETC dysfunction.

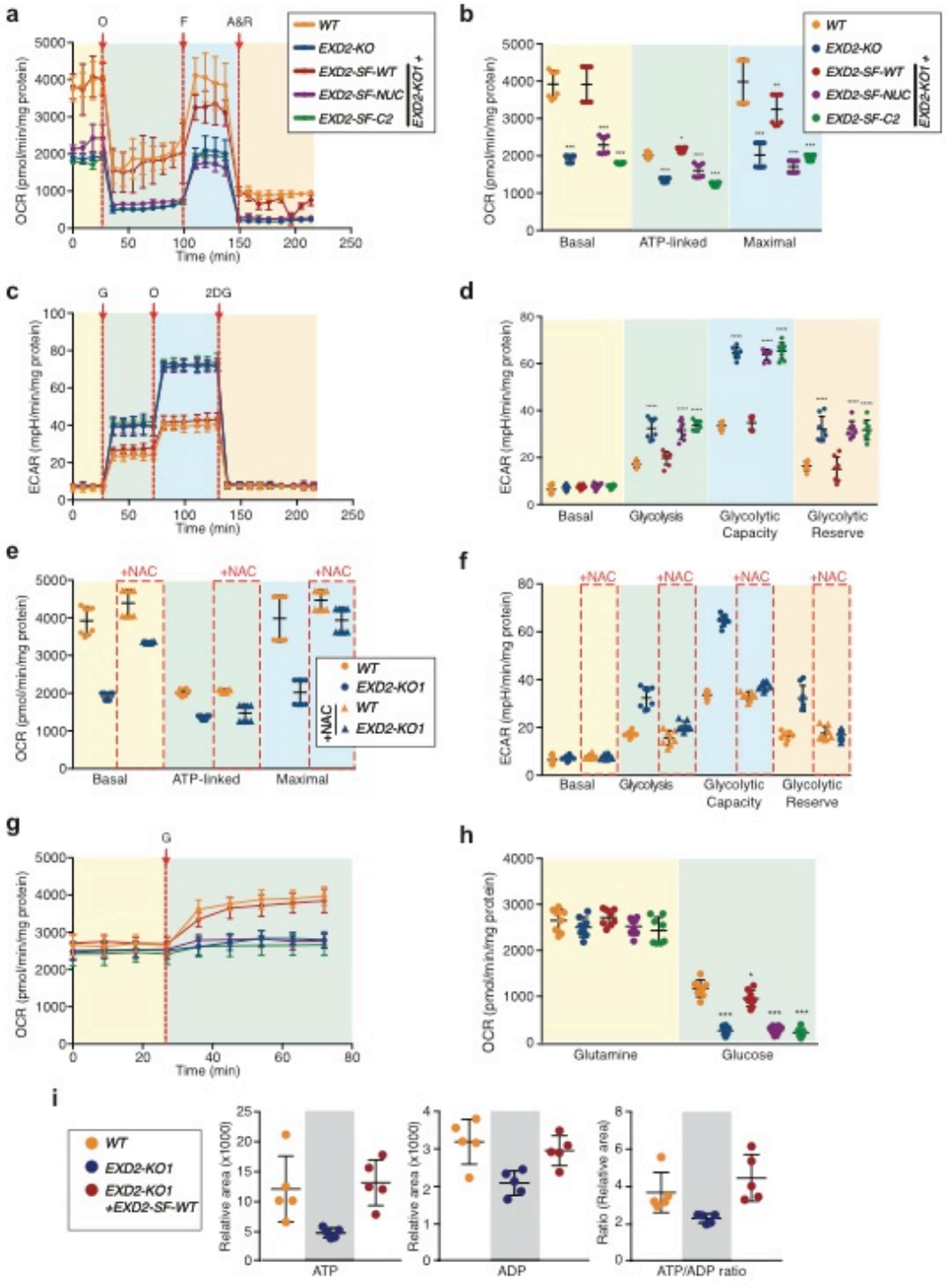

Figure 18: EXD2 is required for OXPHOS activity and ATP production. (**a**) Analysis of oxygen consumption rate (OCR) using the Seahorse Bioassay and the mitochondrial stress test. U2OS cells were treated consecutively with oligomycin (O), FCCP (F), and Antimycin plus Rotenone (A&R) (as described in Materials and Methods) to measure basal respiration, ATP production, maximal respiration and spare respiratory capacity, respectively. EXD2 deficient cells show decreased basal respiration, ATP production and maximal respiration that can be rescued by the expression of *EXD2-SF-WT* but not the *NUC* or *C2* mutant forms. The mean from 2 independent experiments performed in quadruplicate

(n=8 per point) and standard deviation are plotted. (**b**) Graphical representation of OCR (extrapolated from data in (**a**)). Mitochondrial respiration and ATP production are reduced in the absence of functional EXD2. (**c**) Analysis of extracellular acidification rates (ECAR) to assess glycolytic function using the Seahorse Bioassay and Glycolysis stress test. U2OS cells were treated consecutively with glucose (G), oligomycin (O) and 2-deoxy-D-glucose (2DG) (as described in Materials and Methods). EXD2 deficient cells show increased ECAR indicating increased extracellular lactate production. Expression of *EXD2-SF-WT* but not the *NUC* or *C2* mutant forms of EXD2 reduced ECAR in deficient cells. The mean from 2 independent experiments performed in quadruplicate (n=8 per point) and standard deviation are plotted. (**d**) Graphical representation of ECAR (extrapolated from data in (**c**)). (**e**) Treatment of cells with NAC increases OCR but does not alter ATP-linked respiration in *EXD2-KO1* cells. (**f**) Addition of NAC reduces ECAR rates in cells lacking EXD2 or expressing mutant forms. Data in (e) and (f) is compiled from 2 independent experiments performed in quadruplicate (n=8 samples per point). (**g**) EXD2 depletion affects glucose-linked respiration. U2OS cells were treated with glucose to distinguish the OCR coming from glutaminolysis versus glycolysis. (**h**) Graphical representation of OCR (extrapolated from data in (**g**)) shows the impairment in OCR is caused mainly by a defect in glucose usage. Data shown is from 2 independent experiments performed in quadruplicate (n=8) and mean and standard deviation are shown. For Figures 4a to 4l, statistical analysis was performed using one-way ANOVA together with Dunnett's test (***$p < 0.001$, **$p < 0.01$, *$p < 0.05$, analysis of variance compared with the *WT*). (**i**) EXD2 affects the levels of ADP and ATP. *EXD2-KO1* U2OS cells have lower levels of both ADP and ATP compared with *WT* or complemented cell lines. ATP and ADP were made by targeted metabolomics analysis and data shown is from 5 independent cultures with the individual values, mean and standard deviation shown. Statistical analysis was performed using the t test (***$p < 0.001$, *$p < 0.05$, n.s. = non-significant).

EXD2 associates with Complex I of the ETC and the mitoribosome

In order to determine how EXD2 deficiency could influence ATP production and lead to a pronounced metabolic phenotype, we used BioID mass spectrometry (BioID-MS) to identify proximity interactors, by overexpressing EXD2 fused to the BirA* biotin ligase. After 24 hours of expression in the presence or absence of biotin labeling, we could only detect streptavidin signal in the mitochondria of biotin-supplemented cells transiently expressing *EXD2-BirA** or the *EXD2-C2-BirA** mutant (Figure 19a). Identification of biotinylated proteins by mass spectrometry revealed a group of EXD2 proximity interactors that was highly enriched for proteins involved in OXPHOS and composed almost entirely of mitochondrial proteins (Figure 19b and 19c and Supplementary Table 3). Notably, this included almost all of the known matrix exposed subunits of the Complex I N and

Q modules (Sánchez-Caballero *et al*, 2016), many proteins involved in RNA processing or translation at mitoribosomes (GRSF1, TACO1, ACAD9, LETM1) (Hällberg and Larsson, 2014; Jourdain *et al*, 2013), as well as enzymes implicated in redox reactions (POLD4, PYRC1, PYRC2) (Lyle *et al*, 2009; Kuo *et al*, 2016). The majority of these interactions were also observed with the *EXD2-C2* mutant that fails to complement cellular phenotypes of *EXD2-KO1* cells, indicating that this domain is not required for mitochondrial localization or some of the most enriched protein interactions detected, although the representation of mitoribosome components was particulary reduced (Figures 19b and 19c and Supplementary Table 3). To validate these findings, we performed IPs with *EXD2-WT* followed by Western blotting for the NDUF9A subunit of complex I and observed a robust interaction with EXD2 (Figure 19d). In contrast, we could not detect any interaction with a subunit of the Complex I P module, ND6, emphasizing the specificity of the interactome. These results suggested that EXD2 may have a direct role in Complex I regulation, assembly or function, potentially through interactions with proteins in the RNA granules that are involved in RNA processing and translation and localize in close proximity to the mtDNA. The interaction of EXD2 with different subunits of Complex I raised the question of whether this protein could be a novel subunit of Complex I or function as part of the assembly complex. Using BN-PAGE analysis of mitochondria, we were able to detect a decrease in the abundance of complexes I and V and supercomplex I/III in the *EXD2-KO* cells, suggesting that depletion of EXD2 affects the assembly and/or stability of these complexes (Figures 19e and 19f). We next tried to evaluate if EXD2 constituted an unknown component of any of the ETC complexes. Western blot analysis of the native gel showed EXD2 was present in the mitochondrial preparations, however its size does not corresponded to any of the ETC complexes, suggesting EXD2 should function at an indirect level in order to affect their stability (Figure 19e). Complex I has been well-described as one of the major sources of ROS within the cell (Gorenkova *et al*, 2013; Vinogradov and Grivennikova, 2016). To further explore the possibility that EXD2 could affect its activity, we tried to evaluate if the deficiency in respiration we observed in the *EXD2-KO* cells was caused by Complex I dysfunction. In fact, when feeding cells with malate and pyruvate, two substrates of Complex I (Salabei *et al*, 2014), we could see a decrease in OCR in *EXD2-KO* cells that could be rescued in the *EXD2-WT* complemented cells but not in the mutants *EXD2-NUC* or *EXD2-C2* (Figures 19g and 19h). In contrast, when we fed the cells with succinate, a Complex II substrate (Salabei *et al*, 2014), the

difference in OCR was partially rescued, suggesting EXD2 is probably affecting Complex I activity thus leading to accumulation of ROS and mitochondrial dysfunction (Figures 19g and 19h). These data further established the predominant localization and activity of EXD2 are mitochondrial and suggest that EXD2 is important for the assembly of different subunits of the ETC and therefore required for an optimal OXPHOS function.

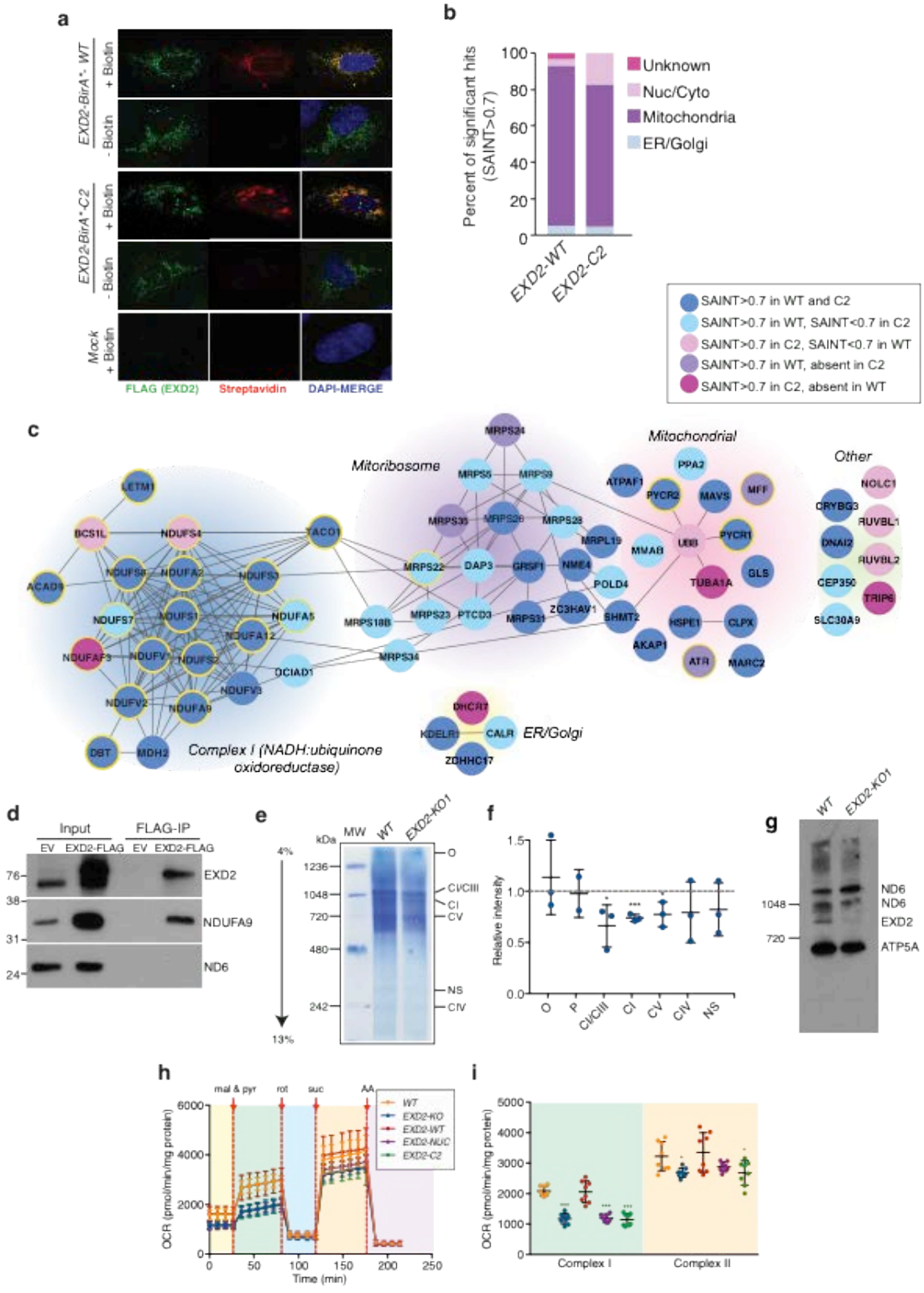

Figure 19: EXD2 interacts with Complex I and the mitoribosome. (**a**) Expression of *EXD2-WT-BirA** or *EXD2-C2-BirA** fusion proteins with or without 24 hours of biotin labeling. Streptavidin staining is exclusively cytoplasmic in each case, consistent with mitochondrial localization. Biotin labeled BirA* expressing control cells are also shown, note diffuse Streptavidin labeling signal. (**b**) Graphical representation of proximity interactor subcellular localization in *EXD2-WT-BirA** or *EXD2-C2-BirA** expressing cells. (**c**) EXD2 associates with primarily mitochondrial proteins and interactors are enriched

for Complex I and many small mitoribosome components. Proteins are color coded based on the statistical analysis (see legend) and those known to be mutated in human hereditary diseases are circled in yellow. See Supplementary Table 3 for data, curation and statistical analysis). (**d**) EXD2 interacts with Complex I component NDUFA9. Results from Immunoprecipitation-Western blotting of U2OS cell extracts are shown. Similar results were obtained in 3 independent experiments. (**e**) Reduced levels of OXPHOS complexes in EXD2 deficient cells. Separation of digitonin-solubilized mitochondrial complexes in BN-PAGE gel; oxoglutarate dehydrogenase complex (O), pyruvate dehydrogenase (P) supercomplex I+III (CI/CIII), complexes I, V and IV (CI, CV and CIV), non-specific band (NS). (**f**) Quantification of the relative band intensity in the *EXD2-KO* (WT set at 1.0), normalized to the background. Statistical analysis was performed using independent t-tests (***$p < 0.001$, *$p < 0.05$). (**g**) Immunoblotting of the BN-PAGE gel for Complex I (ND6) and Complex V (ATP5A) shows EXD2 does not appear to be a subunit of these ETC complexes (**h**) Complex I activity is reduced in cells lacking EXD2. Analysis of OCR using the Seahorse Bioassay to assess the activity of individual OXPHOS complexes by consecutive administration of malate and pyruvate (mal & pyr, Complex I substrate), rotenone (R), succinate (suc, Complex II substrate) and antimycin (A). (**h**) Graphical representation of OCR (extrapolated from data in (**i**) shows that the impairment in OCR is mainly due to a defect in Complex I activity. Data shown is from 2 independent experiments performed in quadruplicate (n=8) and individual values, mean and standard deviation are shown. Statistical analysis was performed using one-way ANOVA together with Dunnett's test (***$p < 0.001$, *$p < 0.05$, analysis of variance compared with the *WT*).

EXD2 can process RNA and is required for mitochondrial translation

To determine if EXD2 plays a role in mitochondrial RNA processing, we examined the *in vitro* activity of bacterially purified EXD2 to determine its substrate specificity. We had to remove the MTS (aa 1-61), as well as a portion of the C-terminus (aa 471-621) to facilitate solubility of the protein (Figure 20a). Given nuclease contaminants are often present in bacterial extracts, we also generated the *EXD2-NUC* mutant to ensure that the observed activity was specific for EXD2 (Figure 20a). *In vitro*, EXD2 exhibited promiscuous 3'-5' exonuclease activity on DNA, RNA and DNA:RNA hybrid substrates that was dependent on the exonuclease domain (Figure 20b). Thus EXD2 has a robust 3'-5' exonuclease activity that appears to lack specificity *in vitro*.

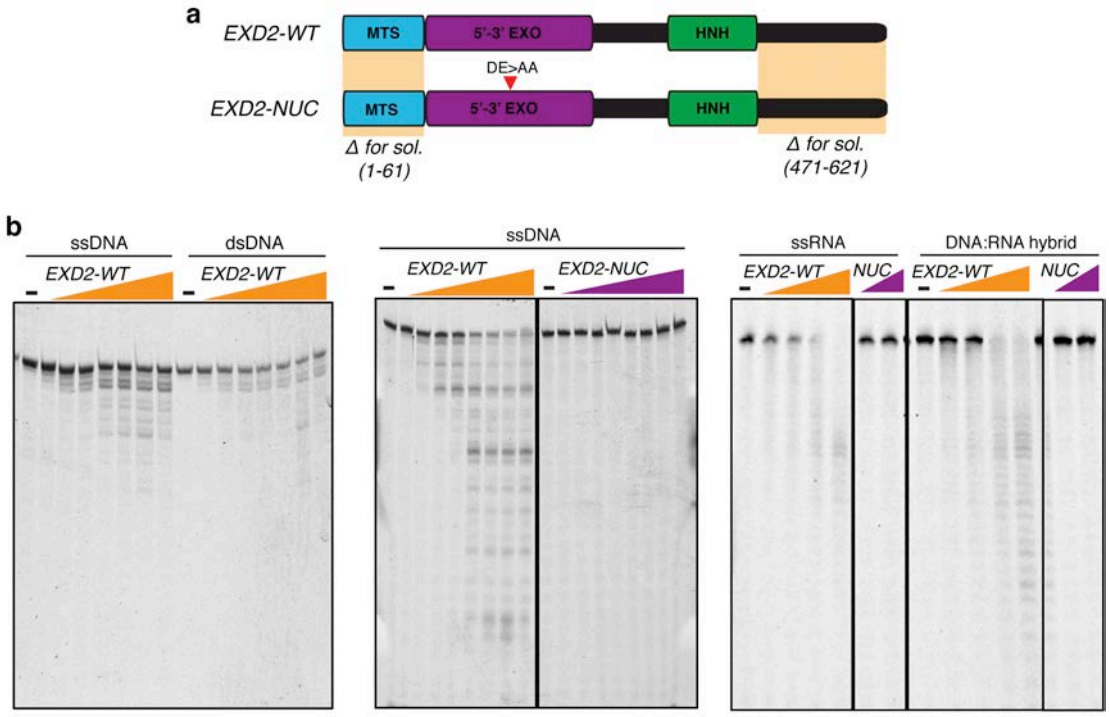

Figure 20: EXD2 is an active exonuclease that lacks specificity *in vitro*. (**a**) Graphical summary of the bacterially produced EXD2-proteins. (**b**) Analysis of *EXD2-WT* and *EXD2-NUC* activity on single-stranded DNA (ssDNA), double-stranded DNA (dsDNA), single-stranded RNA (ssRNA) and DNA:RNA hybrid substrates.

Given its protein-protein interactions with RNA processing proteins and translational components, as well as its influence on mitochondrial function, we wanted to determine if EXD2 could affect the processing or stability of mitochondrial encoded RNA species. The mtDNA is composed of two strands that are transcribed in precursor long polycistronic units, which are then cleaved into the mature rRNAs, tRNAs and mRNAs that will be required for respiratory chain biogenesis (Andersson *et al*, 1998). In order to evaluate if EXD2 could play a role in mitochondrial RNA processing, we performed RT-qPCR and observed a significant decrease in the mRNA levels of different subunits of Complex I (Figure 21a). We also performed MitoString analysis in order to have a more global analysis of the mitochondrial transcripts (Wolf and Mootha, 2014). This assay quantitates several mature and precursor mtDNA transcripts by using probes that target each of the highly abundant mt-mRNA transcripts, probes for regions that are transcribed but are not believed to encode functional proteins and probes overlapping the junctions of two adjacent genes which will only produce signal when bound to the unprocessed precursor

transcript (Figure 21b). While there were minor alterations in the levels of some transcripts and intermediates, we could not detect any significant differences among targets analyzed in the *EXD2-WT* and *EXD2-KO* cells, suggesting that EXD2 does not play a global role in RNA processing. However, we observed a significant reduction in both of the mtDNA-encoded rRNAs in cells lacking EXD2, potentially suggesting alterations in ribosome assembly or translation (Figure 21c). Analysis of mitochondrial translation using metabolic pulse labeling with ^{35}S-Met/Cys revealed that the mitochondrial *de novo* protein synthesis rate was dramatically reduced in the *EXD2-KO* clones (Figures 21d and 21e). The effect appeared to be general, with several mitochondrial proteins being affected, including subunits of the five different complexes of the ETC. This could be rescued in the *EXD2-WT* complemented cells, but not in the mutants *EXD2-NUC* or *EXD2-C2* (Figure 21f), and neither by the addition of NAC to the culture medium (Figure 21g). These results suggest EXD2 is necessary for efficient mitochondrial translation and that it depletion affects key components of the ETC causing defective mitochondrial respiration and subsequent accumulation of ROS.

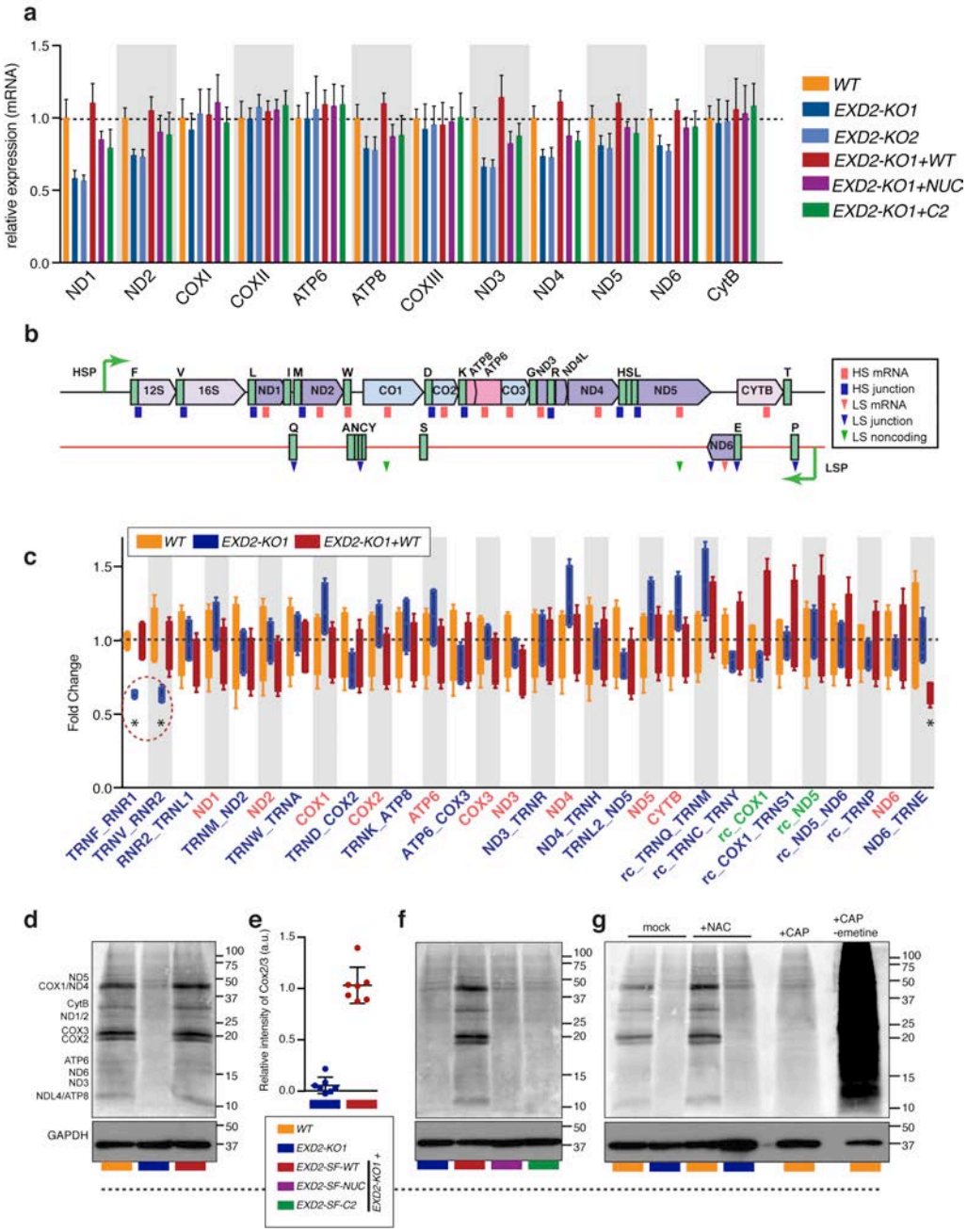

Figure 21: EXD2 can process RNA and is required for mitochondrial translation. (**a**) RT-qPCR analysis of mtDNA encoded RNA expression in the indicated cell line. Mean and standard deviation are shown. Statistical analysis was performed using one-way ANOVA together with Dunnett's test (**b**) Location of MitoString probes on the mtDNA strands. rRNAs, mRNAs and tRNAs encoded by the mtDNA are labeled in black text (tRNAs are annotated by their one letter symbols). The location of mRNA probes is noted in red, junction probes in blue and non-coding probes in green. Rectangles indicate probes targeting the heavy strand, while triangles indicate probes targeting the light strand. (**c**) Graphical analysis of the fold change of each of the MitoString probes compared to *WT*. Normalized quadruplicate values are shown as a box and whiskers minimum to maximum plot for *WT*, *EXD2-KO1* and *EXD2-WT* cells with the standard deviation. Statistical analysis was performed using one-way ANOVA together with Dunnett's test. (**d**) EXD2 is required for efficient mitochondrial translation.

Phosphoimager images of S35 labeled mitochondrial translation products separated by SDS-PAGE and blotted to PVDF membranes are shown for the indicated cell lines. Subsequent Western blotting for GAPDH was performed to ensure equal loading. Approximate size of mitochondrial translation products is indicated to right of gel. (**e**) Quantification of 7 independent experiments compared to the WT sample in each experiment. Each point represents the mean of technical replicates and the overall mean and standard deviation are shown. (**f**) The *WT* but not the *NUC* and *C2* mutant forms of EXD2 can rescue the translation defect of cells lacking EXD2. (**g**) The mitochondrial translation defect is not rescued by the administration of NAC to the culture medium. Additional controls treated with chloramphenicol (CAP), to block mitochondrial translation, or CAP without emetine to allow only cytoplasmic translation are shown.

Chapter 2

EXD2 regulates stem cell homeostasis and lifespan in *Drosophila melanogaster*

Contributors: Joana Silva, Andreu Casali, Suvi Aivio, Acaimo González-Reyes and Travis H. Stracker

CG6744 encodes a putative homolog of human *EXD2*

The fruit fly, *Drosophila melanogaster*, has been used extensively as an animal model in biology, serving as excellent system to investigate the role of new proteins *in vivo*. Sequence similarity searches revealed that the *Drosophila melanogaster* protein *dEXD2* (encoded by *CG6744*) shares an overall amino acid identity of 41% with human *EXD2*, containing both the 3'-5' exonuclease domain and the C-terminal HNH domain punctuated by tandem CxxC motifs (Figure 22a). In order to characterize *dEXD2*, we first analyzed its temporal expression levels in control *Drosophila* (*yellow white*, *yw*) lines. qRT-PCR analysis revealed two peaks of expression, corresponding to the early embryo development (0-4 hours) and pupariation (WPP) (Figure 22b). Interestingly, both of these phases have been associated with high metabolic rates (Merkey *et al*, 2011), suggesting *dEXD2* could play an important role in these stages. To further address the potential effects of *dEXD2* deficiency at an organism level, we took advantage of a transgenic insertion using the P-element construct P{EPgy2} (*dEXD2*^{EY03872}) (Figure 22a). The presence of a mini-white marker allows the differentiation of KO flies through eye color (Figure 22c). Furthermore, conventional PCR and qRT-PCR analysis confirmed that *dEXD2* expression levels were reduced in both males and females (Fig 23c), allowing us to use these as a model to explore the role of *dEXD2 in vivo*.

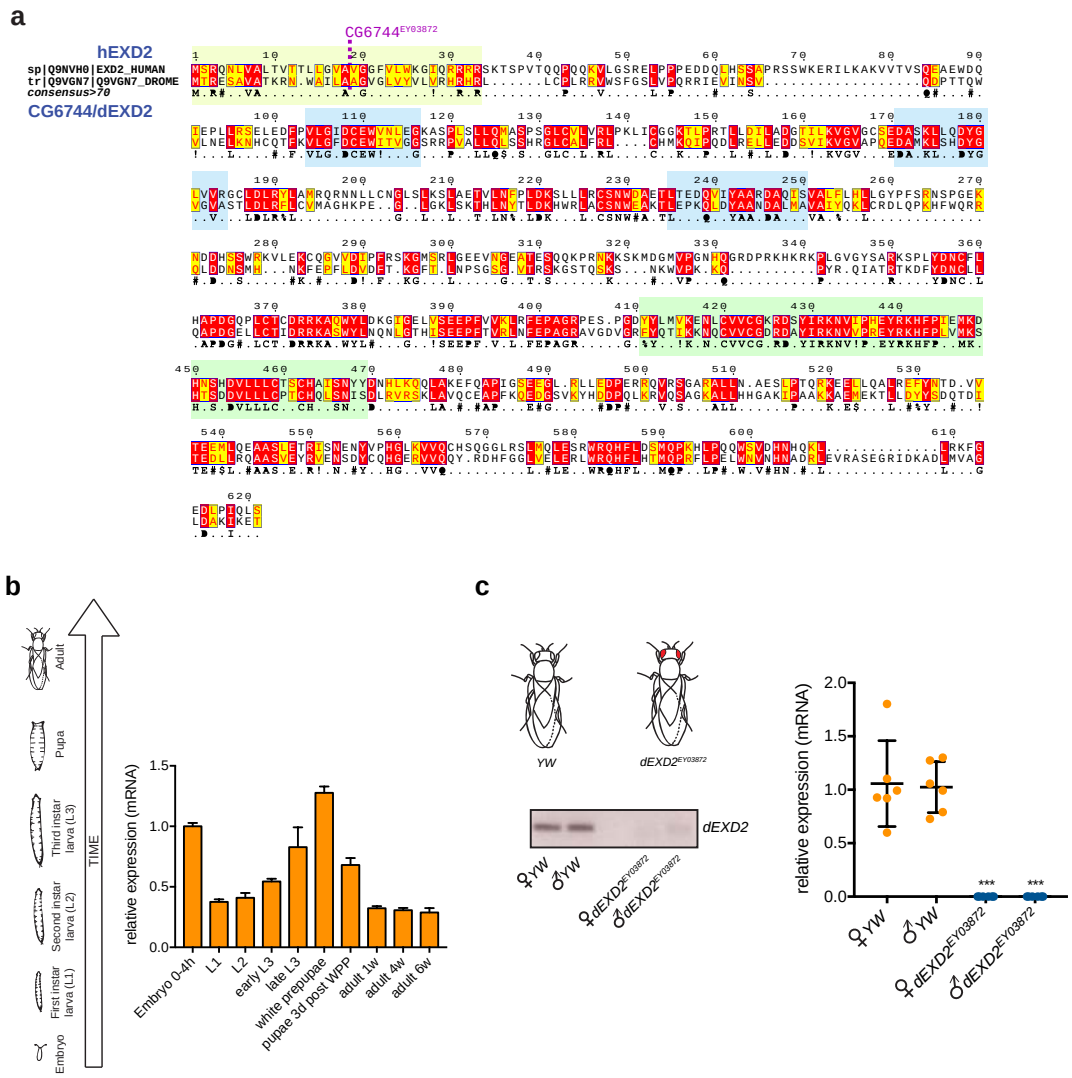

Figure 22: *Drosophila melanogaster* with disrupted expression of dEXD2. (**a**) Protein sequence alignment of human EXD2 and *Drosophila* dEXD2. MTS is shaded in yellow, nuclease domain in blue and HNH-like domain in green for reference. (**b**) qRT-PCR analysis showing differentially expression of dEXD2 along the developmental stages of Drosophila melanogaster. (**c**) Use of P-element for gene disruption allows eye-based color discrimination for the two genotypes (*YW* and *dEXD2*^{EY03872}). Conventional PCR and qRT-PCR showing disrupted dEXD2 expression in the *dEXD2*^{EY03872} flies compared with the *YW*. Data shown is from 2 independent experiments performed in triplicate (n=6) and mean and standard deviation are shown. Statistical analysis was performed using t-test (***$p < 0.001$).

dEXD2 is required for normal development

Given the differential expression pattern of *dEXD2* during development (Figure 22b), we hypothesized that its removal could affect normal growth of

Drosophila. Highly proliferative cells, such as cancer or embryonic stem cells, often require a specialized metabolism that relies on aerobic glycolysis to provide both the energy and building blocks needed to support their rapid growth (Folmes *et al*, 2011; Shyh-Chang and Daley, 2013; Chen *et al*, 2008). This is also the case for the early stages of *Drosophila* development, where a small embryo must be able to exponentially increase its biomass in a short amount of time, in order to give rise to a fully differentiated adult fly (Tennessen *et al*, 2011). Given the central role of mitochondria in energy metabolism, we examined *dEXD2* deficient flies, and found that they also harbor lower levels of mtDNA (Figure 23a) that could translate into less effective OXPHOS function and problems during development (Miyadera *et al*, 2001; Feng *et al*, 2001). In order to explore this possibility, we conducted a phenotypic analysis of our mutant flies, and observed that both embryos and pupae were significantly smaller (Figures 23b and 23c). Furthermore, when analyzing the pupariation rate, we noticed that the $dEXD2^{EY03872}$ flies required more time to reach the pupae stage (Figure 23c). This delay was rescued by feeding the flies with NAC and was further enhanced in flies fed with PQ (Figure 23c), suggesting dEXD2 is affecting the normal development of *Drosophila* probably by affecting their oxidative status. Considering the well-established role of the insulin and ecdysone signaling pathways in growth and developmental timing in *Drosophila* (Caldwell *et al*, 2005; Colombani *et al*, 2005; Mirth *et al*, 2005), we next investigated if *dEXD2* depletion affected the expression levels of these hormones. qRT-PCR analysis revealed a significant decrease of the insulin-like peptides *dILP2*, *dILP3* and *dILP5*, as well as of the insulin and ecdysone receptors (*InR* and *EcR*) in *dEXD2* deficient female flies (Figure 23d). These results are in agreement with previous work that showed that impairment of the insulin and ecdysone pathways result in developmental delay and shorter animals (Caldwell *et al*, 2005; Colombani *et al*, 2005; Mirth *et al*, 2005) and suggest a role for *dEXD2* in the normal development of *Drosophila melanogaster*.

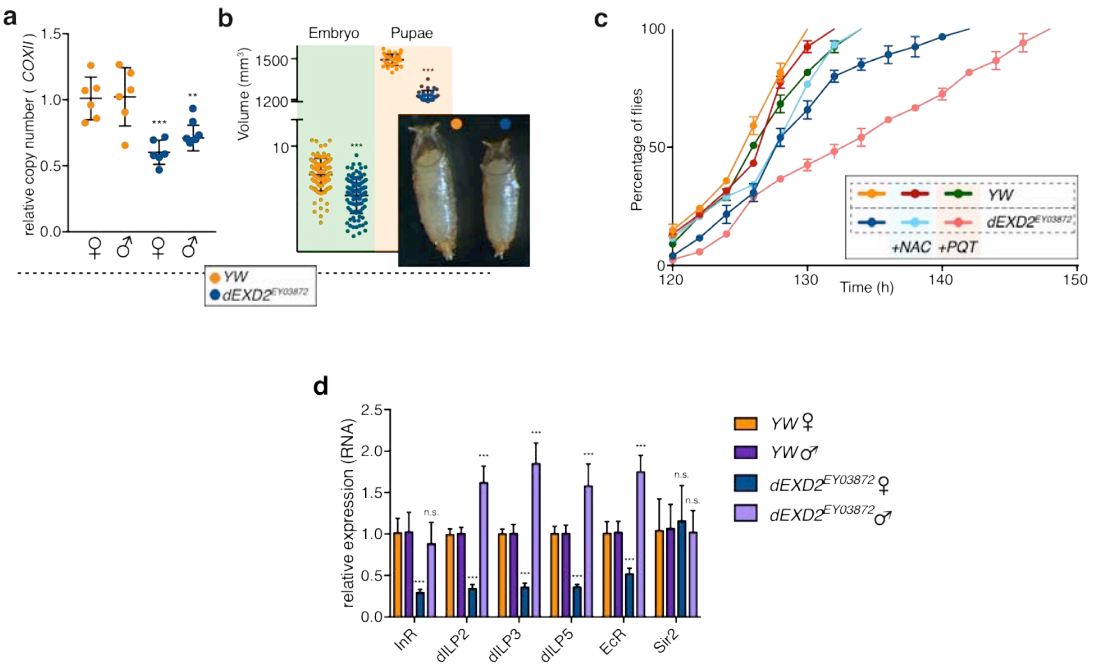

Figure 23: dEXD2 affects normal development in flies. (**a**) mtDNA levels were analyzed using qPCR to COXII and normalized to genomic RNA polymerase II. Mean compiled from 2 independent experiments performed in triplicate (n=6) and the standard deviation are shown. (**b**) Morphological analysis showing *dEXD2*^{EY03872} embryos and pupae are significantly smaller compared with the *YW*. Mean and standard deviation of one hundred embryos and thirty-one pupae are shown. (**c**) Timing of pupariation reveals a delay in *dEXD2*^{EY03872} flies compared with the *YW*. Administration of NAC to the food of flies rescues the phenotype. PQ treatment further enhances the development delay of the *dEXD2*^{EY03872} flies. Mean compiled from 3 independent experiments and the standard deviation are shown**.** (**d**) qRT-PCR analysis shows a differentially expression of InR, dILPs, and EcR in *dEXD2*^{EY03872} flies. Mean compiled from 3 independent experiments performed in triplicate (n=9) and standard deviation are shown. Statistical analysis was performed using t-test (***p < 0.001, **p < 0.01, n.s. = non-significant).

Flies lacking dEXD2 live longer and are more active

In addition to the ecdysone and insulin signaling pathways, many other processes have been implicated in the regulation of aging and development of Drosophila, and these need to be tightly regulated in order to assure the integrity of physiological processes. Among the best studied is the ROS signaling pathway, which has also been shown to coordinate the insulin response. Activation of the IIS pathway requires autophosphorylation of multiple tyrosine residues in the InR. However, this receptor can also be regulated through ROS by stimulating serine

hyperphosphorylation, which promotes the dissociation between the InRβ-subunit and the InR substrate (IRS) and/or the IRS and PI3K, promoting the degradation of the IRS proteins and decrease of specific signaling proteins (Papaconstantinou, 2009). Thus it seems that in long-lived animals presenting with abnormal oxidative status, the insulin pathway also appears to be affected, suggesting that these processes might be interconnected. As increased ROS has been demonstrated to either extend or diminish lifespan in different experimental settings (Kurosu *et al*, 2005; Giorgio *et al*, 2005), we next examined the lifespan of *dEXD2* deficient flies as they showed increased ROS levels (Figure 24a). We found a significant increase in the lifespan of both males and females (Figure 24a), although the effect was much more pronounced in females. Given the strong role that calorie restriction (CR) plays in the regulation of lifespan (Colman *et al*, 2014; Metaxakis and Partridge, 2013), we examined the impact of CR on lifespan in *dEXD2* deficient animals. After submitting both female *YW* and *dEXD2*^{EY03872} flies to a low protein diet, we noticed that CR had the same effect in both groups, extending their lifespan to same degree. These results suggest that the increase in lifespan caused by *dEXD2* deficiency was independent of CR (Figures 24b and 24c). In order to assess a potential effect of oxidative stress in our phenotypes, we fed the flies with a diet enriched in NAC. The addition of NAC was able to rescue the female lifespan extension caused by *dEXD2* deficiency, suggesting that this gene could affecting ROS in order to influence lifespan in *Drosophila* (Figure 24a). Complex I deficiency has been reported to sensitize cells to hypoxia (DeHaan *et al*, 2004). Considering the possible implication of EXD2 in the function of Complex I, we examined the recovery of flies from a hypoxic challenge. Both male and female flies lacking *dEXD2* showed a pronounced defect in recovery from hypoxia (Figure 24d). Finally, we tried to evaluate whether *dEXD2* also affected the healthspan of *Drosophila*. As a fitness indicator, we conducted a climbing activity assay to measure the movement capacity of our flies. Although we could not detect any differences in young flies (3-5 days), we observed a significant increase in the locomotor activity of older *dEXD2* deficient flies (5 weeks) (Figure 24e). In agreement with this, we found that flies lacking *dEXD2* also had an increased capacity to degrade glycogen at older ages (Figure 24f), suggesting a possible role for *dEXD2* in influencing metabolism and energy expenditure. Together these data demonstrated that *dEXD2* affects both lifespan and healthspan of *Drosophila melanogaster*, possibly through the control of the oxidative status of the organism.

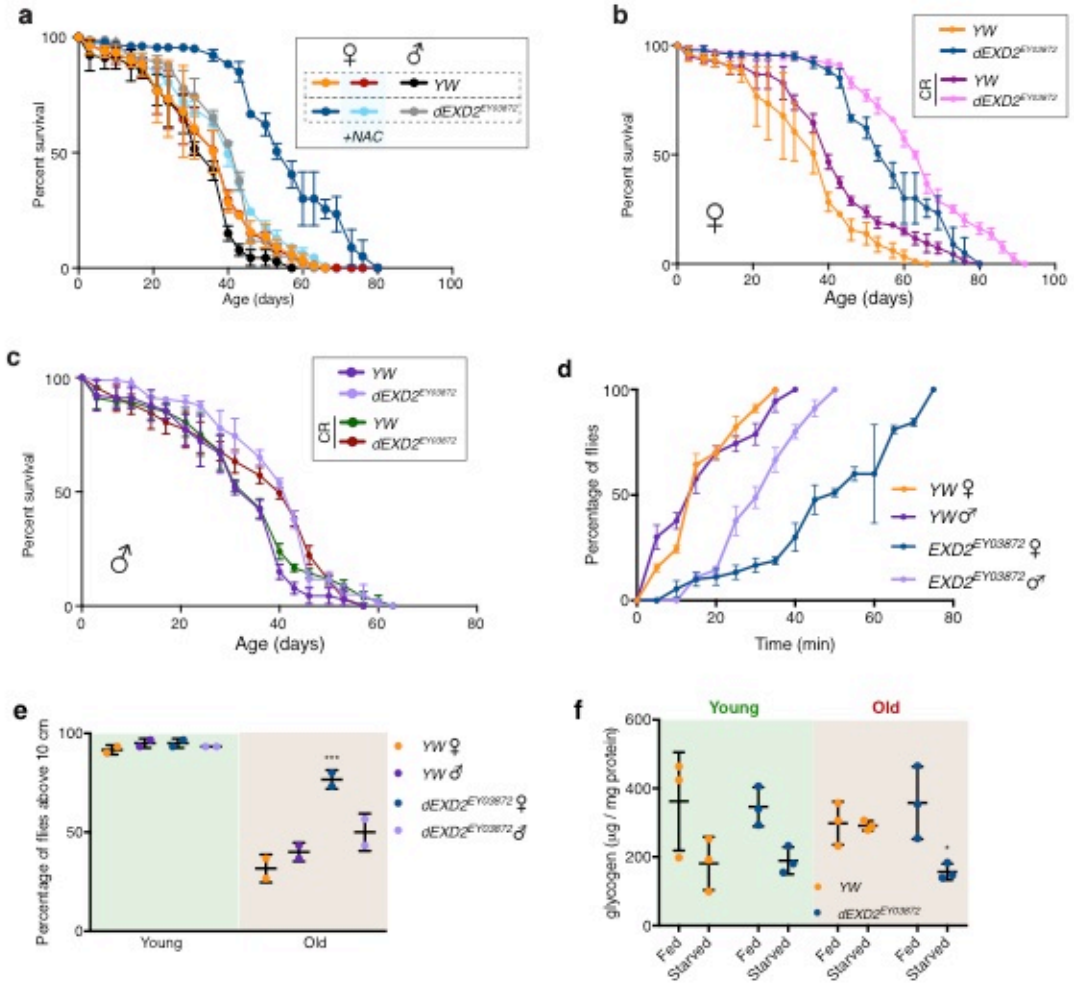

Figure 24: dEXD2 affects the lifespan and healthspan of Drosophila melanogaster. (**a**) Both male and female *dEXD2*^{EY03872} flies have a significantly increased lifespan compared to controls, particularly the females. Addition of NAC to the food normalizes the lifespan of *dEXD2* deficient females. (**b**) CR food extends lifespan in female flies regardless of dEXD2 status. (**c**) CR does not affect male survival regardless of dEXD2 status. For all the lifespan studies a total of 180 flies were used for each condition. The mean was compiled from 3 independent experiments and the standard deviation is shown. Statistical analysis can be found in the Supplementary Table 4. (**d**) Flies lacking dEXD2 need more time to recover from hypoxia. Flies were placed in hypoxia for 30 min and the time of recovery was measured according to their ability to stand up. A total of 90 flies was used for each condition. Mean compiled from 3 independent experiments and standard deviations are shown. Statistical analysis was performed using t-test (***p < 0.001, analysis of variance at the time the last corresponding *YW* recovered). (**e**) Climbing activity assay shows older flies lacking dEXD2 are more active compared with YW. A total of 60 flies were used for each condition. Mean compiled from 2 independent experiments and standard deviation are shown. Statistical analysis was performed using t-test (***p < 0.001). (**f**) Glycogen measurements reveal that older female flies lacking dEXD2 are more capable of degrading the molecule and therefore convert it into energy. A total of 10 flies per group constituted each measurement. Mean compiled from 3 independent experiments and standard deviations are shown. Statistical analysis was performed using t-test (*p < 0.05).

dEXD2 deficiency results in decreased fecundity and premature germ stem cell attrition

In addition to controlling lifespan, it has been shown that the insulin and ROS pathways are also involved in controlling the metabolism of several organisms, in order to balance costly energy processes, namely lifespan, growth and fecundity (Kenyon *et al*, 1993; Clancy *et al*, 2001; Dillin *et al*, 2002; Van Raamsdonk and Hekimi, 2009). Considering that the first two appear to be disturbed in our *dEXD2* deficient flies, we next decided to evaluate wether fecundity was also affected. As qRT-PCR analysis of *dEXD2* levels in different tissues showed high expression in the germline (Figure 25a), we examined fecundity in the female flies that were more clearly affected. Flies lacking *dEXD2* showed decreased egg laying over time with a drop in fecundity at 4 weeks, close to the same time we observed an increase in lifespan (Figure 25b). One cause of reduced fecundity in *Drosophila melanogaster* is the loss of germline stem cells (GSCs) (Zhao *et al*, 2008) (Figure 25c). We therefore examined GSC numbers at several time points during development compared to controls. We observed a clear drop in GSC numbers at 4 weeks of age (Figures 25d and 25e) that could be rescued to near wild type levels by the addition of NAC to the food (Figures 25d and 25e). Furthermore, the addition of NAC also restored the fecundity defect observed in $dEXD2^{EY03872}$ flies (Figure 25b). Histological analysis of ovaries revealed a collapse of the mitochondrial network at later stages, as Cytochrome-C staining was nearly absent and ATP synthase levels were reduced in the *dEXD2* deficient flies (Figure 25f). It has been proposed that accumulation of ROS prompts differentiation in a variety of stem cell populations (Chandel *et al*, 2016; Khacho *et al*, 2016; Ong *et al*, 2016; Owusu-Ansah and Banerjee, 2009). Therefore, we decided to evaluate if ROS levels were affected in the GSCs of our flies. We were able to detect an increase in ROS levels in the GSCs of *dEXD2* deficient flies in both normal conditions and in flies stressed with paraquat (Figure 25g).

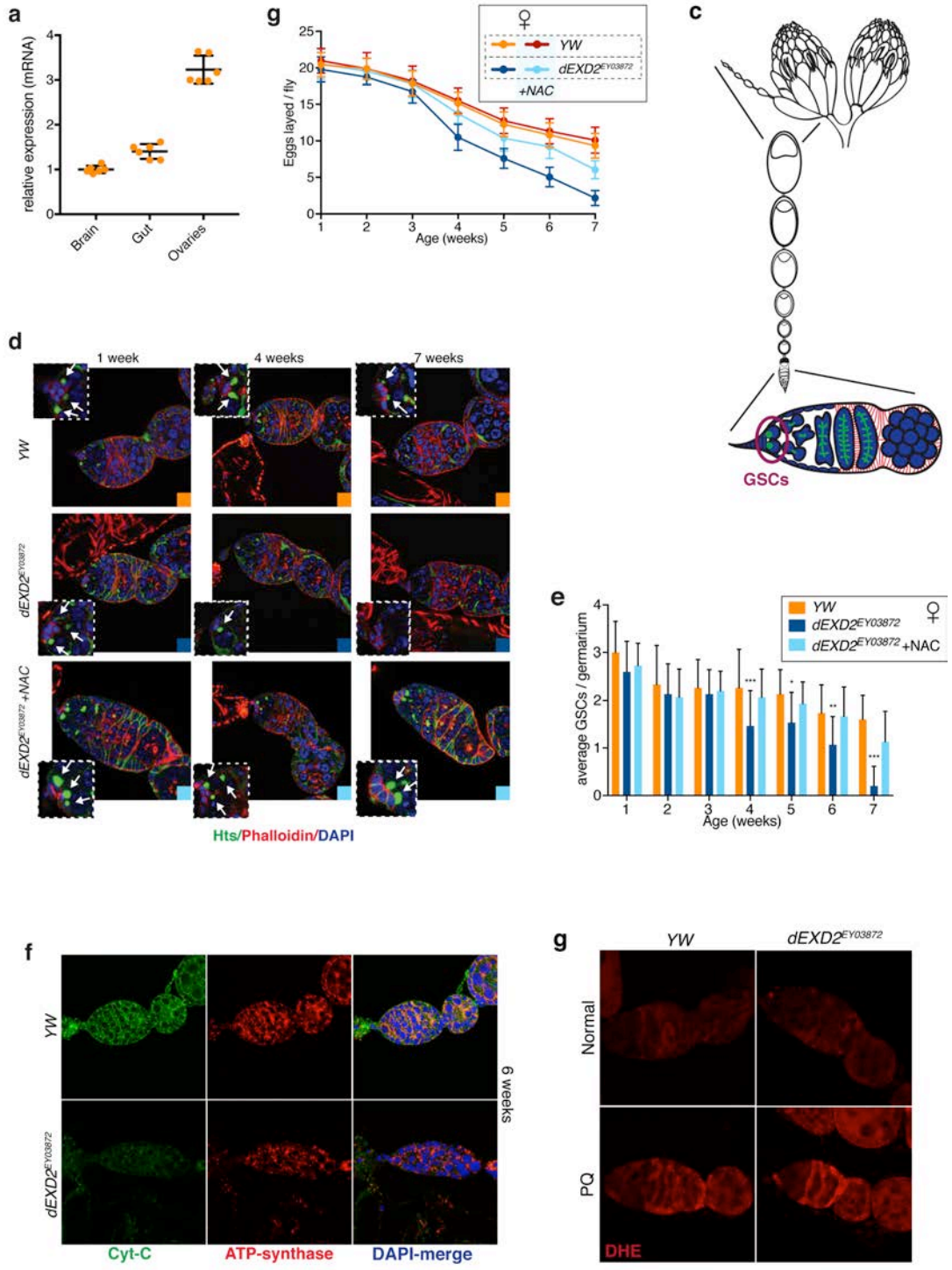

Figure 25: dEXD2 depletion impairs fecundity and leads to premature attrition of GSCs. (**a**) qRT-PCR analysis of different *Drosophila* tissues shows higher mRNA levels in the ovaries of *YW* flies. (**b**) Fecundity is reduced in *dEXD2*^{EY03872} flies and can be partially rescued by NAC treatment. A total of 60 flies were used for each group. Mean and standard deviation are shown. (**c**) Schematic illustration of the ovaries of Drosophila melanogaster, representing the egg differentiation that arises from the GSCs residing in the germarium. (**d**) Immunofluorescence analysis of *Drosophila* germariums reveals an accelerated age dependent attrition of the GSCs in *dEXD2*^{EY03872} flies that can be rescued by NAC

treatment. (**e**) Quantification of GSCs of each genotype for the different ages and upon NAC treatment. Mean compiled from 15 independent germariums and standard deviations are shown. Statistical analysis was performed using t-test (***$p < 0.001$, **$p < 0.01$, *$p < 0.05$). (**f**) Immunofluorescence analysis of *Drosophila* germariums shows a significant decrease in the levels of CytC and ATP synthase in *dEXD2*^{EY03872} flies. (**g**) DHE staining of drosophila germariums reveals an atypical ROS accumulation near the GSCs niche of *dEXD2*^{EY03872} flies, which is further enhanced by PQ treatment.

Together, our findings suggest that reduced levels of *dEXD2* trigger the accumulation of ROS in the GSCs, leading to their premature attrition and a subsequent decrease in fecundity and an increase in *Drosophila melanogaster* lifespan.

Chapter 3

EXD2 influences breast cancer growth in *xenografts*

Contributors: Joana Silva, Suvi Aivio, Miranda Stobbe, Marc Guiu, Roger Gomis and Travis H. Stracker

MDA-MB-231 breast cancer cells deficient for EXD2 are viable

With the hypothesis that EXD2 loss may represent and additional mode to promote the metabolic alterations that drive tumorigenesis, we sought to investigate if this protein affects cancer growth in human tumor *xenografts*. It has been proposed that glutamine dependence, which we saw was affected by EXD2 depletion (Figure 17g), is a hallmark of several types of cancer (Wise *et al*, 2008; DeBerardinis and Cheng, 2010). Uptake of glutamine is essential for the activation of the mTOR pathway, which provides the tumor cells with the nutrients needed for its exponential growth and survival (Jewell *et al*, 2015). It has been shown that this is particularly interesting for basal triple-negative breast cancers, where glutamine depletion severely impairs tumor growth (Kung *et al*, 2011; van Geldermalsen *et al*, 2016). In order to investigate a possible role in tumor growth, we depleted EXD2 from MDA-MB-231 breast cancer cells using two independent short hairpin RNAs (*shEXD2#1* and *shEXD2#2*), each one resulting leading to a significant reduction in expression (Figure 26a). In addition, we also generated cells lacking EXD2 using the CRISPR/CAS9 methodology, with two different RNA guides and complemented them with the different forms mentioned before: *EXD2-WT*, *EXD2-NUC*, *EXD2-C1* and *EXD2-C2* (Figure 26b).

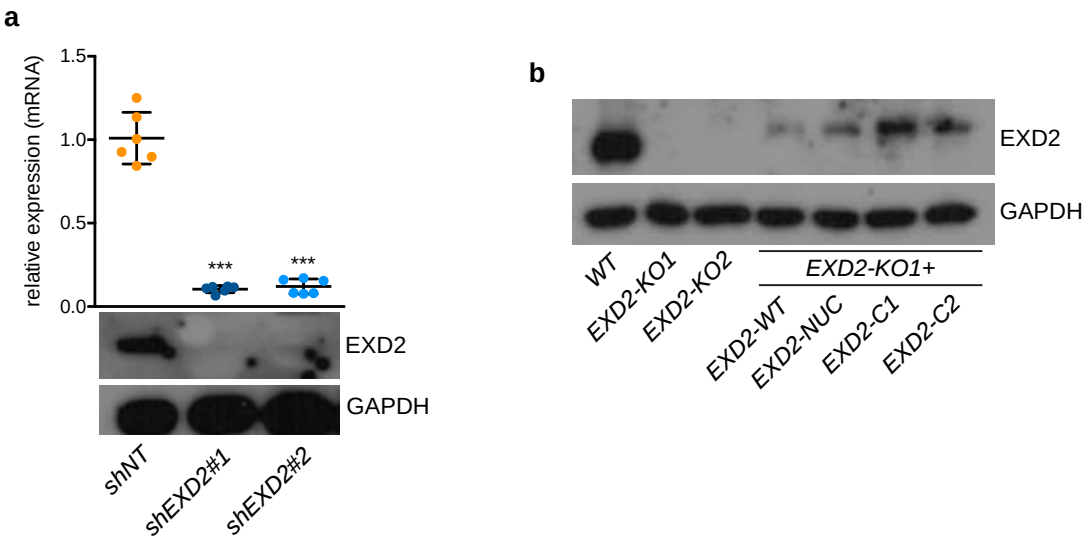

Figure 26: Generation of EXD2 deficient cells. (**a**) Depletion of EXD2 in MDA-MB-231 cells by stable shRNA expression with 2 independent vectors (*shEXD2#1* and *shEXD2#2*) reduces mtRNA and protein levels. Mean compiled from 2 independent experiments performed in triplicate (n=6) and the standard deviations are shown. Statistical analysis was performed using one-way ANOVA together with Dunnett's test (****p* < 0.001, analysis of variance compared with the WT). (**b**) Generation of MDA-MB-231 cells lacking EXD2 using CRISPR/CAS9 targetting and complemented with EXD2 or indicated mutant forms. A representative western blot of U2OS cells showing relative levels of EXD2 is presented.

Depletion of EXD2 causes metabolic changes in MDA-MB-231 cells

In agreement with the results presented above for the U2OS cells, we observed that MDA-MB-231 cells lacking EXD2 also presented with lower levels of mtDNA, which could be restored by the *WT* protein but not by any of the mutants (Figures 27a and 27b). Furtherm ore, EXD2 deficiency also affected the ETC as measured by the Seahorse XF24 bioanalyzer. Compared to the parental cell line or *EXD2-WT* complemented cells, *EXD2-KO* cells exhibited reduced OCR that could not be rescued by any of the mutants *EXD2-NUC* or *EXD2-C2* (Figures 27c and 27d). Similarly to U2OS cells, the defect in respiration appears to be due to mitochondrial dysfunction, as the *EXD2-KO* cells could not reach the same OCR levels as the WT cells even after treatment with the uncoupling agent FCCP (Figures 27c and 27d). We also observed that the *EXD2-KO* and mutant cells presented higher ECAR levels, indicating an increase in aerobic

glycolysis and lactate production, consistent with defective ETC activity (Figures 27e and 27f).

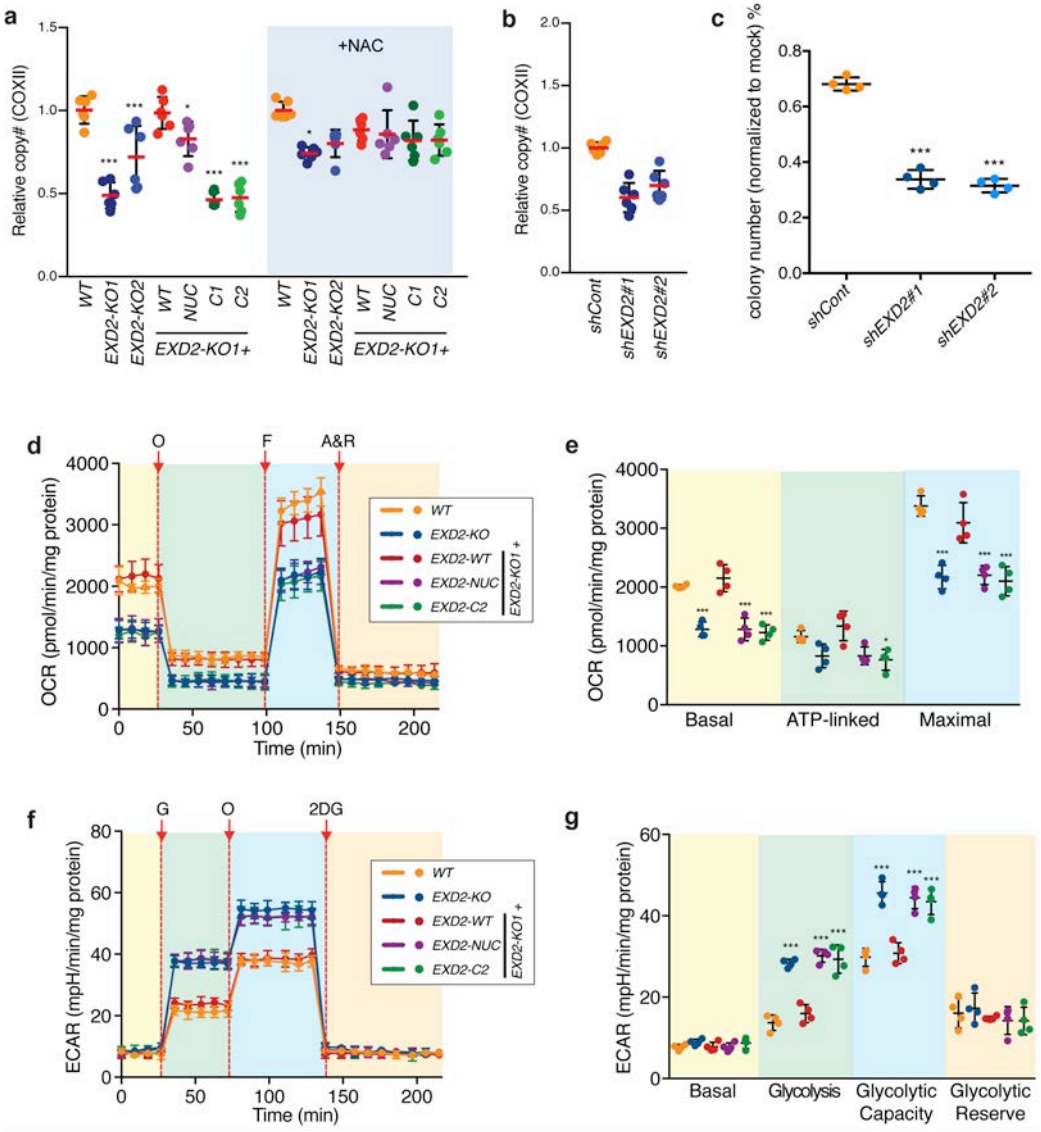

Figure 27: EXD2 deficiency affects mtDNA levels and cellular respiration. (**a**) mtDNA levels were analyzed using qRT-PCR to *COXII* and normalized to genomic DNA (*ACTB*). Cells in parallel were treated with NAC at 5 mM to reduce ROS levels. (**b**) qRT-PCR results for mtDNA levels in cells transfected with shRNA. Results presented are compiled from 2 experiments performed in triplicate with the individual values, mean (red bar) and standard deviation shown. (**c**) MDA-MB-231 cells were grown in media depleted from glutamine and cellular sensitivities were assayed by clonogenic survival assay. The surviving fractions (normalized to mock-treated cultures) are plotted Mean compiled from 2 independent experiments performed in duplicate (n=4) and the standard deviation are shown. (**d**) Analysis of OCR using the Seahorse Bioassay and the mitochondrial stress test. MDA-MB-231 cells were treated consecutively with oligomycin (O), FCCP (F), and Antimycin plus Rotenone (A&R) (as described in Materials and Methods) to measure basal respiration, ATP production, maximal respiration and spare respiratory capacity, respectively. EXD2 deficient cells show decreased basal respiration, ATP production and maximal respiration that can be rescued by the *WT* protein but not by the mutants

NUC or *C2*. The mean from 1 experiment performed in quadruplicate (n=4 per point) and standard deviation are plotted. (**e**) Graphical representation of OCR (extrapolated from data in (**d**)). (**f**) Analysis of ECAR to assess glycolytic function using the Seahorse Bioassay and Glycolysis stress test. MDA-MB-231 cells were treated consecutively with glucose (G), oligomycin (O) and 2-deoxy-D-glucose (2DG) (as described in Materials and Methods). *EXD2-KO* cells present with increased ECAR. Expression of *EXD2-SF-WT* but not the *NUC* or *C2* mutant forms of EXD2 reduced ECAR in deficient cells. The mean from 1 experiment performed in quadruplicate (n=4 per point) and standard deviation are plotted. (**g**) Graphical representation of ECAR (extrapolated from data in (**f**)). Statistical analysis was performed using one-way ANOVA together with Dunnett's test (***$p < 0.001$, *$p < 0.05$, analysis of variance compared with the *WT*).

EXD2 affects cellular migration *in vitro*

The ability of a cell to migrate and invade has been proposed as a hallmark for several types of tumors (Hanahan and Weinberg, 2011). In order escape from the primary tumor and metastasize distant organs, cancer cells require a distinct metabolism that provides both energy and nutrients necessary for such demanding processes. Considering the dramatic effects we saw in several metabolites in EXD2 deficient cells (Figure 16), we sought to investigate if EXD2 could also be disturbing cell migration. To do so, we performed a wound-healing assay and observed a significant impairment in the ability of cells to migrate upon EXD2 depletion (Figures 28a and 28b).

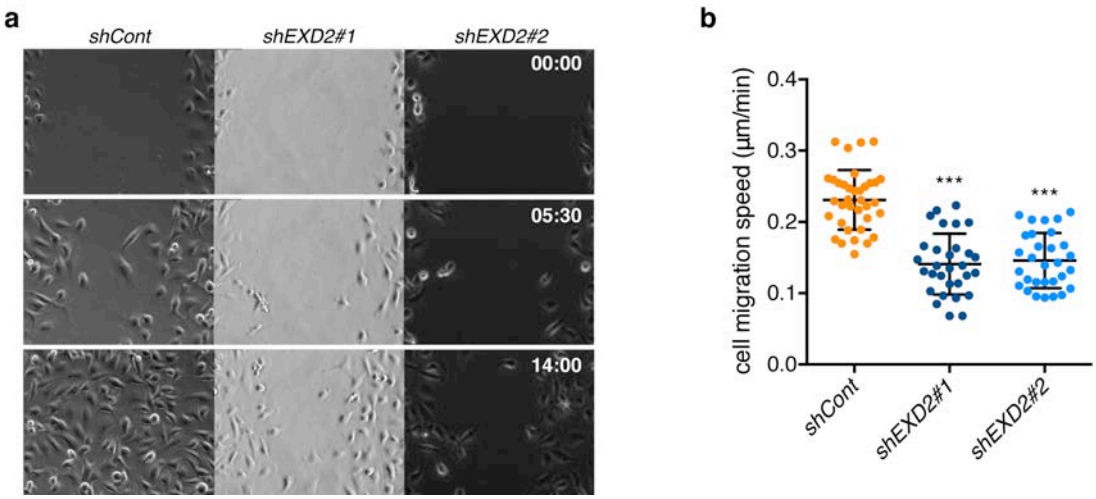

Figure 28: Depletion of EXD2 affects migration of MDA-MB-231 breast cancer cells. After scratchwounding, cells were monitored and pictures were taken every ten minutes. **(a)** Representative

images taken at different time points reveal that EXD2 depletion affects cell migration. The time correspond to the format hh:mm. **(b)** Quantification of at least 30 different fields, mean and standard deviation are shown. Statistical analysis was performed using one-way ANOVA together with Dunnett's test (***$p < 0.001$, *$p < 0.05$, analysis of variance compared with the *WT*).

EXD2 deficiency impairs tumorigenesis in MDA-MB-231 *xenografts*

Considering the metabolic switch observed upon EXD2 depletion, we sought to explore its potential role in tumor development. To do so, we injected luciferase-expressing *shNT*, *shEXD2#1* and *shEXD2#2* MDA-MB-231 cells into the mammary fat pads of immunosuppressed BALB/c nude mice and monitored tumor growth by photon flux after luciferin-injection. Seven weeks after injecting the tumors, we had to sacrifice the animals due to the excessive size of the tumors originating from the *shNT* cells. However, tumors expressing either *shEXD2#1* or *shEXD2#2* were significantly smaller, with photon flux measurements showing an impairment of growth of these cells (Figures 29a and 29b). qRT-PCR analysis of the extracted tumors further confirmed that the silencing of EXD2 was maintained during the experiment (Figure 29c). To investigate the possible mechanisms that could be affected by EXD2 depletion and impairing tumor growth, we performed IHC staining of the tumors for well-known markers of tumorigenesis (Figure 29d). Ki67 staining showed that EXD2 deficiency led to slower proliferation of the cells, particularly in the central region of the tumor, suggesting these cells were more dependent on EXD2 function. As angiogenesis is an important factor to promote tumor growth, we stained the tumors with the vascular marker CD31 and observed that the tumors lacking EXD2 presented with significant reduction of new blood vessels in the central region. Together, these results suggest EXD2 plays a role in carcinogenesis, probably by affecting the ability of the cells to develop of intra-tumoral vasculature that allows for tumor growth.

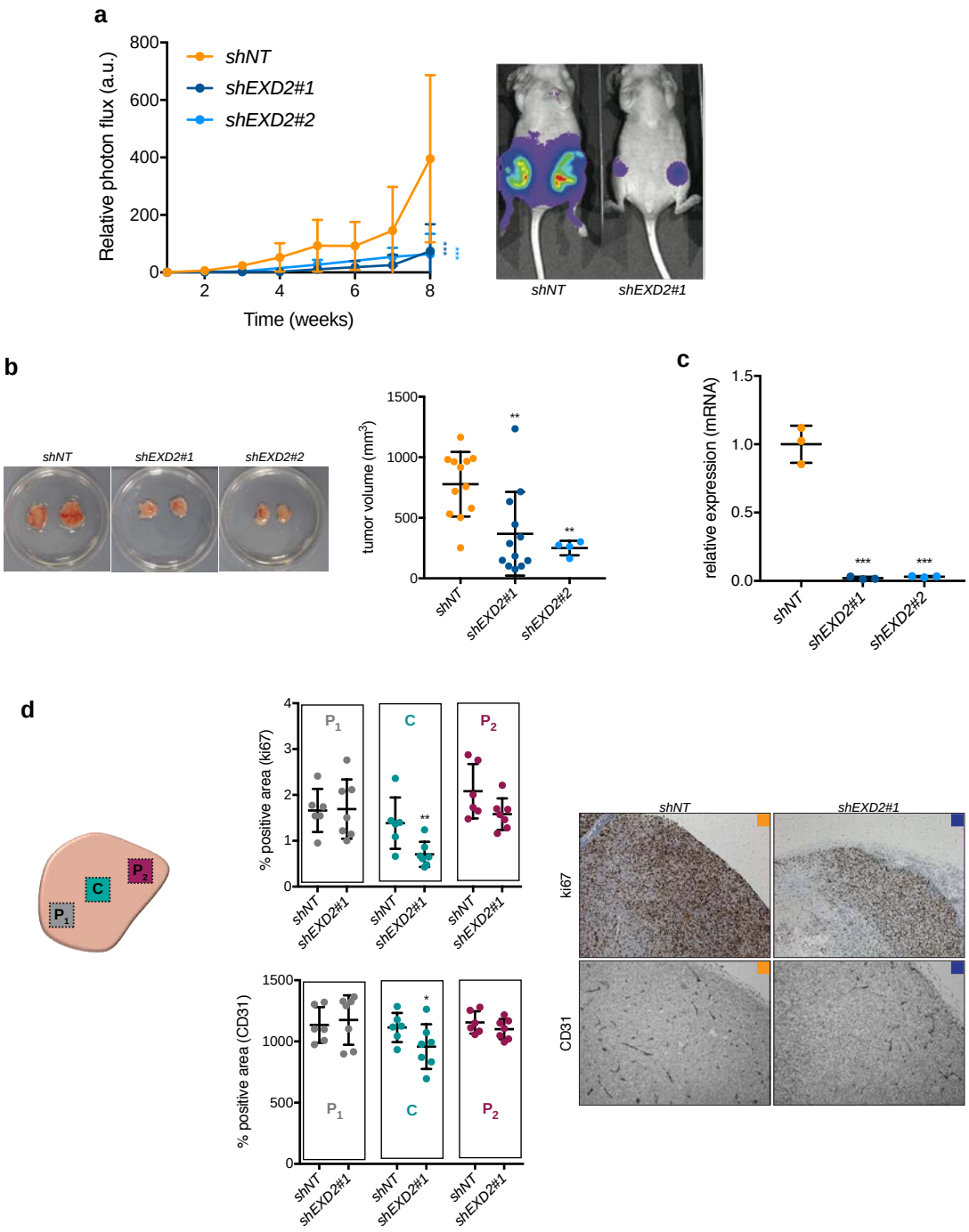

Figure 29: EXD2 influences breast cancer growth. (**a**) Tumor formation of MDA-MB-231 breast cancer cells injected into the mammary fat pad monitored by luciferase expression using an IVIS imager. (**b**) Examples of tumors extracted 7 weeks after the initial injection and respective sizes. Data shown is from a minimum of 4 tumors per condition. Mean and standard deviation are shown. Statistical analysis was performed using one-way ANOVA together with Dunnett's test (***p* < 0.01, analysis of variance compared with the *WT*). (**c**) qRT-PCR analysis of EXD2 expression in the extracted tumors at the end of the experiment. (**d**) Histological analysis of the tumors expressing *shNT* and *shEXD2#1*. Quantification of Ki67 and CD31 show a decrease in staining in the central region of the tumor. A minimum of 6 tumors was analyzed for each condition. Mean and standard deviation are shown. Statistical analysis was performed using t-test (***p* < 0.01, **p* < 0.05).

DISCUSSION

During the course of this project we characterized a novel mitochondrial protein, EXD2, and connected its conserved domains (3'-5' exonuclease and HNH-like) with the maintenance of mitochondrial homeostasis. We propose that EXD2 acts as a regulator for facilitating mitochondrial translation and OXPHOS function, which ultimately control GSCs maintenance and lifespan in *Drosophila melanogaster*.

Mitochondrial protein synthesis is modulated by translational activators, which often bind RNA. Therefore, a deficiency in these activators may lead to an impairment in the expression of mitochondrially encoded proteins and thereby to faulty assembly of the OXPHOS machinery. Although future work will be necessary to identify the precise targets of EXD2, as well as other potential enzymatic activities this protein may have, we believe the most likely scenario is that EXD2 could be involved in rRNA processing, modification of tRNAs and/or degradation of damaged RNAs, which will ultimately have an impact on mitochondrial translation.

The localization of EXD2 (Figure 11), together with its association with the mitoribosome and with Complex I subunits (Figures 19b and 19c) and the effect on mitochondrial translation (Figures 21d-g), support the idea that this exonuclease is important for mitochondrial homeostasis. As a result of its depletion, cells exhibit defective respiration, mitochondrial dysfunction and accumulation of ROS, affecting both fecundity and lifespan in *Drosophila*.

We also observed that EXD2 interacts with mtDNA, likely reflecting the proximity of the mtDNA to ongoing translation. However, EXD2 could play a more direct role in its stabilization and maintenance that we have not uncovered.

Finally, alternative structural predictions also suggest the HNH domain of EXD2 could be related to Tetraheme cytochrome proteins that bind hemes through coordinated cysteine and histidine residues (Figure 10c), backing the hypothesis of a more direct role of EXD2 in the ETC, as suggested by our hemin-agarose pulldown assays where we observed an enrichment for EXD2 that appear to be dependent on its C-terminus (Supplementary Figure 2). Alternatively, this result could reflect the interactions of EXD2 with other heme binding mitochondrial proteins.

One of the few papers describing EXD2 identified both human and *Drosophila* EXD2 as a host factor for the replication of Dengue RNA virus (Sessions *et al*, 2009). It is possible that EXD2 may affect Dengue replication in a direct way, by acting on the ssRNA or some replication intermediates. Consistent with this possibility, our BioID data revealed interactions between EXD2 and ZC3HAV1 and MAVS, both of

which have been implicated in antiviral defense (Figure 19b and Supplementary Table 3) (He *et al*, 2016; Todorova *et al*, 2015; Jablonski and Caputi, 2009; Park *et al*, 1999; Goodier *et al*, 2015; Zhu *et al* 2011; Hayakawa *et al*, 2011).

In contrast to MAVS, ZC3HAV1 has not been shown to localize in the mitochondria, but it was recently identified in a genome wide screen for proteins involved in OXPHOS, suggesting it could have a mitochondrial role (Arroyo *et al*, 2016). However, given our results, the fact that other proteins that are directly involved in cellular metabolism were identified in the screen and that Dengue infection involves metabolic reprogramming, it seems more likely that it plays an indirect role, either by controlling the metabolism of the cell, or by modulating the immune response.

Mitochondria-mediated immune responses might be the result of an evolutionary adaptation by which mitochondria learned how to cope with entry of foreign microorganisms that allowed for them to be part of the cell. However, this feature also makes them the perfect target for all the invading pathogens, including viruses. It is known that most of the viruses modulate mitochondrial processes in a highly specific manner so that they can replicate and produce progeny (El-Bacha and Da Poian, 2013; Anand and Tikoo, 2013; Neumann *et al*, 2015). Thus, it is important for future studies to understand and unravel the potential roles of EXD2 in controlling viral replication.

A previous screen identified EXD2 as a modulator of sensitivity to different DNA crosslinking agents (Smogorzewska *et al*, 2010), and more recently, EXD2 was reported to be localized in the chromatin and play a role in homologous recombination by interacting with the DNA resection machinery (Broderick *et al*, 2016). Using the same method (Broderick *et al*, 2016) we can detect EXD2 in the chromatin (Supplementary Figure 1), however we also see other mitochondrial proteins, suggesting the fractionation protocol leads to chromatin that is highly contaminated with mitochondria.

Our results suggest EXD2 localizes exclusively to the mitochondria (Figure 11) and in an unbiased proteomics approach we identified almost exclusively mitochondrial proteins, supporting the idea that EXD2 mainly resides in the mitochondria. We also found among the interacting proteins POLDIP2 and ATR, which have been implicated in DNA replication (Figure 19b and Supplementary Table

3). However, both of these proteins have additional roles in the mitochondria, which appear to be independent of their nuclear function.

In addition, we did not observe any differences in RPA foci formation or DNA damage sensitivity in our KO clones, in contrast to what was reported by Broderick and colleagues (Figure 15) (Broderick *et al*, 2016). However, it should be taken into account that the authors used a metabolic readout (Alamar Blue) assay for the sensitivity measurements, suggesting that EXD2 deficiency may trigger metabolic defects, as described here. Upon DNA damage, cells have a unique metabolic requirement to provide nucleotides for DNA repair while limiting proliferation.

Analysis of both mouse embryonic fibroblasts and different human cell lines exposed to DNA-damaging agents showed a specific inhibition of glutamine consumption, which was due to an upregulation of the mRNA levels of *Sirt4* (Jeong *et al*, 2013). *Sirt4* has been previously described to reduce glutamate dehydrogenase (GDH), the enzyme that converts glutamate to α-ketoglutarate, inhibiting glutaminolysis (Haigis *et al*, 2006). Therefore, it is possible that cells dependent on glutamine, such as those lacking EXD2 (Figures 17g and 27c), could have metabolic defects following DNA damage. However, using the colony formation assay, we could not detect any significant differences in survival between *EXD2-WT* and *EXD2-KO* when exposing cells to different dosages of CPT and MMC (Figure 14).

As for *in vivo* data, one paper described in flies a role for *dEXD2* in somatic recombination (Cox *et al*, 2007). However, it must be taken into consideration the authors identified this gene, in a BLASTP search, as a possible exonuclease with strong homology to *WRN* gene, which has been well studied as key player in DNA replication and recombination.

In addition, although detecting a significant increase in recombination in flies lacking *dEXD2* compared with wild-type, this was not remotely comparable with the increase seen in *CG7670* flies, which is the true orthologue of *WRN* in *Drosophila*.

Thus, although we cannot completely discard a function for EXD2 in DNA repair, we believe that its main role is to preserve mitochondrial homeostasis, by controlling mitochondrial translation and OXPHOS function.

We observed that EXD2 depletion disturbed glucose usage, causing the cells to rely on glutamine to survive (Figure 16). Several metabolites were affected, including glutathione, which has been described to be essential for the antioxidant defenses of the cell, along with several compounds of the TCA cycle and nucleotide

biosynthesis. Overall, our results suggest that upon EXD2 depletion, cells undergo a metabolic “switch”, where much of the glucose is converted into lactate while the TCA is fueled by glutamine. These metabolic changes are typical of the Warburg effect, often observed in cancer cells (Warburg *et al*, 1927).

Several studies have reported that cancer cells usually have a higher glycolytic metabolism in order to fulfill the high demand for proliferation, while relying on glutamine for biomass production. When testing the influence of EXD2 in tumorigenesis, we saw that its deficiency severely impaired breast cancer growth (Figure 29). Although cells lacking EXD2 show the perfect “signature” for tumor proliferation, the limiting existence of glutamine *in vivo* prevents this hypothetical advantage, rendering these cells less fit for growth. Consistently, *ex vivo* analysis of the tumors showed a decrease in proliferation and vascular growth.

Given that glutamine is a nonessential amino acid, several therapies have been explored related to its metabolism (Hensley *et al*, 2013; Wise and Thompson, 2010). Inhibition of glutaminolysis has been shown to impair tumor growth in several models and many clinical agents targeting this pathway are being explored. Thus, by depleting EXD2 and causing the cells to rely exclusively on glutamine to survive, we believe EXD2 could become a potential biomarker and/or target for cancer treatment.

In addition to the metabolic defects described previously, we also saw that EXD2 is necessary for oxidative metabolism (Figure 18). Cells lacking EXD2 have a significant decrease in OCR and ATP levels. In addition, ECARs were elevated, indicating an increase in aerobic glycolysis and lactate production, which often accompany defective OXPHOS activity (Invernizzi *et al*, 2012; Robinson *et al*, 2012). Moreover, we saw that this defect is probably due, at least in part, to reduced Complex I activity (Figures 19h-i), indicating that EXD2 could be controlling its activity.

We saw that EXD2 associates with the matrix exposed subunits of Complex I (Figure 19b and Supplementary Table 3) and its depletion affects the stability of different ETC units (Figures 19e-f). Complexes I and III have been proposed to be the major sources of ROS within the cell and consistent with this, we saw that EXD2 deficient cells show higher levels of mitochondrial ROS (Figure 17a), which could be due to a defective OXPHOS. This could result in the damage of mtDNA, thus leading to its decrease, as shown here (Figures 17c and 27b).

Moreover, we were able to rescue most of the phenotypes by NAC treatment, reinforcing the idea that EXD2 deficiency causes problems in OXPHOS function that ultimately force the metabolic switch and cause mitochondrial dysfunction.

We saw that EXD2 affects mitochondrial translation that is required for the generation of important ETC subunits. Although we are still trying to identify the specific targets of EXD2, we believe EXD2 acts on RNA metabolism to affect translation. *In vitro* data showed that EXD2 is able to degrade several substrates, including RNAs (Figure 20).

We performed RT-qPCR analysis of several mitochondrial transcripts and observed a specific depletion of transcripts for subunits of Complex I in our KO cells (Figure 21a). Although we cannot discard that this result could be due to the fact that Complex I transcripts have a shorter half-life and are therefore more prone to degradation (Chujo *et al*, 2012), we believe EXD2 could have additional roles regarding Complex I assembly. Supporting the regulatory complexity that this complex represents, a recent metabolic labeling study showed that the matrix arm proteins of Complex I had a distinct turnover rate compared with the ones in the membrane arm (Kim *et al*, 2012), consistent with the idea that the matrix arm proteins might exist as free monomers or in less stable and smaller subcomplexes and that EXD2 could be important for the handling of such structures.

To date, there is only one protein that has been proposed to be involved in the assembly of the N module of Complex I. NUBPL has been described to have a conserved CxxC motif that binds iron-sulfur and affects protein biogenesis (Sheftel *et al*, 2009). Together with our BioID results (Figure 19b and Supplementary Table 3), it is possible that EXD2 could play a role in the assembly of the matrix arm of Complex I, thus affecting its stability and activity. Moreover, given that Complex I has the most mitochondrial encoded proteins out of all the ETC complexes, it is possible that its activity is differentially affected upon inhibition of global mitochondrial translation.

As the nuclease activity of EXD2 is required to complement all of the phenotypes we have identified, we performed MitoString analysis to identify possible defects in the processing of several mature and precursor mtDNA transcripts (Figure 21c). In contrast to our RT-qPCR data, we could not detect any significant differences in any of the mRNA transcripts and no defects in processing were evident. We believe this could be due to the fact that despite the high coverage, this assay is far

less sensitive compared with qPCR. However, we noticed a significant decrease in both MT-RNR1 and MT-RNR2, encoding for mitochondrial 12S and 16S ribosomal RNAs, which could indicate a problem with ribosomal biogenesis, and therefore translation, that could also be explained by the interaction seen between EXD2 and the mitoribosme (Figure 19b and Supplementary Table 3).

Previous studies have found a role for GRSF1, here identified as a potential EXD2 interactor, in the regulation of mitochondrial RNAs. GRSF1 localizes to RNA granules and is required for precursor RNA cleavage and it preferentially associates with light strand transcripts. GRSF1 depletion affects rRNAs and some mRNAs and causes impaired ribosome assembly (Antonicka *et al*, 2013; Jourdain *et al*, 2013). Additionally, it has been recently shown to control RMRP levels in the mitochondria, and its depletion led to a decrease in OCR (Noh *et al*, 2016). Future work will be required in order to understand and define the precise targets of EXD2 and the relevance of each of its proximity interactions.

Mitochondria are responsible for generating energy stores in the form of ATP and NADH, which serve as fuel for physiological processes and lifespan, as well as ROS. Thus it is crucial to understand mitochondrial function in order to identify and characterize the pathways associated with longevity. We observed that the lifespan extension in female dEXD2 deficient flies was independent of *Sir2* and CR (Figures 23 and 24), two main pathways that have been strongly implicated in longevity. Thus, we propose that this difference is primarily due the premature attrition of the GSCs (Figures 25d and 25e).

Several mitochondrial genes have been implicated in GSCs maintenance or differentiation in both male and female *Drosophila*, contributing to defective fecundity and a consequent increase in lifespan (Yu *et al*, 2016; Teixeira *et al*, 2015; Schultz and Sinclair, 2016). Several papers have reported that accumulation of ROS prompts differentiation in a variety of stem cell populations (Khacho *et al*, 2016; Ong *et al*, 2016; Kong *et al*, 2016; Owusu-Ansah and Banerjee, 2009).

Although increased ROS production has been widely associated with aging and age-related diseases (Morais *et al*, 2014; Forster *et al*, 1996; Harman, 1965), it has also been shown that increased oxidative stress caused by inhibition of the ETC complexes or deletion of antioxidant enzymes increases lifespan in *C. elegans* and yeast **(**Dillin *et al*, 2002; Van Raamsdonk and Hekimi, 2009; Mesquita *et al*, 2010). Recently, it has been proposed that mitochondrial ROS produced specifically through

Complex I reverse electron transport extends lifespan in *Drosophila* (Scialò *et al*, 2016), with some of its subunits (CG32230 and CG2014) affecting strongly the females (Copeland *et al*, 2009). These recent findings have forced the scientific community to reevaluate the role of ROS in the aging process (Hekimi *et al*, 2011; López-Otín *et al*, 2013).

We observed that flies lacking dEXD2 are more sensitive to oxidative stress (Figure 24d) and that feeding them a NAC diet was enough to partially rescue most of the phenotypes, supporting the idea that EXD2 is acting through oxidative metabolism in order to control fecundity and lifespan. Moreover, it has been shown that the mitochondrial respiratory chain is essential for HIF1 activation *in vivo* and organismal adaptation to hypoxia (Hamanaka *et al*, 2016).

There are several processes involved in the regulation of aging that need to be tightly regulated in order to assure optimal physiological progress. In addition to ROS, defects in the insulin/IGF-1 pathway have also been described to extend lifespan in different organisms (Kenyon *et al*, 1993; Clancy *et al*, 2001; Tatar *et al*, 2003). Moreover, this pathway seems to be intrinsically linked to ROS and ecdysone signaling. Activation of the insulin/IGF-1 pathway requires autophosphorylation of multiple tyrosine residues the insulin receptor (IR). However, this receptor can also be regulated through ROS by stimulating serine hyperphosphorylation, which promotes the dissociation between the IRβ-subunit and the IR substrate (IRS) and/or the IRS and PI3K, promoting the degradation of the IRS proteins and decrease of specific signaling proteins (reviewed in Papaconstantinou, 2009). Some models of long-lived animals display alterations in these pathways. One example is the overexpression of *Klotho* in mice, which results in an increase of lifespan, through the manipulation of ROS and insulin pathways (Kurosu *et al*, 2005). $p66^{Shc}$ activity has been linked to IRβ-subunit and $p66^{Shc}$ mutant animals are also long-lived and display accumulation of ROS due to defective mitochondrial ETC (Giorgio *et al*, 2005). Moreover, it has been shown in *D. melanogaster* that insulin can act directly in the ovaries and distress hormonal synthesis, with IR-mutants showing lower levels of ecdysone (Tu *et al*, 2002). In addition, it has also been shown that ecdysone mutant flies have increased lifespan (Simon *et al*, 2003).

We observed that female flies deficient for dEXD2 present lower levels of several insulin-like peptides, insulin receptor and ecdysone receptor (Figure 23d). Insulin and ecdysone pathways are responsible for the rate of larval growth and the

length of that growth period, respectively, and it has been shown that impairment of these pathways results in developmental delay and shorter animals (Caldwell *et al*, 2005; Colombani *et al*, 2005; Mirth *et al*, 2005), which is in agreement with our data (Figure 23b). Thus, we propose that dEXD2 depletion in the germ line causes oxidative stress, damaging the GSCs and thus affecting fecundity and leading to an increase of lifespan. This is consistent with the expression pattern of dEXD2, the effects of NAC on GSCs attrition, fecundity and lifespan, and the close correlation between the age of GSCs loss and lifespan extension.

Analysis of mRNAs enriched in the germ plasm of *Xenopus*, which is rich in mitochondria and RNA binding proteins, identified *xEXD2* (Cuykendall and Houston, 2010), supporting the possibility that it may have a role in the GSCs niche in vertebrates. It will be interesting in future works to see if EXD2 affects mammalian fertility or lifespan, and if it can be used to study aging and age-related diseases.

Our BioID data showed a strong interaction between EXD2 and several Complex I proteins (Figure 19b and Supplementary Table 3). Mutations in most of these proteins have been associated with several metabolic diseases, including Leigh Syndrome (Martín *et al*, 2005). Moreover, deletions in chromosome 14q24, that harbors EXD2 among other genes, have been associated with several diseases including heart failure, brachydactyly and intellectual disability (Oehl-Jaschkowitz *et al*, 2014). Together, this supports the idea that EXD2 could be considered a potential candidate for undiagnosed human metabolic diseases.

It has also been shown that defects in Complex I assembly are involved in the metabolic switch from OXPHOS to glycolysis (Rafikov *et al*, 2015), and a recent report showed EXD2 was upregulated in response to a BET-inhibitor treatment of Complex I-deficient cells, together with several other proteins involved in OXPHOS regulation (Barrow *et al*, 2016). Thus, it is possible that by controlling Complex I function, EXD2 can have an indirect role in the metabolism of the cell. Consistent with this idea, two recent reports identified several EXD2 interactors as new regulators of the ETC (Floyd *et al*, 2016) and as being essential for OXPHOS function (Arroyo *et al*, 2016). Depletion of SHMT2, another of the proteins identified in the proximity assay, has also been associated with increase of mitochondrial ROS, lower levels of $NADPH/NADP^+$ and GSH/GSSG ratios and these phenotypes were rescued when cells were treated with NAC (Martínez-Reyes and Chandel, 2014). Although the individual contribution of EXD2 deficiency to these metabolic defects

still remains to be discovered, it will be interesting to explore its potential use as a biomarker for metabolic pathologies.

Given the high metabolic demands displayed by tumor cells, targeting mitochondrial ATP production has emerged as a viable therapeutic strategy against cancer. Epidemiological and laboratory-based studies have shown that the anti-diabetic drug metformin prevents cancer progression (Evans *et al*, 2005; Wheaton *et al*, 2014). In addition to diminishing glucose and insulin levels, metformin also functions by inhibiting ETC Complex I (El-Mir *et al*, 2000; Owen *et al*, 2000), which has been shown to be essential for its antitumorigenic effects (Wheaton *et al*, 2014). Interestingly, the administration of metformin causes metabolite alterations similar to those reported here, including a decrease of aspartate, glutathione and NAD^+ levels (Liu *et al*, 2016; Gui *et al*, 2016).

Inhibition of mitochondrial translation has also been explored as a potential therapy for cancer treatment. A recent report has shown that several mitochondria-targeted drugs, including chloramphenicol, effectively eradicate cancer stem cells, preventing tumor growth in several cancer cell lines (Lamb *et al*, 2015). Considering EXD2 depletion causes defects in mitochondrial translation, GSC maintenance and tumor growth, we consider it could constitute a novel therapeutic biomarker or target.

Mitochondrial disorders can result from a dysfunctional respiratory chain due to several causes, including mutations in ETC subunits and/or chaperone proteins required for proper OXPHOS function, defective mtDNA maintenance and protein translation, and also problems in RNA processing and abundance. Hence, the discovery and characterization of unknown proteins that enable mitochondrial function will allow for a better understanding and treatment of several pathologies, including metabolic disorders and cancer.

CONCLUSIONS

EXD2 is a mitochondrial protein that contains a MTS in its N-terminal region that is both necessary and sufficient for its localization

EXD2 is required for normal metabolism and its depletion impairs glucose usage and confers glutamine dependence

EXD2 deficiency leads to increased levels of mitochondrial ROS, depolarization of the mitochondrial membrane and decreased levels of mtDNA

EXD2 is required for OXPHOS activity and ATP production and its deficiency impairs cellular respiration

EXD2 associates with the matrix subunits of Complex I and the mitoribosome and its deficiency impairs ETC complex assembly or stabilization

EXD2 is an active, evolutionarily conserved 3'-5' exonuclease that is able to degrade RNA, DNA and RNA:DNA hybrids *in vitro*

EXD2 is required for efficient mitochondrial translation

EXD2 is required for normal aging and metabolic homeostasis in *Drosophila melanogaster*

EXD2 deficiency leads to ROS dependent premature attrition of the GSCs and reduced female fecundity

EXD2 deficiency impairs breast cancer growth in *xenografts* possibly by imposing glutamine addiction and/or preventing angiogenesis

SUPPLEMENTARY MATERIAL

Chromatin Fractionation (Supplementary Figure 1)

Alternative chromatin fractionation was performed in agreement with a previous publication (Broderick *et al*, 2016). U2OS cells were resuspended in buffer A (10mM HEPES-KOH pH=7.9, 10mM KCl, 1.5mM MgCl2, 340mM sucrose, 10% glycerol, 1mM DTT, 1x protease inhibitor cocktail) and phosphatase inhibitor cocktail, and Triton X-100 was added to a final concentration of 0.1%. After incubation on ice for 5min, samples were centrifuged at 1300xg for 4 min. Pelleted nuclei were washed with buffer A, resuspended in buffer B (3mM EDTA, 0.2mM EGTA, 1mM DTT, 1x protease inhibitor cocktail and phosphatase inhibitor cocktail) and lysed for 20min on ice. After centrifugation at 1700xg for 5min, the supernatant (nuclear soluble fraction) was collected, and the pellet (chromatin fraction) was washed with buffer B, resuspended in urea buffer (9M urea, 50mM Tris-HCl pH=7.3) and sonicated.

Hemin-Agarose Pulldowns (Supplementary Figure 2)

HEK293 cells were transfected with *EXD2-WT*, *EXD2-NUC*, *EXD2-C1* and *EXD2-C2* cloned into a SF-TAP vector. Cells were washed with PBS (1x protease inhibitor cocktail and phosphatase inhibitor cocktail) and collected in lysis buffer (50mM TrisHCl pH=7.5, 150mM NaCl, 1% Tween-20, 0.5% NP-40, 1x protease inhibitor cocktail and phosphatase inhibitor cocktail). Samples were centrifuged at 12000xg and the lysates were incubated with pre-washed hemin-agarose beads for 1 hour at 37°C in a mechanical rotator. After extensive washes, the beads were incubated with SDS-PAGE buffer and boiled for 5 minutes, allowing the elution of the heme-binding proteins, which were then identified by Western Blot.

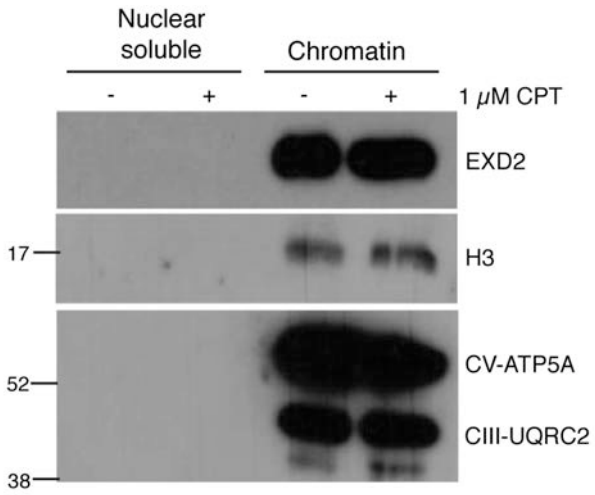

Supplementary Figure 1: Subcellular fractionation using previously reported methods (Broderick *et al*, 2016) in the presence or absence of DNA damage induced by CPT. The presence of EXD2 in the chromatin fraction is accompanied by other mitochondrial proteins, suggesting this protocol co-enriches mitochondria with this fraction.

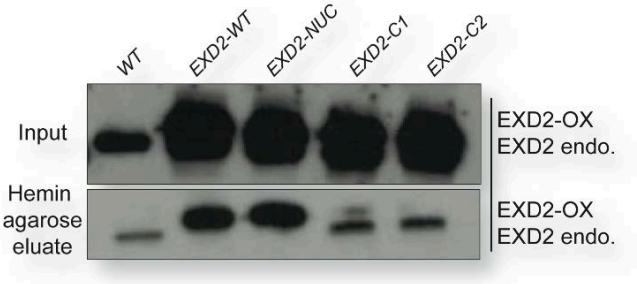

Supplementary Figure 2: Hemin-agarose pulldowns assays show enrichment for EXD2. This interaction seems to be dependent on the C-terminal region, as it is lost in both *EXD2-C1* and *C2* mutants while the *EXD2-NUC* mutant is still able to associate with the hemin group.

Supplementary Table 1: LC/MS and GC/MS analysis. Metabolon data that was analyzed to generate Figures 16a and 16b.

Biochemical	*shCont*					*shEXD2#1*				
	Tech 1	Tech 2	Tech 3	Tech 4	Tech 5	Tech 1	Tech 2	Tech 3	Tech 4	Tech 5
1,2-dipalmitoylglycerol	1.0759	1.4696	0.7137	1.1648	1.1298	0.7229	0.7535	1.0232	1.0289	1.1291
1-arachidonoylglycerophosphoethanolamine*	1.3998	0.9702	1.4487	0.8678	0.7755	0.6067	1.0088	0.8956	1.5352	0.5758
1-arachidonoylglycerophosphoinositol*	1.1976	0.9348	1.0033	1.1148	0.8812	0.7431	1.2599	1.3593	1	0.9713
1-methylnicotinamide	0.7699	1	0.7192	1.2251	1.4399	0.9239	0.7788	1.3616	1.5187	0.9722
1-myristoylglycerophosphocholine	0.8597	1.0745	1.3509	0.9437	0.9554	0.8862	1.2222	1.014	1.0506	1.0163
1-oleoylglycerophosphocholine	0.5886	1.1441	2.9572	1.1433	1.0085	0.821	0.7943	1	1.2408	0.5759
1-oleoylglycerophosphoethanolamine	1.3008	1.1179	1.4363	0.4627	0.5702	0.5827	1.3712	0.9182	1.2777	0.5462
1-oleoylglycerophosphoinositol*	1.4117	1.2068	1.1774	0.8491	0.9258	0.7238	1.3319	1	1.439	0.8348
1-palmitoleoylglycerophosphocholine*	0.973	1.0672	1.8836	0.7641	0.721	1	1.391	0.9788	1.0289	1.0529
1-palmitoylglycerophosphocholine	0.5031	0.9458	2.6748	1.2262	1.1469	0.6951	0.8829	1.1173	1.7925	0.4541
1-palmitoylglycerophosphoethanolamine	1.0761	1.1495	1.0071	0.5033	0.1929	0.6021	1	0.6957	1.2854	0.4278
1-palmitoylglycerophosphoinositol*	1.7427	1.2466	1.1775	0.9144	1.041	0.771	1.159	0.9915	1.3164	0.8777
1-palmitoylplasmenylethanolamine*	1.4905	1.0857	1.6439	0.8209	0.6634	0.3887	1.0149	0.7378	1.3371	0.5026
1-pentadecanoylglycerophosphocholine*	1.2752	0.6951	2.0558	0.6867	0.579	0.8755	1.191	0.6252	0.912	1.0077
1-stearoylglycerol (1-monostearin)	1.1138	1.5678	1.4981	0.8902	0.9567	0.7888	1.1674	1.1203	1.3941	0.6532
1-stearoylglycerophosphocholine	1.1042	2.4126	6.7326	0.3337	0.3893	1.3076	1.0524	0.2965	0.4182	0.9239
1-stearoylglycerophosphoethanolamine	1.3502	1.1952	1.393	0.6093	0.5479	0.2065	1	0.7303	1.2039	0.2428
1-stearoylglycerophosphoinositol	1.3876	1.1753	1.0941	1.4093	1.2047	0.5696	1	0.9982	1.0385	0.6966
10-heptadecenoate (17:1n7)	1.2094	1.0539	0.9603	1	1.0293	0.8516	0.8495	0.9283	1.1417	0.9226
10-nonadecenoate (19:1n9)	0.9835	1.3575	1.0454	1.3342	1.4458	0.8042	0.7943	0.7221	1.1015	0.9141
13-methylmyristic acid	1.0447	1.0259	1	0.9485	0.8776	1.0128	1.102	0.9548	1.2073	1.154
17-methylstearate	1	1.1101	1.7075	0.755	0.9152	1.0474	0.9325	0.7931	1.1647	0.6022
2'-deoxyinosine	0.8489	0.6185	1.0326	0.5801	0.4218	0.6951	1.1027	0.6512	1	0.8454
2-aminoadipate	1.3212	1.5307	1.217	1.2392	1.1895	0.6371	0.6451	0.6745	0.7892	0.694
2-arachidonoylglycerophosphocholine*	1.0213	1.1338	1.8224	1.1012	1	0.7453	1.2314	0.7554	0.9593	0.7484
2-arachidonoylglycerophosphoethanolamine*	1.1814	1.1661	1.5221	1.0286	0.9791	0.8304	1.1898	0.8422	0.9472	0.9206

2-docosahexaenoylglycerophosphocholine*	1	1.072	1.3843	1.0687	0.8871	0.8103	1.1784	0.9243	1.1043	0.8001
2-docosahexaenoylglycerophosphoethanolamine*	1.1197	1.1354	1.3353	1.0688	0.9419	0.7789	1.0629	0.8638	1	0.8421
2-docosapentaenoylglycerophosphocholine*	1.1657	1.3078	1.9194	1.1117	0.956	0.6567	1.2627	0.8079	0.8808	0.7789
2-docosapentaenoylglycerophosphoethanolamine*	1	1.6848	1.8602	1.0133	1.0021	0.6772	1.1453	0.8229	0.926	0.7005
2-eicosatrienoylglycerophosphocholine*	0.9959	0.8977	2.6217	1	1.0773	0.92	1.2635	0.8657	1.2623	0.8082
2-hydroxyglutarate	0.8155	0.9452	0.8541	0.7785	0.6331	1.1252	1	1.5083	1.4074	1.4923
2-hydroxypalmitate	1.0336	1.3011	1.0948	1	1.083	0.3165	0.3244	0.2946	0.4485	0.3374
2-hydroxystearate	1.3122	1.1837	1.0939	1	0.6636	0.3575	0.3903	0.404	0.6551	0.4083
2-linoleoylglycerophosphocholine*	0.9866	1.0433	1.2775	0.7842	0.732	1	1.7177	1.1152	0.9043	1.0583
2-linoleoylglycerophosphoethanolamine*	0.4374	1.0078	1.1322	0.6082	0.6912	0.9607	1.3294	1.1685	1.4232	1
2-methylbutyrylcarnitine (C5)	1.9873	2.1364	1.6764	1.7959	1.971	0.9121	0.8818	1.0138	1	0.9956
2-myristoylglycerophosphocholine*	1	1.125	1.4028	1.3509	1.4082	0.969	1.1577	1.2446	1.345	0.9893
2-oleoylglycerophosphocholine*	0.569	0.7466	1.6951	1.0101	1	0.6309	1.061	1.0066	1.292	0.5601
2-oleoylglycerophosphoethanolamine*	0.5921	0.9401	1.8737	1.0797	1.0708	0.7159	1	0.8534	1.1657	0.6265
2-oleoylglycerophosphoinositol*	1.53	1.6114	1.1323	1.0301	1.1682	0.6785	1.2163	1	1.3927	0.9043
2-palmitoleoylglycerophosphocholine*	1.0451	1.0415	1.3197	1.0201	1.0867	0.8452	1.1807	0.9956	1.2722	0.9045
2-palmitoleoylglycerophosphoethanolamine*	0.9624	0.8912	1.1409	1.0718	1.025	1.0533	1.0242	1	1.2098	0.864
2-palmitoylglycerophosphocholine*	0.9278	0.8944	1.6215	1	1.0247	0.8264	1.3798	1.0141	1.2749	0.8701
2-palmitoylglycerophosphoethanolamine*	0.6947	0.9779	1.6319	0.9344	1.1386	0.8868	1.3281	0.9869	1.1142	0.759
3'-dephosphocoenzyme A	0.6448	0.6639	1.2796	0.993	0.766	1.1927	1	0.8718	0.6396	0.9405
3-(4-hydroxyphenyl)lactate	0.6734	0.6598	0.6927	0.53	0.5024	1.2226	1.39	1.046	1.1416	1.2918
3-dehydrocarnitine*	1.2728	1.1601	0.8994	1.3123	0.9988	1.2495	1.0012	0.8219	0.7849	1.0777
3-hydroxyisobutyrate	0.6119	0.9427	0.6119	0.7174	0.7544	1.6214	0.6119	0.9262	1.0573	1.1243
3-phosphoserine	1.3768	1.4239	1	0.3478	0.9384	0.3478	0.6356	1.2709	1.0221	0.9942
4-hydroxybutyrate (GHB)	1.2133	1.6863	1.3466	0.741	1.2629	0.7721	0.8176	1.1983	1.2094	1.1824
5,6-dihydrouracil	1.338	1.5639	1.1575	1	0.7784	0.7426	0.8712	0.8653	1.0985	1.055
5-aminovalerate	1.0068	1.0712	0.8022	1	0.8698	1.2476	1.0645	1.1096	1.1238	1.1952
5-methyltetrahydrofolate (5MeTHF)	1.5319	1.7809	1.5492	1.2933	1.4989	0.9007	0.91	1	1.3623	1.1176
5-methylthioadenosine (MTA)	1.1181	1.163	1.1309	1.1029	1.3105	0.9286	0.8505	0.9337	0.8962	0.9549
5-methyluridine (ribothymidine)	1.1025	0.9927	1.1188	1.0035	0.8143	0.5959	0.7591	0.7063	0.812	0.8435
5-oxoproline	1.1955	1.0948	1.0991	1.0608	0.7747	0.7451	0.7604	0.6867	0.566	0.7618

7-alpha-hydroxycholesterol	1.7418	1.134	1.4253	1.0981	1.4957	0.8846	0.8448	0.6522	0.9673	0.6522
7-beta-hydroxycholesterol	1.0712	1.4522	1.0299	1.0538	1.0811	0.7699	0.785	1.1613	0.8934	0.9744
7-ketocholesterol	1.0072	1.3227	1.0067	0.9571	1.3551	0.7818	1	1.1989	1.2002	0.9136
acetyl CoA	1.4119	1	1.282	1.1295	1.3097	0.7714	0.87	0.7604	1.1295	1.5446
acetylcarnitine	1.3795	1.4659	1.257	1.2141	1.0323	1	0.9063	0.725	0.9172	1.1002
acetylphosphate	0.9906	1.0705	0.8098	1.3583	1.6679	1.7523	0.9202	1.0493	1.059	1.2263
adenine	1.0446	1.2907	1.0271	1.1698	1	0.7917	0.7854	0.8534	1.0259	0.847
adenosine	0.7287	0.7691	1.2605	0.9511	1.0527	1.4085	1	1.1954	0.8987	1.1657
adenosine 5'-diphosphate (ADP)	1	1.5888	1.017	0.9765	1.3473	1.2718	0.9902	1.1976	1.1492	1.396
adenosine 5'-monophosphate (AMP)	0.8362	1.3781	0.9442	1.0213	1.4945	1.3662	1	1.6425	1.4758	1.5623
adenosine 5'-triphosphate (ATP)	1.0386	1.4109	0.8711	1.1196	1.3954	1.0029	0.8727	1.0604	0.9101	1
alanine	1.0012	1.0258	0.9497	0.8259	0.7579	1.0267	1.0665	1.0297	1.2502	1.2047
alpha-tocopherol	0.367	1.3394	0.5048	0.8096	1.1556	0.9917	2.0906	1.1677	1.5626	1.0083
arachidonate (20:4n6)	1.6558	0.8813	0.8968	1.6241	1.0779	0.8086	0.7112	0.6853	2.0175	0.8113
arginine	1.1647	0.8981	0.952	1.0762	0.9501	1	1.0264	0.877	1.2156	1.0602
asparagine	1.0448	1.0315	1.2229	0.8546	0.7235	0.7534	0.9024	0.7808	1.3513	1.1952
aspartate	1.6889	1.8777	1.6639	1.4161	1.4679	0.7755	0.9	0.876	1	1.0043
aspartylleucine	1.1409	1.2247	1.2913	1.0384	0.8604	0.6994	1	0.669	2.3782	1.1991
aspartylphenylalanine	1.2003	1.3016	1.2529	1.0588	1	0.7902	1.2705	0.9423	2.8858	1.5742
aspartylvaline	1.2136	1.4798	1.0772	1.0205	1.2826	0.5917	0.8346	0.7235	2.0913	1.0276
beta-alanine	0.767	1.121	0.6438	1.2521	0.9005	2.029	1	1.1586	1.0267	1.254
butyrylcarnitine	0.8767	1	0.6899	0.8374	0.9968	2.1899	1.7284	2.0708	1.8314	1.812
caprate (10:0)	0.8028	1.0308	1.0492	1.2294	1	0.7668	1.0717	1.1663	1.3242	0.8012
carnitine	0.7904	1.1715	0.7562	1.4388	1.8175	0.9066	0.7591	1.5413	1.6755	0.8848
cholesterol	1.1232	1.2821	1.1351	0.9906	1.0523	0.8374	1.0136	1.0958	1.1428	1
choline	1.3008	0.97	1.2153	0.8315	0.6502	1.0101	1.1553	0.7031	0.6722	1
choline phosphate	0.6537	1.1571	0.5884	1.0241	1.3785	1.3151	1	1.6397	1.72	1.4409
cis-vaccenate (18:1n7)	1.2446	1.2539	1.2033	0.9604	1.1141	0.964	1.0148	1.1989	0.994	0.9014
citrate	1.0998	1.3113	1.0603	1.1772	1.3591	1.0663	0.939	1.1104	0.5983	0.7671
coenzyme A	0.7118	0.9324	0.7812	1.0219	1.234	1.1961	1	1.0259	0.5997	1.1534
creatine	0.8164	0.9233	0.8287	1.1087	1.1308	1	0.8479	1.1472	1.2182	1.0281

cystathionine	1.0528	1.2808	1.069	0.9009	1.0047	0.8675	0.8947	0.9476	1.0146	0.9204
cysteine	1.8758	1.9103	1.6013	1.3901	1.1723	0.2808	0.3528	0.322	0.3534	0.4073
cysteine-glutathione disulfide	1.4928	1.5132	1.4876	1.6042	1.375	0.2232	0.1765	0.1789	0.1645	0.2207
cysteinylglycine	0.6606	1.0685	0.8827	0.6801	0.961	1.131	1.7793	2.0159	2.0292	1.6059
cystine	2.7587	1.8276	2.0641	1.1492	0.7991	0.2937	0.2937	0.2937	0.2937	0.2937
cytidine	0.6423	0.6423	1.096	1	0.6468	0.8103	0.7738	0.7486	0.6423	0.8644
cytidine 5'-diphosphocholine	1.035	1.059	0.8896	1.3689	1.3135	0.492	0.5851	1	1.964	0.7453
cytidine 5'-monophosphate (5'-CMP)	0.975	1.1581	1.1985	0.8592	1	1.4426	1.2981	1.1419	0.8967	1.4305
deoxycarnitine	1.0065	0.9935	0.7131	1.3011	1.272	1.1577	1.0874	1.0318	0.9015	0.9582
dihomo-linoleate (20:2n6)	1.1868	1.319	1.0837	1.6696	1.8433	0.8256	0.7375	0.91	0.6303	0.8629
dihomo-linolenate (20:3n3 or n6)	1.161	1	0.86	1.0542	1.0505	0.8381	0.8169	0.5744	1.201	0.7078
dihydrocholesterol	1.2496	0.7223	1.2851	0.8527	0.8778	0.9021	0.7223	1.3818	0.7223	1.16
dimethylarginine (SDMA + ADMA)	1.0918	1.0133	1.3911	0.8003	0.5961	0.9937	1.3423	0.6585	1.2401	1.4178
docosadienoate (22:2n6)	1.1143	1.125	1.1371	0.9891	0.9576	1.0983	0.9898	1.0779	1.3787	1.175
docosahexaenoate (DHA; 22:6n3)	1.1014	0.9826	0.969	1.0699	1.2241	0.9371	0.8169	1	1.4845	0.9915
docosapentaenoate (n3 DPA; 22:5n3)	1.0373	1.0541	0.7444	1.2574	1	0.8277	0.508	0.7081	1.1867	0.9087
docosapentaenoate (n6 DPA; 22:5n6)	0.8609	1.0262	0.7503	1.4058	1.1506	0.9451	0.5452	0.7057	1.7286	1
docosatrienoate (22:3n3)	1.0253	1.1092	1.0655	0.765	1.027	0.5111	0.599	1.0234	1.3753	0.6198
eicosenoate (20:1n9 or 11)	1.348	1.3047	1.1084	1.0346	1.0243	0.8603	0.8945	1	1.3125	0.9727
erythritol	0.9461	1.2557	1.0475	0.9423	0.6913	0.8572	1.1188	1.2763	0.9085	1.2673
erythronate*	0.8473	0.5241	0.763	0.5955	0.6077	0.9776	1.4096	1.0645	1.153	1
ethanolamine	1.8188	1.5362	2.0907	1.2431	0.8708	0.8386	0.8332	1.134	0.9878	1.2041
flavin adenine dinucleotide (FAD)	1.0997	1.2509	1.1872	1.0801	1.0958	0.8915	1.0549	0.9768	0.9853	0.9535
fructose	1.4989	0.9013	1.8161	1	0.4441	0.5064	0.3122	0.3887	1.1629	0.9767
fructose-6-phosphate	2.5234	2.0047	1.3893	1.2627	0.7089	0.3786	0.3523	0.2304	0.8211	0.3559
fumarate	1.1119	1.2342	1.1794	0.9187	0.9416	1	1.1946	1.2258	1.2286	0.9196
gamma-aminobutyrate (GABA)	0.8635	1.0512	0.7314	1.0086	1	1.7466	1.3693	1.3884	1.3636	1.3618
gamma-glutamylcysteine	1.314	1.0287	1	1.2284	0.7977	0.4324	0.5366	0.5129	0.3863	0.5543
gamma-glutamylglutamate	1.0349	1.065	1	1.1748	1.0024	0.6697	0.5874	0.6194	0.3788	0.6089
gamma-glutamylglutamine	1.1246	1.0162	0.9685	1.1057	1	0.4651	0.467	0.5272	0.3347	0.4241
gamma-glutamylisoleucine*	0.9772	1.0752	0.9443	0.9139	1.0591	1.0211	0.9868	1.0572	1.0985	1.0918

gamma-glutamylleucine	1.0757	1.1694	1.0879	0.9875	0.9655	0.8732	0.8486	1	0.9429	1.0337
gamma-glutamylmethionine	1.2626	1.1551	1.2742	1.5582	1.1346	0.6875	0.643	0.7884	0.5649	0.5799
gamma-glutamylphenylalanine	1.3178	1.3152	1.3361	1.2571	1.1457	0.9374	1.012	0.9257	0.9097	0.9461
gamma-glutamyltyrosine	1.3985	1.302	1.3511	1.1305	1	0.8288	0.8658	1.0136	0.9968	1.0379
gamma-glutamylvaline	0.8895	0.9133	0.7864	0.7112	0.8121	1.0839	1	1.0383	1.005	1.153
gluconate	1.108	0.832	1.0825	0.4656	0.3661	0.6977	1	1.2987	2.295	0.6781
glucose	1.2988	1	1.8041	1.1349	0.9563	0.7057	0.7808	0.4934	0.7709	0.6882
glucose 1-phosphate	1.4559	2.1329	1.4098	1.7159	1.3803	0.8614	0.7328	1	1.2821	0.9614
glucose-6-phosphate (G6P)	2.777	1.8477	2.2235	1.243	0.687	0.0965	0.35	0.2017	0.7327	0.2825
glutamate	0.8297	0.9437	0.8207	1	1.0768	0.9499	0.8722	1.0445	1.1028	0.934
glutamate, gamma-methyl ester	0.7828	0.9569	0.9598	1.0397	0.8665	1.4125	1.1684	1.1459	0.6631	1.0028
glutamine	1.1005	1.0613	0.9126	0.9523	0.8968	0.9185	0.9324	0.99	0.9482	1
glutathione, oxidized (GSSG)	0.5742	0.8738	0.6635	0.7909	1.0734	1.4484	1.4113	1.3781	1.4233	1.5075
glutathione, reduced (GSH)	0.6397	0.9465	0.7018	0.7946	1.0439	1.6443	1.634	1.6039	1.7601	1.7526
glycerate	1.2861	1	1.1569	0.8066	0.4557	0.7994	0.6356	0.5576	0.4557	0.4557
glycerol 2-phosphate	1.4663	1.7536	1.3603	1.3689	1.3103	0.7332	0.7504	0.9517	1	0.9574
glycerol 3-phosphate (G3P)	1.6631	1.9758	1.5841	1.2235	1.474	0.6652	0.8228	1.0149	1.0507	0.7765
glycerophosphorylcholine (GPC)	1.2538	1.5115	1.2482	1.6387	1.9131	0.8125	0.7298	1.0797	1.1799	0.8248
glycine	1.249	1.3915	1.2026	1.0573	1	0.6744	0.7864	0.7716	0.8589	0.8552
glycylglutamate	1.1334	0.9242	0.6527	1.0025	0.9975	0.816	1.1334	1.0207	0.7861	1.1766
glycylglycine	1.004	1.1124	1.025	1.1601	0.8161	1.1593	0.9712	0.9834	1.7811	1.3187
glycylleucine	0.8258	1	1.069	0.9241	1.0957	1.2172	1.1579	1.3407	1.3282	1.1733
glycylproline	1.0111	0.7888	0.9772	0.7888	1.2163	0.8163	1.1402	1.0097	1.662	1.2375
glycylserine	0.8366	0.8432	0.8472	0.9405	0.8912	1.3799	1.4055	1.3419	2.0962	1.1061
glycylvaline	1.5705	1	1.1006	0.8515	1.1168	1.2633	0.638	1.1971	1.1496	0.9277
guanosine	0.5588	0.4173	1.1394	0.5242	0.4355	0.8496	1.2751	0.7307	1	0.7287
guanosine 5'- monophosphate (5'-GMP)	0.7955	1.128	0.9749	1.0079	1.2791	1.1284	0.9661	1.3193	1.2799	1.2561
guanosine 5'-diphospho-fucose	1.4017	1.5157	1.463	1.287	1.4275	0.9367	1.1548	0.9544	0.915	1.069
gulono-1,4-lactone	0.9062	1.2813	1	0.7219	0.8401	0.9708	1.2009	1.4284	1.1421	1.0008
histidine	0.9806	1.016	1	0.964	0.8224	1.0041	1.0811	0.933	1.0722	1.1242
homocysteine	1.2632	1.7171	1.5622	1.236	1	0.7928	0.7668	0.7239	0.8739	0.9471

hypoxanthine	1.0734	0.8318	1.1683	0.9433	0.6688	0.7158	1.0573	0.7565	1	0.8593
inosine	1.1293	0.7586	1.1701	0.9673	0.6013	0.6433	1	0.6837	1.1257	0.8136
inositol 1-phosphate (I1P)	1.2682	1.5468	0.8405	1.0299	1.1874	1	0.9181	1.2993	1.3878	1.2141
Isobar: UDP-acetylglucosamine, UDP-acetylgalactosamine	0.8708	0.9007	1	1.1632	1.1315	0.7138	0.6977	0.9798	1.0665	0.7497
isobutyrylcarnitine	0.7914	1.3527	1.0133	0.7981	1	0.7528	0.7273	1.1953	0.904	0.7273
isoleucine	1.2369	1.1196	0.9781	0.9503	0.9606	1.0299	1.0402	1.0259	1.1002	1.1138
isoleucylglycine	1.0677	1.542	1.3815	1	1.2568	1.3746	1.0114	1.4912	0.9229	0.8525
isovalerylcarnitine	1.2169	1.3008	1.0267	1.4049	1.5069	0.8456	1.0008	0.7552	0.7491	0.4029
kynurenine	1.2993	1.079	0.9118	1.6365	1	0.8123	0.6785	0.8368	1.1013	1.2624
lactate	1.3843	1.3919	1.1861	1.0469	1	0.795	0.9067	0.9573	1.2118	1.1219
lactose	1.3237	1.2197	1.0508	0.9499	0.8494	0.9716	1.1189	1.6552	1.4828	1.1102
lanthionine	0.8366	1	0.8187	0.8317	0.8636	0.8164	1.0535	1.0142	1.2458	1.0379
lathosterol	0.928	1.0498	1.0744	0.8213	1.2504	1.2631	1.2454	1.2557	0.9222	1.5684
laurate (12:0)	1.0048	1.0067	0.947	1.0064	1.0494	1.0574	0.8261	1	1.0884	1.1079
leucine	1.0576	1.1022	1	0.9605	0.9096	1.0355	1.023	0.938	1.0963	1.1658
lysine	1.0803	1.0474	1	1.0591	0.8862	1.2304	1.0441	0.9448	1.252	1.1668
malate	1.3115	1.3666	1.1728	1	1.1142	0.9503	0.9286	1.1347	1.0137	1.0213
mead acid (20:3n9)	1.1299	1.0896	0.9244	1.5365	1.8819	0.5869	0.5145	0.6329	1	0.4706
methionine	1.0377	1.0744	1.0081	0.9696	0.8769	1	1.0491	0.9054	1.0952	1.1181
methylphosphate	0.8611	1	1.2741	0.9596	0.9324	1.1491	0.8305	1.1746	0.7941	0.9698
myo-inositol	0.8231	0.9277	0.7099	0.6735	0.6275	1.2418	1.4526	1.5913	1.676	1.5142
myristate (14:0)	1.0673	1.0171	1.0067	0.973	1	1.064	0.9639	1.0182	1.1056	1.1029
myristoleate (14:1n5)	1.2776	1.0683	1.0362	0.8468	0.8443	1.183	1.2113	1.2368	0.9702	1.2428
N-acetyl-aspartyl-glutamate (NAAG)	0.686	0.746	0.6984	0.7548	0.7886	1.1861	1.1413	1.2467	1.3415	1.2341
N-acetylalanine	1	0.9918	1.1087	0.9489	1.0195	0.9506	1.1108	1.001	1.3005	1.2392
N-acetylaspartate (NAA)	0.9976	1.1124	0.9896	1.0087	1	1.4177	1.3564	1.3568	1.4936	1.5248
N-acetylglutamate	0.5846	0.8247	0.5437	0.9375	0.8612	1.2256	1.0841	1.2873	1.0435	1.1537
N-acetylmethionine	0.9509	0.9892	1.0798	1	0.8498	0.9385	1.0816	1.0162	1.363	1.1352
N-acetylneuraminate	1.2754	1.397	1.2107	1.1429	1.1103	0.7364	1	0.8353	1.0155	0.7842
N-acetylserine	0.9282	1.0883	0.9593	0.7182	0.8768	0.9512	1.1245	1.2346	1.3803	1.1622
N-acetylthreonine	0.942	0.7102	1	1.0067	0.8043	0.8867	1.1509	0.9712	1.2119	0.992

n-Butyl Oleate	1.4597	1.1731	1.1033	0.8967	0.7012	0.8442	0.2653	0.2653	1.1871	1.6318
N-formylmethionine	1.1495	1.2808	1.1939	1.2421	1.181	0.8878	0.9574	0.9596	0.9917	0.9847
N1-methyladenosine	1.2725	0.6113	1.403	0.7593	0.4103	0.4572	1	0.5598	1.4914	1.0114
N1-methylguanosine	1.0533	0.8593	1.2572	0.7528	0.5085	0.5085	1.1058	0.5394	1.4872	1
N2-methylguanosine	1.1328	0.5291	1.3547	0.5587	0.4407	0.4407	0.9944	0.4407	2.3094	1.0056
N6-carbamoylthreonyladenosine	1.2749	0.8532	2.2508	0.7818	0.6747	0.6399	0.7642	0.6399	1.5205	0.8619
nicotinamide	1.4403	1.3788	1.6266	0.9821	1	0.6712	0.9874	0.7455	2.194	1.2548
nicotinamide adenine dinucleotide (NAD+)	0.5177	0.7158	0.557	1.5181	1.5391	0.8512	0.7896	1.5855	0.5065	0.6455
nicotinamide adenine dinucleotide phosphate (NADP+)	0.7905	1.0577	0.807	1.2446	1.5433	0.641	0.7648	1.3656	1	1.3299
nicotinamide adenine dinucleotide reduced (NADH)	0.6666	1.1043	0.5729	1.1844	1.2548	1.5541	0.8227	0.9969	0.9157	1.1446
nonadecanoate (19:0)	1.2622	1.0494	1.462	1.2899	0.9514	0.9419	0.9447	1	1.1966	0.817
oleate (18:1n9)	1.0226	1.2407	1.0684	1.0257	1	0.9013	0.9966	1.2363	0.87	0.9331
oleoylcarnitine	1	1.8065	0.9668	1.3299	1.4242	1.331	0.8516	1.4502	0.6504	1.013
ornithine	1.0775	1.2626	0.9499	1.0823	1	1.1861	0.8882	1.1278	0.9018	1.2465
palmitate (16:0)	1.1852	1.1076	1.0601	1	1.0604	0.9798	0.9932	0.993	1.1958	0.932
palmitoleate (16:1n7)	1.13	1.2824	1.0421	0.9323	0.989	1.0494	0.7937	1.006	1	0.9245
palmitoyl sphingomyelin	1.1323	1.331	1.0957	1	1.1024	0.8565	0.9593	1.1143	1.0989	1.0497
palmitoylcarnitine	0.9983	1.1919	0.8732	1.2617	1.2423	1.2739	1.102	1.1971	0.6106	0.9496
pantothenate	1.2154	1.2963	1.1362	1.1169	1.1801	0.9507	0.9581	1	1.0091	1.0302
penicillin G	1.4353	1.0466	1.1363	0.8739	0.8417	0.9443	0.8251	1.0455	1.0559	0.8839
pentadecanoate (15:0)	1.0549	1.0772	1.0834	0.9842	1	0.9874	1.0431	0.9822	1.2518	0.9639
phenol red	1.1503	1	1.0059	0.8811	0.7973	1.0001	1.1387	1.1769	1.2669	1.029
phenol sulfate	1.0439	1.0234	1.039	1	1.0175	0.9466	0.872	0.9575	0.9175	0.8377
phenylacetylglycine	1.2207	1	0.8753	0.9616	1.0241	0.8948	1.0644	1.0779	1.0693	1.0639
phenylalanine	1.1074	1	0.9505	0.8612	0.8347	1.0421	1.0834	1.0446	1.1419	1.2486
phenylalanylglutamate	0.8717	1.5363	1	1.0145	1.4285	1.4819	1.1835	1.4865	0.4803	1.0043
phenylalanylserine	1	1.3049	1.0924	1.2217	1.3249	0.9874	0.9513	1.2389	1.5004	1.0219
phosphate	1.0652	1.059	1.1256	0.9559	0.93	0.9217	1.0326	1.0188	0.9915	0.9979
phosphoethanolamine	0.6899	1.3733	1.5076	0.6756	1	0.6756	0.6756	0.6756	1.1169	1.0653
proline	1	1.0428	0.9944	0.974	0.9828	1.0981	1.0695	1.0816	1.1424	1.1818
propionylcarnitine	1.4087	1.7506	1.3844	1.3734	1.304	0.8907	1.0858	0.833	1	1.0152

pseudouridine	1.2434	0.9553	1.2587	1	0.7662	0.8547	1.2577	0.9892	1.8299	1.3828
putrescine	1.0086	1.1416	0.9853	1.2183	1.0699	1.6144	0.9799	1	1.1013	1.2596
pyridoxal	1.0367	0.8472	1.0409	0.9187	0.8399	1.2412	0.8286	1.0494	1.1983	1.3878
pyridoxine (Vitamin B6)	1.1185	1	0.8254	0.9936	0.9397	1.9315	1.6538	2.01	0.7709	1.3168
pyroglutamine*	0.6882	0.7836	0.6632	0.9469	1.0489	1.009	0.8482	1.0986	1.1414	1
pyroglutamylvaline	0.7277	0.8073	0.739	0.4375	0.8782	1.641	1.6826	1.4808	1.6859	1.6155
pyrophosphate (PPi)	0.9061	1.3332	0.6771	1.1719	1.4828	1.5605	1	1.6049	0.9268	1.25
ribitol	1.1094	0.7234	1.0209	0.6796	0.5232	0.727	0.8865	0.9233	1.0172	1
ribose	1.8834	0.6425	2.1241	0.9082	0.3726	0.5656	1.1648	0.6492	0.8985	0.5472
ribulose	0.9661	0.7791	0.7089	0.6203	0.5443	0.7437	1.0347	0.8768	1.8061	0.5443
S-adenosylhomocysteine (SAH)	1.0232	1.0485	1.2043	0.8981	0.8324	0.8779	1	0.9419	1.2459	1.0789
S-methylcysteine	2.1558	2.6408	2.2832	0.6924	1.364	0.2461	0.2461	0.5992	0.7402	0.735
sedoheptulose-7-phosphate	2.006	1.4774	1.7926	1.1863	0.4913	0.4184	0.7205	0.5133	0.982	0.4968
serine	1.2309	1.1912	1.0536	0.9268	0.828	0.8192	1	0.9612	1.276	1.1304
serylphenyalanine	0.804	0.7892	0.7517	1.2071	1.0172	1.6438	1.3081	1.6229	1.5076	1.2664
sorbitol	1.4037	1.9043	1.1157	1.386	0.7391	1	0.8794	1.2305	1.3324	0.8415
spermidine	1.2554	1.3238	1.1239	1.0723	1.1398	1.0434	0.9632	0.8534	0.9147	1.0066
sphinganine	1.0462	1.4254	0.971	1	1.2976	1.1013	0.8346	1.4457	2.726	1.5763
sphingosine	1.0297	1.7033	0.998	1.2464	1.6753	1	0.9171	1.1492	1.4071	1.1956
stearoyl sphingomyelin	1.3701	1.0287	1.4861	1.3608	1.5946	0.8438	1	0.8608	0.772	0.7964
succinate	1.0491	1	1.2406	0.8659	0.8723	1.0113	1.0433	1.1168	0.7135	1.045
thiamin (Vitamin B1)	0.7436	0.8428	0.5576	1.572	1.7079	0.7384	0.6724	1.5643	1.6412	0.8646
threonine	1.1137	1.0374	0.979	0.9622	0.9775	1.034	1	0.9646	1.1556	1.0823
threonylleucine	0.9258	1.1913	0.9279	1	1.0254	1.3527	1.2261	1.5327	1.3082	1.1549
thymidine	1	0.594	1.2142	0.7396	0.465	0.6596	1.2012	0.4168	0.678	0.5353
thymidine 5'-monophosphate	0.8702	0.8449	1.0118	0.8521	0.7396	1	1.2358	1.1798	1.2336	1.1643
thymine	2.2949	1	2.1977	0.9412	0.8594	0.2082	0.9054	0.6406	1.2804	0.7187
tryptophan	1.0275	1.0608	1	0.919	0.8998	1.0072	1.0382	1.0185	1.1556	1.1194
tyrosine	1.0409	1.0107	1	0.901	0.8457	1.069	1.0834	1.0349	1.2232	1.2121
UDP-galactose	0.9438	1.2917	1.1574	1.1602	1.0281	0.8141	0.981	1	1.079	1.4482
UDP-glucuronate	1.0699	1.2653	1.158	1.1484	1.1644	1.0471	0.9445	0.8972	0.8813	1

uracil	1.6544	1.0169	2.0108	1.0905	0.5098	0.3396	1	0.4205	0.4498	0.5447
urea	1.1255	1.2487	1.3448	0.8664	1	0.7708	1.1126	1.0798	1.2175	0.9172
uridine	1.1887	0.891	1.277	1	0.7584	0.7129	0.9027	0.6049	0.8107	0.7316
uridine 5'-diphosphate (UDP)	1	1.342	0.8798	1.1706	1.2095	1.0462	0.9569	1.1824	1.1572	1.3328
uridine 5'-triphosphate (UTP)	0.7867	1.1141	0.5178	1.4102	1.5943	1	0.6915	1.1192	0.8527	1.0118
uridine monophosphate (5' or 3')	0.9795	1.1192	1.0638	0.9661	0.6536	1.145	1.1035	1.3772	1.6155	1.4023
valine	1.0761	1.0777	1.0001	0.943	0.9013	1.0292	1.0526	0.9931	1.0754	1.08
xanthine	1.3112	0.9336	1.2243	1	0.6721	0.5851	1.0513	0.7871	0.9056	0.9959
xanthosine	1.3196	0.9559	1.6724	1.256	0.5026	0.9956	0.5026	0.7351	0.9535	1.0044
xylonate	0.2591	0.7366	0.6746	0.2591	0.2591	1.3916	1.1081	1.3799	1.5995	0.7135

Supplementary Table 2: Stable isotope analysis. Source data that is summarized in Figure 16d and some results plotted in Figure 16c.

Resonances	shCont						shEXD2#1					
	[U-^{13}C]-Glc			[U-^{13}C]-Gln			[U-^{13}C]-Glc			[U-^{13}C]-Gln		
	Tech 1	Tech 2	Tech 3	Tech 1	Tech 2	Tech3	Tech 1	Tech 2	Tech 3	Tech 1	Tech 2	Tech 3
Cytidine [C1'-riboside]	0.66	0.75	0.74									
Aspartate [β(CH2) downfield]	0.59	0.45	0.50	0.78	0.85	0.83				0.85	0.78	0.86
Aspartate [β(CH2) upfield]	0.56	0.40	0.46	0.69	0.79	0.71				0.82	0.74	0.84
Glutamate [γ(CH2)]	0.30	0.37	0.51	0.42	0.55	0.50				0.53	0.41	0.66
Glutamate [α(CH)]				0.59	0.68	0.62				0.56	0.53	0.72
Glutathione [β(CH2)-Glu]				0.50	0.63	0.57				0.55	0.42	0.65
Glutathione [α(CH)-Glu,Cys]				0.22	0.40	0.28						
Glutathione [γ (CH2)-Glu]	0.54	0.39	0.46									
Glutathione [α(CH)-Cys]	0.89	0.87	0.67									
Glutathione ox [β(CH2)-Cys]	0.95	0.96	0.71									
Glycine [α(CH2)]	0.36	0.15	0.44									
Guanidinoacetate [α(CH2)]	0.84	0.68	0.89									
Adenosine [H8-adenine]	0.58	0.38	0.72									
ADP [H8-adenine]	0.60	0.79	0.75									
AXP [C1'-riboside]	0.55	0.47	0.67									
dCMP [C6-H cytosine]	0.73	0.56	0.76									
Uridine [C6-H uracil]				0.52	0.58	0.37						
Uridine [C5-H uracil]				0.42	0.48	0.25						
Uridine [C1'-riboside]	0.68	0.40	0.68									
UDPGs [C6-H uracil]	0.60	0.46	0.62	0.42	0.57	0.40				0.51	0.39	0.54
UDPGs [C1'-riboside]	0.64	0.58	0.73									
UDP-Glucuronate [C1"-H]	0.99	0.85	0.98				0.89	0.22	0.84			
UDP-Glucose [C1"-H]	0.95	0.82	0.95				0.86	0.69	0.96			
UDP-GlcNac [C1"-H]	0.91	0.81	0.96				0.71	0.28	0.89			
UDP-GalNac [C1"-H]	1.00	0.82	1.00									
Fumarate [2x(CH)]	0.70	0.58	0.71	1.00	1.00	0.99				1.00	1.00	1.00
Succinate [2x(CH2)]				0.71	0.90	0.77				0.88	0.85	0.91
Acetates [(CH3-)]	0.60	0.46	0.55									
Glycerol [C1,C3 (CH2a)]	0.79	0.70	0.74									
Glycerol [C1,C3 (CH2b)]	0.53	0.37	0.55									
o-phosphocholine (CH3)3-N-	0.74	0.46	0.41									
o-phosphocholine -CH2-O-P	0.58	0.35	0.40									

Supplementary Table 3: BioID data. Results of BioID analysis and notes regarding the localization and function of individual hits. Data is plotted schematically in Figure 19c.

			*EXD2-WT-BirA*FLAG*				*EXD2-C2-BirA*FLAG*				
Gene Name	**Top-2-CTL**		**Tech 1**	**Tech 2**	**Total**	**SAINT**	**Tech 1**	**Tech 2**	**Total**	**SAINT**	**Notes: summarized from Uninprot (uniprot.org) and Biogrid (the biogrid.org) unless indicated otherwise**
EXD2	2	2	3998	4333	8331		5137	4178	9315		*BirA* fused protein*
ZC3HAV1	56	49	296	311	607	1.00	138	144	282	0.99	Cytoplasmic, Nuclear, RBP, RNA decay, retroviral restriction, interaction with MRPS9, MRPS31, MRPL35, implicated in OXPHOS; PMID:27667664
MAVS	10	8	133	157	290	1.00	70	72	142	1.00	Mitochondrial outer membrane, RNA antiviral signaling
AKAP1	15	15	143	116	259	1.00	38	53	91		Mitochondrial outer membrane, cristae, matrix, RNA binding, PKA signaling
SHMT2	27	25	119	121	240	1.00	91	95	186	1.00	Mitochondrial serine and glycine catabolism, redox balance PMID:25186498
HSPE1			91	92	183	1.00	42	41	83	1.00	Mitochondrial matrix
NDUFS1	6	5	89	66	155	1.00	45	45	90	1.00	Complex I core subunit, mutated in mitochondrial Complex I deficiency (OMIM)
NDUFS3	6	6	72	73	145	1.00	39	55	94	1.00	Complex I core subunit, mutated in mitochondrial Complex I deficiency (OMIM)
NDUFA9	12	6	62	45	107	1.00	28	45	73	0.78	Complex I accessory subunit, mutated in Leigh Syndrome (OMIM)
CLPX	5	3	55	49	104	1.00	19	32	51	0.95	Mitochondrial matrix, chaperone functions, regulates TFAM, heme biosynthesis and translation
NDUFS2	7	5	56	42	98	1.00	24	34	58	1.00	Complex I core subunit, mutated in mitochondrial Complex I deficiency
POLDIP2			46	29	75	1.00	3	3	6		Mitochondrial nucleoid, nucleus, polymerase, alternative splicing and NADPH oxidase functions
DNAI2			35	34	69	1.00		18	18		Associates with multiple chaperonin complexes
NDUFV2			34	34	68	1.00	13	23	36	1.00	Complex I core subunit, flavoprotein complex with NDUFV1 and NDUFV2, mutated in mitochondrial Complex I deficiency (OMIM)
NDUFV3			33	34	67	1.00	12	19	31	1.00	Complex I core subunit, flavoprotein complex with NDUFV1 and NDUFV2
CRYBG3	4	3	29	35	64	1.00	34	32	66	1.00	Cytoplasm, nucleus, PKA regulation
PYCR2			36	25	61	1.00	34	30	64	1.00	Mitochondrial, Proline biosynthesis, NAD^+ or NADP used as a substrate, mutated in hypomyelinating leukodystrophy 10 (OMIM)
DAP3	5	4	35	24	59	1.00	7	6	13		Mitoribosome (MRPS29), regulates transcription/translation, RNA binding
MRPS9	5	4	34	23	57	1.00	7	13	20		Mitochondrial small ribosomal subunit (28S), interaction with ZC3CHAV1
MRPS24	1		24	25	49	1.00					Mitochondrial small ribosomal subunit (28S)
PYCR1			23	24	47	1.00	26	19	45	1.00	Mitochondrial, Proline biosynthesis, NAD^+ or NADP used as substrate, mutated in Cutis Laxa Type IIB and IIIB (OMIM)
NDUFV1	3		23	24	47	1.00	18	13	31	0.98	Complex I core subunit, flavoprotein complex with NDUFV1 and NDUFV2, mutated in mitochondrial Complex I deficiency (OMIM)
LETM1			28	17	45	1.00	14	15	29	1.00	Mitochondrial inner membrane, matrix, required for normal mitochondrial morphology, deleted in Wolf-Hirschhorn Syndrome (OMIM)
MRPS23	4	3	22	19	41	1.00	3		3		Mitochondrial small ribosomal subunit (28S)
MRPS26			22	17	39	1.00	7	15	22	1.00	Mitochondrial small ribosomal subunit (28S)

NDUFA5	5	3	22	17	39	1.00	10	11	21		Complex I subunit, required for assembly and/or stability of Complex I (OMIM)
ZDHHC17			21	17	38	1.00	33	29	62	1.00	Golgi, palmitoyltransferase activity
NDUFA2			20	16	36	1.00	4	4	8	1.00	Complex I accessory subunit, mutated in Leigh Syndrome (OMIM)
NDUFS8	1		17	18	35	1.00	4	12	16	1.00	Complex I core subunit, iron-sulfur protein, mutated in Leigh Syndrome (OMIM)
MARC2			14	19	33	1.00	9	15	24	1.00	Mitochondrial, oxidized base detoxification PMID:22924387
TACO1			14	18	32	1.00	13	15	28	1.00	Mitochondrial, translational activator, mutated in Leigh Syndrome (OMIM)
ATPAF1			18	9	27	1.00	5	11	16	1.00	Complex IV assembly
NDUFA12	3	2	16	11	27	1.00	4	8	12	1.00	Complex I accessory subunit, mutated in Leigh Syndrome (OMIM)
GRSF1	2		12	13	25	1.00	7	14	21	1.00	Mitochondrial RNA granule component, RNA processing
MRPS22			17	8	25	1.00	9		9		Mitochondrial small ribosomal subunit (28S), mutated in mitochondrial oxidative phosphorylation deficiency 5 (OMIM)
DBT	2		15	9	24	1.00	7	8	15	1.00	Mitochondrial nucleoid component, branched chain amino acid catabolism, mutated in Maple Syrup Urine Disease (OMIM)
NME4			12	11	23	1.00	18	11	29	1.00	Mitochondrial, interacts with OPA1, bioenergetics and lipid signaling PMID:23150663
MRPL19			9	12	21	1.00	3	5	8	0.99	Mitochondrial large ribosomal subunit (39S)
KDELR1	10	6	13	6	19	1.00	13	12	25	1.00	ER, ER-Golgi protein transport
ACAD9			9	10	19	1.00	5	12	17	1.00	Complex I assembly, fatty acid oxidation, mutated in mitochondrial Complex I deficiency (OMIM)
MMAB			10	8	18	1.00	4		4		Mitochondrial, vitamin B12 metabolism, mutated in Isolated methylmalonic aciduria patients (OMIM)
MDH2			5	10	15	1.00	8	9	17	1.00	Mitochondrial, TCA cycle, malate to oxaloacetate, NAD^+ used as a cofactor to generate NADH
MRPS34	1		9	6	15	1.00	3	3	6		Mitochondrial small ribosomal subunit (28S)
MRPS28			9	6	15	1.00		1	1		Mitochondrial small ribosomal subunit (28S)
CEP350			7	5	12	1.00		7	7		Centrosomal, microtubule anchoring
MRPS18B	2	2	4	5	9	1.00		3	3		Mitochondrial small ribosomal subunit (28S)
MFF			4	4	8	1.00					Mitochondrial, peroxisome and mitochondrial fusion/fission, mutations implicated in mitochondrial encephalopathy (OMIM)
PTCD3	6	5	21	19	40	0.99	6	9	15		Mitochondrial small ribosomal subunit (28S) (MRPS29), RNA binding, required for mitochondrial translation and respiration
GLS			10	3	13	0.99	11	15	26	1.00	Mitochondrial, initiates catabolism of glutamine, targeted by BPTES
SLC30A9			7	3	10	0.99	2		2		Zinc transporter
PPA2	2		6	3	9	0.99	6	3	9		Mitochondrial, yeast homologue implicated in mtDNA maintenance PMID:16300924
NDUFS7	6	6	28	24	52	0.98	9	14	23		Complex I core subunit, mutated in Leigh Syndrome (OMIM)
CALR	1		3	3	6	0.96	1		1		ER resident protein, Ca^{2+} storage
MRPS31	10	6	32	24	56	0.95	6	9	15		Mitochondrial small ribosomal subunit (28S), interaction with Z3CHAV1, DAP3
OCIAD1	3	2	16	12	28	0.94	2	6	8		Mitochondrial
ATR			2	4	6	0.77					Nuclear, mitochondrial outer membrane, replication stress signaling, apoptosis, mutated in Seckel Syndrome (OMIM)

MRPS5	6	4	12	11	23	0.70	8	11	19		Mitochondrial small ribosomal subunit (28S)
MRPS35	5	5	13	12	25						Mitochondrial small ribosomal subunit (28S)
RUVBL2	169	165	311	358	669		756	651	1407	1.00	Nucleus, cytoplasm, Golgi, chaperone like activity, ATPase and ssDNA binding
RUVBL1	178	174	301	330	631		688	663	1351	1.00	Nucleus, cytoplasm, Golgi, chaperone like activity, ATPase and ssDNA binding
UBB	13	7	20	15	35		59	49	108	0.95	Ubiquitous, covalent protein modifier
NDUFS4			10	8	18		6	5	11	1.00	Complex I accessory subunit, mutated in mitochondrial Complex I deficiency (OMIM)
BCS1L			8	9	17		12	8	20	1.00	Mitochondrial Complex III assembly, mutated in mitochondrial Complex III deficiency, GRACILE, Bjornstadt and Leigh Syndromes (OMIM)
NOLC1	9	8	5	3	8		34	41	75	1.00	Nucleus, nucleoli
TUBA1A	25	22					91	72	163	1.00	Nucleus, cytoplasm, microtubules
TRIP6	7	6					37	33	70	1.00	Nucleus, cytoplasm
DHCR7	2						6	3	9	0.99	ER, nuclear outer membrane
NDUFAF3							3	3	6	0.98	Complex I accessory subunit, mutated in mitochondrial Complex I deficiency (OMIM)

REFERENCES

Acín-Pérez R, Fernández-Silva P, Peleato ML, Pérez-Martos A, Enríquez JA (2008) Respiratory active mitochondrial supercomplexes. *Mol Cell*. 32(4): 529-39

Allen JF (1993) Control of gene expression by redox potential and requirement for chloroplast and mitochondrial genomes. *J Theor Biol*. 165(4): 609-31

Almuhaideb A, Papathanasiou N and Bomanji J (2011) 18F-FDG PET/CT imaging in oncology. *Ann Saudi Med*. 31(3): 3-13

Anand SK and Tikoo SK (2013) Viruses as modulators of mitochondrial functions. *Adv Virol*. 2013: 738794

Anderson S, Bankier AT, Barrell BG, de Brujin MH, Coulson AR, Drouin J, Eperon IC, Nierlich DP, Roe BA, Sanger F, Schreier PH, Smith AJ, Staden R and Young IG (1981) Sequence and organization of the human mitochondrial genome. *Nature*. 890(5806): 457-65

Andersson SG, Zomorodipour A, Andersson JO, Sicheritz-Pontén T, Alsmark UC, Podowski RM, Näslund AK, Eriksson AS, Winkler HH and Kurland CG (1998) The genome sequence of Rickettsia prowazekii and the origin of mitochondria. *Nature*. 396(6707): 133-40

Andreyev AY, Kushnareva YE and Starkov AA (2005) Mitochondrial metabolism of reactive oxygen species. *Biochemistry (Mosc)*. 70(2): 200-14

Andziak B, O'Connor TP, Qi W, DeWaal EM, Pierce A, Chaudhuri AR, Van Remmen H and Buffenstein R (2006) High oxidative damage levels in the longest-living rodent, the naked mole-rat. *Aging Cell*. 5(6): 463-71

Antonicka H, Ogilvie I, Taivassalo T, Anitori RP, Haller RG, Vissing J, Kennaway NG and Shoubridge EA (2003) Identification and characterization of a common set of complex I assembly intermediates in mitochondria from patients with complex I deficiency. *J Biol Chem*. 278(44): 43081-8

Antonicka H, Sasarman F, Nishimura T, Paupe V and Shoubridge EA (2013) The mitochondrial RNA-binding protein GRSF1 localizes to RNA granules and is required for posttranscriptional mitochondrial gene expression. *Cell Metab*. 17(3): 386-98

Antonicka H and Shoubridge EA (2015) Mitochondrial RNA Granules Are Centers for Posttranscriptional RNA Processing and Ribosome Biogenesis. *Cell Rep*. S2211-1247(15)00055-8

Arroyo JD, Jourdain AA, Calvo SE, Ballaranco CA, Doench JG, Root DE and Mootha VK (2016) A Genome-wide CRISPR Death Screen Identifies Genes Essential for Oxidative Phosphorylation. *Cell Metab*. S1550-4131(16)30433-8

Bahadorani S and Hiliker AJ (2008) Cocoa confers life span extension in Drosophila melanogaster. *Nutr Res*. 28(6): 377-82

Banci L, Bertini I, Cefaro C, Ciofi-Baffoni S, Gallo A, Martinelli M, Sideris DP, Katrakili N and Tokatlidis K (2009) MIA40 is an oxidoreductase that catalyzes oxidative protein folding in mitochondria. *Nat Struct Mol Biol*. 16(2): 198-206

Barrow JJ, Balsa E, Verdeguer F, Tavares CD, Soustek MS, Hollingsworth LR 4th, Jedrychowski M, Vogel R, Paulo JA, Smeitink J, Gygi SP, Doench J, Root DE and Puigserver P (2016) Bromodomain Inhibitors Correct Bioenergetic Deficiency Caused by Mitochondrial Disease Complex I Mutations. *Mol Cell*. 64(1): 163-175

Birsoy K, Possemato R, Lorbeer FK, Bayraktar EC, Thiru P, Yucel B, Wang T, Chen WW, Clish CB and Sabatini DM (2014) Metabolic determinants of cancer cell sensitivity to glucose limitation and biguanides. *Nature*. 508(7494): 108-12

Blobel G and Dobberstein B (1975a) Transfer of proteins across membranes. I. Presence of proteolytically processed and unprocessed nascent immunoglobulin light chains on membrane-bound ribosomes of murine myeloma. *J Cell Biol*. 67(3): 835-51

Blobel G and Dobberstein B (1975b) Transfer of proteins across membranes. II. Reconstitution of functional rough microsomes from heterologous components. *J Cell Biol*. 67(3): 852-62

Bobrowicz AJ, Lightowlers RN and Chrzanowska-Lightowlers ZM (2008) Polyadenylation and degradation of mRNA in mammalian mitochondria: a missing link?. *Biochem Soc Trans*. 36(Pt 3): 517-9

Borowski LS, Dziembowski A, Hejnowicz MS, Steppien PP and Szczesny RJ (2013) Human mitochondrial RNA decay mediated by PNPase-hSuv3 complex takes place in distinct foci. *Nucleic Acids Res*. 41(2): 1223-40

Brandt U (2006) Energy converting NADH:quinone oxidoreductase (complex I). *Annu Rev Biochem*. 75: 69-92

Bratic I and Trifunovic A (2010) Mitochondrial energy metabolism and ageing. *Biochim Biophys Acta*. 1797(6-7): 961-7

Breuer ME, Koopman WJ, Koene S, Nooteboom M, Rodenburg RJ, Willems PH and Smeitink JA (2013) The role of mitochondrial OXPHOS dysfunction in the development of neurological diseases. *Neurobiol Dis*. 51: 27-34

Broderick R, Nieminuszczy J, Baddock HT, Deshpande RA, Gileadi O, Paull TT, McHugh PJ and Niedzwiedz W (2016) EXD2 promotes homologous recombination by facilitating DNA end resection. *Nat Cell Biol*. 18(3): 271-80

Brown TA, Tkachuk AN, Shtengel G, Kopek BG, Bogenhagen DF, Hess HF and Clayton DA (2011) Superresolution fluorescence imaging of mitochondrial nucleoids reveals their spatial range, limits, and membrane interaction. *Mol Cell Biol*. 31(24): 4994-5010

Cahova M, Palenickova E, Dankova H, Sticova E, Burian M, Drahota Z, Cervinkova Z, Kucera O, Gladkova C, Stopka P, Krizova J, Papackova Z, Oliyarnyk O and Kazdova L (2015) Metformin prevents ischemia reperfusion-induced oxidative stress in the fatty liver by attenuation of reactive oxygen species formation. *Am J Physiol Gastrointest Liver Physiol*. 309(2): G100-11

Cairns RA, Harris IS and Mak TW (2011) regulation of cancer cell metabolism. *Nat Rev Cancer*. 11(2): 85-95

Caldwell PE, Walkiewicz M and Stern M (2005) Ras activity in the Drosophila prothoracic gland regulates body size and developmental rate via ecdysone release. *Curr Biol*. 15(20): 1785-95

Cámara Y, Asin-Cayuela J, Park CB, Metodiev MD, Shi Y, Ruzzenente B, Kukat C, Habermann B, Wibom R, Hultenby K, Franz T, Erdjument-Bromage H, Tempst P, Hällberg BM, Gustafsson CM and Larsson NG (2011) MTERF4 regulates translation by targeting the methyltransferase NSUN4 to the mammalian mitochondrial ribosome. *Cell Metab*. 13(5): 527-39

Cao Y, Fang Y, Cai J, Li X, Xu F, Yuan N, Zhang S and Wang J (2016) ROS functions as an upstream trigger for autophagy to drive hematopoietic stem cell differentiation. *Hematology*. 21(10): 613-8

Chacinska A, Koehler CM, Milenkovic D, Lithgow T and Pfanner N (2009) Importing mitochondrial proteins: machineries and mechanisms. *Cell*. 138(4): 628-44

Chan TM and Exton JH (1976) A rapid method for the determination of glycogen content and radioactivity in small quantities of tissue or isolated hepatocytes. *Anal Biochem*. 71(1): 96-105

Chandel NS (2014) Mitochondria as signaling organelles. *BMC Biol*. 12: 34

Chandel NS, Jasper H, Ho TT and Passegué E (2016) Metabolic regulation of stem cell function in tissue homeostasis and organismal ageing. *Nat Cell Biol*. 18(8): 823-32

Chandra D and Singh KK (2011) Genetic insights into OXPHOS defect and its role in cancer. *Biochim Biophys Acta*. 1807(6): 620-5

Chang CC, Rodriguez J and Ross J (2015) Mitochondrial-Nuclear Epistasis Impacts Fitness and Mitochondrial Physiology of Interpopulation Caenorhabditis briggsae Hybrids. *G3 (Bethesda)*. 6(1): 209-19

Chen JL, Lucas JE, Schroeder T, Mori S, Wu J, Nevins J, Dewhirst M, West M and Chi JT (2008) The genomic analysis of lactic acidosis and acidosis response in human cancers. *PLoS Genet*. 4(12): e1000293

Chinnery PF (2015) Mitochondrial disease in adults: what's old and what's new?. *EMBO Mol Med*. 7(12): 1503-12

Chujo T, Ohira T, Sakaguchi Y, Goshima N, Nomura N, Nagao A, Suzuki T (2012) LRPPRC/SLIRP suppresses PNPase-mediated mRNA decay and promotes polyadenylation in human mitochondria. *Nucleic Acids Res*. 40(16): 8033-47

Clancy DJ, Gems D, Harshman LG, Oldham S, Stocker H, Hafen E, Leevers SJ and Partridge L (2001) Extension of life-span by loss of CHICO, a Drosophila insulin receptor substrate protein. *Science*. 292(5514): 104-6

Clayton DA (1982) Replication of animal mitochondrial DNA. *Cell*. 28(4): 693-705

Colman RJ, Beasley TM, Kemnitz JW, Johnson SC, Weindruch R and Anderson RM (2014) Caloric restriction reduces age-related and all-cause mortality in rhesus monkeys. *Nat Commun*. 5: 3557

Colombani J, Bianchini L, Layalle S, Pondeville E, Dauphin-Villemant C, Antoniewski C, Carré C, Noselli S and Léopold P (2005) Antagonistic actions of ecdysone and insulins determine final size in Drosophila. *Science*. 310(5748): 667-70

Comfort A (1964) Ageing, The Biology of Senescence*. Holt, Rinehart and Winston. New York*

Cong L, Ran FA, Cox D, Lin S, Barretto R, Habib N, Hsu PD, Wu X, Jiang W, Marraffini LA and Zhang F (2013) Multiplex genome engineering using CRISPR/Cas system. *Science*. 339(6121): 819-23

Copeland JM, Cho J, Lo T Jr, Hur JH, Bahadorani S, Arabyan T, Rabie J, Soh J and Walker DW (2009) Extension of Drospphila life span by RNAi of the mitochondrial respiratory chain. *Curr Biol*. 19(19): 1591-8

Cox LS, Clancy DJ, Boubriak I and Saunders RD (2007) Modeling Werner Syndrome in Drosophila melanogaster: hyper-recombination in flies lacking WRN-like exonuclease. *Ann NY Acad Sci*. 1119: 274-88

Crosby AH, Patel H, Chioza BA, Proukakis C, Gurtz K, Patton MA, Sharifi R, Harlalka G, Simpson MA, Dick K, Reed JA, Al-Memar A, Chrzanowska-Lightowlers ZM, Cross He and Lighowlers RN (2010) Defective mitochondrial mRNA maturation is associated with spastic ataxia. *Am J Hum Genet*. 87(5): 655-60

Csiszar A, Labinskyy N, Perez V, Recchia FA, Podlutsky A, Mukhopadhyay P, Losonczy G, Pacher P, Austad SN, Bartke A and Ungvari Z (2008) Endothelial function and vascular oxidative stress in long-lived GH/IGF-deficient Ames dwarf mice. *Am J Physiol Heart Circ Physiol*. 295(5): H1882-94

Cuykendall TN and Houston DW (2010) Identification of germ plasm-associated transcripts by microarray analysis of Xenopus vegetal cortex RNA. *Dev Dyn*. 239(6): 1838-48

Darwin C (1859) The Origin of Species. Vol XI. The Harvard Classics. *New York: P.F. Collier & Son*, 1909-14

DeBerardinis RJ and Cheng T (2010) Q's next: the diverse functions of glutamine in metabolism, cell biology and cancer. *Oncogene*. 29(3): 313-24

DeHaan C, Habibi-Nazhad B, Yan E, Salloum N, Parliament M and Allalunis-Turner J (2004) Mutation in mitochondrial complex I ND6 subunit is associated with defective response to hypoxia in human glioma cells. *Mol Cancer*. 3: 19

Detmer SA and Chan DC (2007) Functions and dysfunctions of mitochondrial dynamics. *Nat Rev Mol Cell Biol*. 8(11): 870-9

Diaz-Vivancos P, de Simone A, Kiddle G and Foyer CH (2015) Glutathione-linking cell proliferation to oxidative stress. *Free Radic Biol Med*. 89: 1154-64

Dillin A, Hsu AL, Arantes-Oliveira N, Lehrer-Graiwer J, Hsin H, Fraser AG, Kamath RS, Ahringer J and Kenyon C (2002) Rates of behavior and aging specified by mitochondrial function during development. *Science*. 298(5602): 2398-401

Dimauro I, Pearson T, Caporossi D and Jackson MJ (2012) A simple protocol for the subcellular fractionation of skeletal muscle cells and tissue. *BMC Res Notes*. 5: 513

DiMauro S and Schon EA (2003) Mitochondrial respiratory-chain diseases. *N Engl J Med*. 348(26): 2656-68

Dmochowska A, Golik P and Stepien PP (1995) The novel nuclear gene DSS-1 of Saccharomyces cerevisiae is necessary for mitochondrial biogenesis. *Curr Genet*. 28(2): 108-12

Doonan R, McElwee JJ, Matthijssens F, Walker GA, Houthoofd K, Back P, Matscheski A, Vanfleteren JR and Gems D (2008) Against the oxidative damage theory of aging: superoxide dismutase protect against oxidative stress but have little or no effect on life span in Caenorhabditis elegans. *Genes Dev*. 22(23): 3236-41

Dröge W (2002) Free radicals in the physiological control of cell function. *Physiol Rev*. 82(1): 47-95

Dzbek J and Korzeniewski B (2008) Control over the contribution of the mitochondrial membrane potential (DeltaPsi) and proton gradient (DeltapH) to the protonmotive force (Deltap). In silico studies. *J Biol Chem*. 283(48): 33232-9

El-Bacha T and Da Poian AT (2013) Virus-induced changes in mitochondrial bioenergetics as potential targets for therapy. *Int J. Biochem Cell Biol*. 45(1): 41-6

El-Mir MY, Nogueira V, Fontaine E, Avéret N, Rigoulet M and Leverve X (2000) Dimethylbiguanide inhibits cell respiration via an indirect effect targeted on the respiratory chain complex I. *J Biol Chem*. 275(1): 223-8

Emanuelsson O, Nielsen H, Brunak S and Heijne G (2000) Predicting subcellular localization of proteins based on their N-terminal amino acid sequence. *J Mol Biol*. 300(4): 1005-16

Enríquez JA (2016) Supramolecular Organization of Respiratory Complexes. *Annu Rev Physiol*. 78: 533-61

Escribano A, Amor M, Pastor S, Castillo S, Sanz F, Codoñer-Franch P and Dasí F (2015) Decreased glutathione and low catalase activity contribute to oxidative stress in children with α-1 antitrypsin deficiency. *Thorax*. 70(1): 82-3

Evans AM, deHaven CD, Barrett T, Mitchell M and Milgram M (2009) Integrated, nontargeted ultrahigh performance liquid chromatography/electrospray ionization tandem mass spectrometry platform for the identification and relative quantification of the small-molecule complement of biological systems. *Anal Chem*. 81: 6656-67

Evans JM, Donnelly LA, Emslie-Smith AM, Alessi DR and Morris AD (2005) Metformin and reduced risk of cancer in diabetic patients. *BMJ*. 330(7503): 1304-5

Feng J, Bussière F and Hekimi S (2001) Mitochondrial electron transport is a key determinant of life span in Caenorhabditis elegans. *Dev Cell*. 1(5): 633-44

Floyd BJ, Wilkerson EM, Veling MT, Minogue CE, Xia C, Beebe ET, Wrobel RL, Cho H, Kremer LS, Alston CL, Gromek KA, Dolan BK, Ulbrich A, Stefely JA, Bohl Sl, Werner KM, Jochem A, Westphall MS, Rensvold JW, Taylor RW, Prokisch H, Kim JJ, Coon JJ, Pagliarini DJ (2016) Mitochondrial Protein Interaction Mapping Identifies Regulators of Respiratory Chain Function. *Mol Cell*. 63(4): 621-32

Folmes CD, Nelson TJ, Martinez-Fernandez A, Arrell DK, Lindor JZ, Dzeja PP, Ikeda Y, Perez-Terzic C and Terzic A (2011) Somatic oxidative bioenergetics transitions into pluripotency-dependent glycolysis to facilitate nuclear reprogramming. *Cell Metab*. 14(2): 264-71

Forster MJ, Dubey A, Dawson KM, Stutts WA, Lal H and Sohal RS (1996) Age-related losses of cognitive function and motor skills in mice are associated with oxidative protein damage in the brain. *Proc Natl Acad Sci USA*. 93(10): 4765-9

Fraga CG, Shigenaga MK, Park JW, Degan P and Ames BN (1990) Oxidative damage to DNA during aging: 8-hydroxy-2'-deoxyguanosine in rat organ DNA and urine. *Proc Natl Acad Sci USA*. 87(12): 4533-7

Ghezzi D and Zeviani M (2012) Assembly factors of human mitochondrial respiratory chain complexes: physiology and pathophysiology. *Adv Exp Med Biol*. 748:65-106

Giorgio M, Migliaccio E, Orsini F, Paolucci D, Moroni M, Contursi C, Pelliccia G, Luzi L, Minucci S, Marcaccio M, Pinton P, Rizzuto R, Bernardi P, Paolucci F and Pelicci PG (2005) Electron transfer between cytochrome c and p66Shc generates reactive oxygen species that trigger mitochondrial apoptosis. *Cell*. 122(2): 221-33

Gloeckner CJ, Boldt K, Schumacher A, Roepman R and Ueffing M (2007) A novel tandem affinity purification strategy for the efficient isolation and characterisation of native protein complexes. *Proteomics*. 7: 4228-4234

Gohil VM, Nilsson R, Belcher-Timme CA, Luo B, Root DE and Mootha VK (2010) Mitochondrial and nuclear genomic responses to loss of LRPPRC expression. *J Biol Chem*. 285(18): 13742-7

Goodier JL, Pereira GC, Cheung LE, Rose RJ and Kazazian HH Jr (2015) The Broad-Spectrum Antiviral Protein ZAP Restricts Human Retrotransposition. *PLoS Genet*. 11(5): e1005252

Gorenkova N, Robinson E, Grieve DJ and Galkin A (2013) Conformational change of mitochondrial complex I increases ROS sensitivity during ischemia. *Antioxid Redox Signal.* 19(13): 1459-68

Greaves LC, Reeve AK, Taylor RW and Turnbull DM (2012) Mitochondrial DNA and disease. *J Pathol*. 226(2): 274-86

Gui DY, Sullivan LB, Luengo A, Hosios AM, Bush LN, Gitego N, Davidson SM, Freikman E, Thomas CJ and Vander-Heiden MG (2016) Environment Dictates Dependence on Mitochondrial Complex I for NAD+ and Aspartate Production and Determines Cancer Cell Sensitivity to Metformin. *Cell Metab*. 24(5): 716-27

Gupta GD, Coyaud É, Gonçalves J, Mojarad BA, Liu Y, Wu Q, Gheiratmand L, Comartin D, Tkach JM, Cheung SW, Bashkurov M, Hasegan M, Knight JD, Lin ZY, Schueler M, Hildebrandt F, Moffat J, Gingras AC, Raught B and Pelletier L (2015) A Dynamic Protein Interaction Landscape of the Human Centrosome-Cilium Interface. *Cell*. 163(6): 1484-99

Haack TB, Kopajtich R, Freisinger P, Wieland T, Rorbach J, Nicholls TJ, Baruffini E, Walther A, Danhauser K, Zimmermann FA, Husain RA, Schum J, Mundy H, Ferrero I, Strom TM, Meitinger T, Taylor RW, Minczuk M, Mayr JA and Prokisch H (2013) ELAC2 mutations cause a mitochondrial RNA processing defect associated with hypertrophic cardiomyopathy. *Am J Hum Genet*. 93(2): 211-23

Haigis MC, Mostoslavsky R, Haigis KM, Fahie K, Christodolou DC, Murphy AJ, Valenzuela DM, Yancopoulos GD, Karow M, Blander G, Wolberger C, Prolla TA, Weindruch R, Alt FW and Guarente L (2006) SIRT4 inhibits glutamate dehydrogenase and opposes the effects of calorie restriction in pancreatic beta cells. *Cell*. 126(5): 941-54

Hällberg BM and Larsson NG (2011) TFAM forces mtDNA to make a U-turn. *Nat Struct Mol Biol*. 18(11): 1179-81

Hällberg BM and Larsson NG (2014) Making proteins in the powerhouse. *Cell Metab*. 20(2): 226-40

Hamanaka RB, Weinberg SE, Reczek CR and Chandel NS (2016) The Mitochondrial Respiratory Chain is Required for Organismal Adaptation to Hypoxia. *Cell Rep*. 15(3): 451-9

Hamilton B, Dong Y, Shindo M, Liu W, Odell I, Ruvkun G and Lee SS (2005) A systematic RNAi screen for longevity genes in C. elegans. *Genes Dev*. 19(13): 1544-55

Hanahan D and Weinberg RA (2011) Hallmarks of cancer: the next generation. *Cell*. 144(5): 646-74

Harman D (1956) Aging: a theory based on free radical and radiation chemistry. *J Gerontol.* 11(3): 298-300

Harman D (1965) The free radical theory of aging: effect of age on serum copper levels. *J Gerontol*. 20: 151-3

Hayakawa S, Shiratori S, Yamato H, Kameyama T, Kitatsuji C, Kashigi F, Goto S, Kameoka S, Fujikura D, Yamada T, Mizutani T, Kazumata M, Sato M, Tanaka J, Asaka M, Ohba Y, Miyazaki T, Imamura M and Takaoka A (2011) ZAPS is a potent stimulator of signaling mediated by the RNA helicase RIG-I during antiviral responses. *Nat Immunol*. 12(1): 37-44

He S and Fox TD (1997) Membrane translocation of mitochondrially coded Cox2p: distinct requirements for export of N and C termini and dependence on the conserved protein Oxa1p. *Mol Biol Cell*. 8(8): 1449-60

He Z, Zhu X, Wen W, Yuan J, Hu Y, Chen J, An S, Dong X, Lin C, Yu J, Wu J, Yang Y, Cai J, Li J and Li M (2016) Dengue Virus Subverts Host Inate Immunity by Targeting Adaptor Proteins MAVS. *J Virol*. 90(16): 7219-30

Hekimi S, Lapointe J and Wen Y (2011) Taking a “good” look at free radicals in the aging process. *Trends Cell Biol*. 21(10): 569-76

Hensley CT, Wasti AT and DeBerardinis RJ (2013) Glutamine and cancer: cell biology, physiology, and clinical opportunities. *J Clin Invest*. 123(9): 3678-84

Herrmann JM and Neupert W (2000) Protein transport into mitochondria. *Curr Opin Microbiol.* 3(2): 210-4

Holec S, Lange H, Kühn K, Alioua M, Börner T and Gagliardi D (2006) Relaxed transcription in Arabidopsus mitochondria is counterbalanced by RNA stability control mediated by polyadenylation and polynucleotide phosphorylase. *Mol Cell Biol*. 26(7): 2869-76

Huang W, Choi W, Chen Y, Zhang Q, Deng H, He W and Shi Y (2013) A proposed role for glutamine in cancer cell growth through acid resistance. *Cell Res*. 23(5): 724-7

Idzorek S (1976) Antiparkinsonian agents and fluphenazine decanoate. *Am J Psychiatry*. 133(1): 80-2

Invernizzi F, D’Amato I, Jensen PB, Ravaglia S, Zeviani M and Tiranti V (2012) Microscale oxygraphy reveals OXPHOS impairment in MRC mutant cells. *Mitochondrion*. 12(2): 328-35

Jablonski JA and Caputi M (2009) Role of cellular RNA processing factors in human immunodeficiency virus type 1 mRNA metabolism, replication, and infectivity. *J Virol*. 83(2): 981-92

Jacobs HT (1991) Structural similarities between a mitochondrially encoded polypeptide and a family of prokaryotic respiratory toxins involved in plasmid maintenance suggest a novel mechanism for the evolutionary maintenance of mitochondrial DNA. *J Mol Evol*. 32(4): 333-9

Jewel JL, Kim YC, Russell RC, Yu FX, Park HW, Plouffe SW, Tagliabracci VS and Guan KL (2015) Metabolism. Differential regulation of mTORC1 by leucine and glutamine. *Science*. 347(6218): 194-8

Jeong SM, Xiao C, Finley LW, Lahusen T, Souza AL, Pierce K, Li YH, Wang X, Laurent G, German NJ, Xu X, Li C, Wang RH, Lee J, Csibi A, Cerione R, Blenis J, Clish CB, Kimmerlman A, Deng CX and Haigis MC (2013) SIRT4 has tumor-suppressive activity and regulates the cellular metabolic response to DNA damage by inhibiting mitochondrial glutamine metabolism. *Cancer Cell*. 23(4): 450-63

Jourdain AA, Koppen M, Wydro M, Rodley CD, Lightowlers RN, Chrzanowska-Lightowlers ZM and Martinou JC (2013) GRSF1 regulates RNA processing in mitochondrial RNA granules*. Cell Metab*. 17(3): 399-410

Kaczmarczyk AN and Koop A (2011) Germline stem cell maintenance as a proximate mechanism of life-history trade-offs? Drosophila selected for prolonged fecundity have a slower rate of germline stem cell loss. *Bioessays.* 33(1): 5-12

Kenyon C, Chang J, Gensch E, Rudner A and Tabtiang R (1993) A C. elegans mutant that lives twice as long as wild type. *Nature*. 366(6454): 461-4

Khacho M, Clark A, Svoboda DS, Azzi J, MacLaurin JG, Meghaizel C, Sesaki H, Lagace DC, Germain M, Harper ME, Park DS and Slack RS (2016) Mitochondrial Dynamics Impacts Stem Cell Identity and Fate Decisions by Regulating a Nuclear Transcriptional Program. *Cell Stem Cell*. 19(2): 232-47

Kim I, Rodriguez-Enriquez S and Lemasters JJ (2007) Selective degradation of mitochondria by mitophagy*. Arch Biochem Biophys*. 462(2): 245-53

Kim TY, Wang D, Kim AK, Lau E, Lin AJ, Liem DA, Zhang J, Zong NC, Lam MP and Ping P (2012) Metabolic labeling reveals proteome dynamics of mouse mitochondria. *Mol Cell Proteomics*. 11(12): 1586-94

Kirkwood TB (1977) Evolution of ageing. *Nature*. 270(5635): 301-4

Koehler CM, Merchant S and Schatz G (1999) How membrane proteins travel across the mitochondrial intermembrane space. *Trends Biochem Sci*. 24(11): 428-32

Kong Y, Song Y, Hu Y, Shi MM, Wang YT, Wang Y, Zhang XH, Xu LP, Liu KY, Deng HK and Huang XJ (2016) Increased reactive oxygen species and exhaustion of quiescent CD34-positive bone marrow cells may contribute to poor graft function after allotransplants. *Oncotarget.* 7(21): 30892-906

Kotiadis VN, Duchen MR and Osellame LD (2014) Mitochondrial quality control and communications with the nucleus are important in maintaining mitochondrial function and cell health. *Biochim Biophys Acta*. 1840(4): 1254-65

Kroemer G and Pouyssegur J (2008) Tumor cell metabolism: cancer's Achilles' heel. *Cancer Cell*. 13(6): 472-82

Kudlow BA, Kennedy BK and Monnat RJ Jr (2007) Werner and Hutchinson-Gilford progeria syndromes: mechanistic basis of human progeroid diseases. *Nat Rev Mol Cell Biol.* 8(5): 394-404

Kühlbrandt W (2015) Structure and function of mitochondrial membrane protein complexes. *BMC Biol.* 13:89

Kung HN, Marks JR and Chi JT (2011) Glutamine synthetase is a genetic determinant of cell type-specific glutamine independence in breast epithelia. *PLoS Genet*. 7(8): e1002229

Kuo ML, Lee MB, Tang M, den Besten W, Hu S, Sweredoski MJ, Hess S, Chou CM, Changou CA, Su M, Jia W, Su L and Yen Y (2016) PYCR1 and PYCR2 Interact and Collaborate with RRM2B to Protect Cells from Overt Oxidative Stress. *Sci Rep.* 6: 18846

Kurosu H, Yamamoto M, Clark JD, Pastor JV, Nandi A, Gurnani P, McGuinness OP, Chikuda H, Yamaguchi M, Kawaguchi H, Shimomura I, Takayama Y, Herz J, Kahn CR, Rosenblatt KP and Kuro-o M (2005) Suppression of aging in mice by the hormone Klotho. *Science.* 309(5742): 1829-33

Kwong LK and Sohal RS (1998), Substrate and site specificity of hydrogen peroxide generation in mouse mitochondria. *Arch Biochem Biophys*. 350(1): 118-26

Lamb R, Ozsvari B, Lisanti CL, Tanowitz HB, Howell A, Martinez-Outschoorn UE, Sotgia F and Lisanti MP (2015) Antibiotics that target mitochondria effectively eradicate cancer stem cells, across multiple tumor types: treating cancer like an infectious disease. *Oncotarget*. 6(7): 4569-84

Lapuente-Brun E, Moreno-Loshuertos R, Acín-Pérez R, Latorre-Pellicer A, Colás C, Balsa E, Perales-Clemente E, Quirós PM, Calvo E, Rodríguez-Hernandéz MA, Navas P, Cruz R, Carracedo Á, López-Otín C, Pérez-Martos A, Fernández-Silva P, Fernández-Vizarra E, Enríque JA (2013) Supercomplex assembly determines eléctron flux in the mitochondrial electron transport chain. *Science*. 340(6140): 1567-70

Lee CM, Sedman J, Neupert W and Stuart RA (1999) The DNA helicase, Hmi1p, is transported into mitochondrial by a C-terminal cleavable targeting signal. *J Biol Chem*. 274(30): 20937-42

Lenaz G, Tioli G, Falasca AI and Genova ML (2016) Complex I function in mitochondrial supercomplexes. *Biochim Biophys Acta*. 1857(7): 991-1000

Lieberman BP, Ploessl K, Wang L, Qu Z, Zha Z, Wise DR, Chodosh LA, Belka G, Thompson CB and Kung HF (2011) PET imaging of glutaminolysis in tumors by 18F-(2S,4R)4-fluoroglutamine. *J Nucl Med*. 52(12): 1947-55

Lightowlers RN and Chrzanowska-Lightowlers ZM (2012) Exploring our origins-the importance of OriL in mtDNA maintenance and replication. *EMBO Rep*. 13(12): 1038-9

Litonin D, Sologub M, Shi Y, Savkina M, Anikin M, Falkenberg M, Gustafsson CM and Temiakov D (2010) Human mitochondrial transcription revised: only TFAM and TF2BM are required for transcription of the mitochondrial genes in vitro. *J Biol Chem*. 285(24): 18129-33

Liu X, Romero IL, Litchfield LM, Lengyel E and Locasale JW (2016) Metformin Targets Central Carbon Metabolism and Reveals Mitochondrial Requirements in Human Cancers. *Cell Metab*. 24(5): 728-739

López-Otín C, Blasco MA, Partridge L, Serrano M and Kroemer G (2013) The hallmarks of aging. *Cell.* 153(6): 1194-217

Lyle AN, Deshpande NN, Taniyama Y, Seidel-Rogol B, Pounkova L, Du P, Papaharalambus C, Lassègue B and Griendling KK (2009) Poldip2, a novel regulator of Nox4 and cytoskeletal integrity in vascular smooth muscle cells. *Circ Res*. 105(3): 249-59

Mannella CA, Buttle K, Rath BK and Marko M (1998) Electron microscopic tomography of rat-liver mitochondria and their interaction with the endoplasmic reticulum. *Biofactors*. 8(3-4): 225-8

Marchi S, Giorgi C, Suski JM, Agnoletto C, Bononi A, Bonora M, De Marchi E, Missiroli S, Patergani S, Poletti F, Rimessi A, Duszynski J, Wieckowski MR and Pinton P (2012) Mitochondria-ros crosstalk in the control of cell death and aging. *J Signal Transduct*. 2012:329635

Margossian SP, Li H, Zassenhaus HP and Butow RA (1996) The DExH box protein Suv3p is a component of a yeast mitochondrial 3'-to-5' exoribonuclease that suppresses group I intron toxicity. *Cell*. 84(2): 199-209

Marnett LJ, Hurd HK, Hollstein MC, Levin DE, Esterbauer H and Ames BN (1985) Naturally occurring carbonyl compounds are mutagens in Salmonella tester strain TA104. *Mutat Res*. 148(1-2): 25-34

Martín MA, Blázquez A, Gutierrez-Solana LG, Fernandéz-Moreira D, Briones P, Andreu AL, Garesse R, Campos Y and Arenas J (2005) Leigh syndrome associated with mitochondrial complex I deficiency due to a novel mutation in the NDUFS1 gene. *Arch Neurol*. 62(4): 659-61

Martínez-Reyes I and Chandel NS (2014) Mitochondrial one-carbon metabolism maintains redox balance during hypoxia. *Cancer Discov*. 4(12): 1371-3

Mercer TR, Neph S, Dinger ME, Crawford J, Smith MA, Shearwood AM, Haugen E, Bracken CP, Rackham O, Stamatoyannopoulos JA, Filipovska A and Mattick JS (2011) The human mitochondrial transcriptome. *Cell.* 146(4): 645-58

Merkey AB, Wong CK, Hoshizaki DK and Gibbs AG (2011) Energetics of metamorphosis in Drosophila melanogaster. *J Insect Physiol*. 57(10): 1437-45

Mesquita A, Weinberger M, Silva A, Sampaio-Marques B, Almeida B, Leão C, Costa V, Rodrigues F, Burhans WC and Ludovico P (2010) Caloric restriction or catalase

inactivation extends yeast chronological lifespan by inducing H2O2 and superoxide dismutase activity. *Proc Natl Acad Sci USA*. 107(34): 15123-8

Metaxakis A and Partridge L (2013) Dietary Restriction Extends Lifespan in Wild-Derived Populations of Drosophila melanogaster. *PLoS One*. 8(9): e74681

Metodiev MD, Lesko N, Park CB, Cámara Y, Shi Y, Wibom R, Hultenby K, Gustafsson CM and Larsson NG (2009) Methylation of 12S rRNA is necessary for in vivo stability of the small subunit of the mammalian mitochondrial ribosome. *Cell Metab*. 9(4): 386-97

Milenkovic D, Ramming T, Müller JM, Wenz LS, Gebert N, Schulze-Specking A, Stojanovsi D, Rospert S and Chacinska A (2009) Identification of the signal directing Tim9 and Tim10 into the intermembrane space of mitochondria. *Mol Biol Cell*. 20(10): 2530-9

Mimaki M, Wang X, McKenzie M, Thorburn DR, Ryan MT (2012) Understanding mitochondrial complex I assembly in health and disease. *Biochim Biophys Acta*. 1817(6): 851-62

Mirth C, Truman JW and Riddiford LM (2005) The role of the prothoracic gland in determining critical weight for metamorphosis in Drosophila melanogaster. *Curr Biol*. 15(20): 1796-807

Miwa S, Riyahi K, Patridge L and Brand MD (2004) Lack of correlation between mitochondrial reactive oxygen species production and life span in Drosophila. *Ann NY Acad Sci*. 1019: 388-91

Miyadera H, Amino H, Hiraishi A, Taka H, Murayama K, Miyoshi H, Sakamoto K, Ishii N, Hekimi S and Kita K (2001) Altered quinone biosynthesis in the long-lived clk-1 mutants of Caenorhabditis elegans. *J Biol Chem*. 276(11): 7713-6

Mockett RJ, Bayne AC, Kwong LK, Orr WC and Sohal RS (2003) Ectopic expression of catalase in Drosophila mitochondria increases stress resistance but not longevity. *Free Radic Biol Med*. 34(2): 207-17

Monaghan RM and Whitmarsh AJ (2015) Mitochondrial Proteins Moonlighting in the Nucleus. *Trends Biochem Sci*. 40(12): 728-35

Montoya J, Gaines GL and Attardi G (1983) The pattern of transcription of the human mitochondrial rRNA genes reveals two overlapping transcription units. *Cell*. 34(1): 151-9

Mootha Vk, Lepage P, Miler K, Bunkenborg J, Reich M, Hjerrild M, Delmonte T, Villeneuve A, Sladek R, Xu F, Mitchell GA, Morin C, Mann M, Hudson TJ, Robinson B, Rioux JD and Lander ES (2003) Identification of a gene causing human cytochrome c oxidase deficiency by integrative genomics. *Proc Natl Acad Sci USA*. 100(2): 605-10

Morais VA, Haddad D, Craessaerts K, De Bock PJ, Swerts J, Vilain S, Aerts L, Overbergh L, Grünewald A, Seibler P, Klein C, Gavaert K, Verstreken P and De Strooper B (2014) PINK1 loss-of-function mutations affect mitochondrial complex I activity via NdufA10 ubiquinone uncoupling. *Science*. 344(6180): 203-7

Morgan B, Ezerina D, Amoako TN, Riemer J, Seedorf M and Dick TP (2013) Multiple glutathione disulfide removal pathways mediate cytosolic redox homeostasis. *Nat Chem Biol*. 9(2): 119-25

Murphy MP, Holmgren A, Larsson NG, Halliwell B, Chang CJ, Kalyanaraman B, Rhee SG, Thornalley PJ, Partridge L, Gems D, Nyström T, Belousov V, Schumacker PT and Winterbourn CC (2011) Unraveling the biological roles of reactive oxygen species. *Cell Metab*. 13(4): 361-6

Nagaike T, Suzuki T, Katoh T and Ueda T (2005) Human mitochondrial mRNAs are stabilized with polyadenylation regulated by mitochondria-specific poly(A) polymerase and polynucleotide phosphorylase. *J Biol Chem*. 280(20): 19721-7

Neuman S, El Maadidi S, Faletti L, Haun F, Labib S, Schejtman A, Maurer U and Borner C (2015) How do viruses control mitochondria-mediated apoptosis. *Virus Res.* 209: 45-55

Nielsen H, Engelbrecht J, Brunak S and von Heijne G (1997) Identification of prokaryotic and eukaryotic signal peptides and prediction of their cleave sites. *Protein Eng,* 10(1): 1-6

Noh JH, Kim KM, Abdelmohsen K, Yoon JH, panda AC, Munk R, Kim J, Curtis J, Moad CA, Wohler CM, Indig FE, de Paula W, Dudekula DB, De S, Piao Y, Yang X, Martindale JL, de Cabo R and Gorospe M (2016) HuR and GRSF1 modulate the nuclear export and mitochondrial localization of the lncRNA RMRP. *Genes Dev*. 30(10): 1224-39

Nouws J, Nijtmans LG, Smeitink JA and Vogel RO (2012) Assembly factors as a new class of disease genes for mitochondrial complex I deficiency: cause, pathology and treatment options. *Brain*. 135(Pt 1): 12-22

Oehl-Jaschkowitz B, Vanakker OM, De Paepe A, Menten B, Martin T, Weber G, Christmann A, Krier R, Scheid S, McNerlan SE, McKee S and Tzchach A (2014) Deletions in 14q24.1q24.3 are associated with congenital heart defects, brachydactyly, and mild intellectual disability. *Am J Med Genet A*. 164A(3): 620-6

Ojala D, Montoya J and Attardi G (1981) tRNA punctuation model of RNA processing in human mitochondria. *Nature*. 290(5806): 470-4

Ong C, Lee QY, Cai Y, Liu X, Ding J, Yung LY, Bay BH and Baeg GH (2016) Silver nanoparticles disrupt germline stem cell maintenance in the Drosophila testis. *Sci Rep*. 6: 20632

Orr WC, Mockett RJ, Benes JJ and Sohal RS (2003) Effects of overexpression of copper-zinc and manganese superoxide dismutases, catalase, and thioredoxin reductase genes on longevity in Drosophila melanogaster. *J Biol Chem*. 278(29): 26418-22

Ostrander DB, Zhang M, Mileykovskaya E. Rho M and Dowhan W (2001) Lack of mitochondrial anionic phospholipids causes an inhibition of translation of protein components of the electron transport chain. A yeast genetic model system for the study of anionic phospholipid function in mitochondria. *J Biol Chem*. 276(27): 25262-72

Owen MR, Doran E and Halestrap AP (2000) Evidence that metformin exerts its anti-diabetic effects through inhibition of complex 1 of the mitochondrial respiratory chain. *Biochem J*. 348(Pt 3): 607-14

Owusu-Ansah E and Banerjee U (2009) Reactive oxygen species prime Drosophila haematopoietic progenitors for differentiation. *Nature*. 461(7263): 537-41

Palade GE (1952) The fine structure of mitochondria. *Anat Rec*. 114(3): 427-51

Pancrudo J, Shanske S, Coku J, Lu J, Mardach R, Akman O, Krishna S, Bonilla E and DiMauro S (2007) Mitochondrial myopathy associated with a novel mutation in mtDNA. *Neuromuscul Disord*. 17(8): 651-4

Papaconstantinou J (2009) Insulin/IGF-1 and ROS signaling pathway cross-talk in aging and longevity determination. *Mol Cell Endocrinol*. 299(1): 89-100

Park YW, Wilusz J and Katze MG (1999) Regulation of eukaryotic protein synthesis: selective influenza viral mRNA translation is mediated by the cellular RNA-binding protein GRSF1. *Proc Natl Acad Sci USA*. 96(12): 6694-9

Partridge L, Prowse N and Pignatelli P (1999) Another set of responses and correlated responses to selection on age at reproduction in Drosophila melanogaster. *Proc Biol Sci*. 266(1416): 255-61

Pietromonaco SF, Denslow ND and O'Brien TW (1991) Proteins of mammalian mitochondrial ribosomes. *Biochimie*. 73(6): 827-35

Poburko D, Santo-Domingo J and Demaurex N (2011) Dynamic regulation of the mitochondrial proton gradient during cytosolic calcium elevations. *J Biol Chem*. 286(13): 11672-84

Popot JL and de Vitry C (1990) On the microassembly of integral membrane proteins. *Annu Rev Biophys Chem*. 19: 369-403

Quinlan CL, Goncalves RL, Hey-Mogensen M, Yadava N, Bunik VI and Brand MD (2014) The 2-oxoacid dehydrogenase complexes in mitochondria can produce superoxide/hydrogen peroxide at much higher rates than complex I. *J Biol Chem*. 289(12): 8312-25

Rafikov R, Sun X, Rafikova O, Meadows ML, Desai AA, Khalpey Z, Yuan JX, Fineman JR and Black SM (2015) Complex I dysfunction underlies the glycolytic switch in pulmonary hypertensive smooth muscle cells. *Redox Biol*. 6: 278-86

Reyes A, Yasukawa T, Cluett TJ and Holt IJ (2009) Analysis of mitochondrial DNA by two-dimensional agarose gel electrophoresis. *Methods Mol Biol*. 554: 15-35

Ristow M and Zarse K (2010) How increased oxidative stress promotes longevity and metabolic health: The concept of mitochondrial hormesis (mitohormesis). *Exp Gerontol*. 45(6): 410-8

Ristow M and Schmeisser S (2011) Extending life span by increasing oxidative stress. *Free Radic Biol Med*. 51(2): 327-36

Robinson GL, Dinsdale D, Macfarlane M and Cain K (2012) Switching from aerobic glycolysis to oxidative phosphorylation modulates the sensitivity of mantle cell lymphoma cells to TRAIL. *Oncogene*. 31(48): 4996-5006

Rorbach J, Nicholls TJ and Minczuk M (2011) PDE12 removes mitochondrial RNA poly(A) tails and controls translation in human mitochondria. *Nucleic Acids Res*. 39(17): 7750-63

Rubio MA, Rinehart JJ, Krett B, Duvezin-Caubet S, Reichert AS, Söll and Alfonzo JD (2008) Mammalian mitochondria have the innate ability to import tRNAs by a mechanism distinct from protein import. *Proc Natl Acad Sci USA*. 105(27): 9186-91

Ryan MT and Hoogenraad NJ (2007) Mitochondrial-nuclear communications. *Annu Rev Biochem*. 76: 701-22

Sabharwal SS and Schumacker PT (2014) Mitochondrial ROS in cancer: initiators, amplifiers or an Achilles' heel?. *Nat Rev Cancer*. 14(11): 709-21

Sagan L (1967) On the origin of mitosing cells. *J Theor Biol*. 14(3): 255-74

Salabei JK, Gibb AA and Hill BG (2014) Comprehensive measurement of respiratory activity in permeabilized cells using extracellular flux analysis. *Nat Protoc*. 9(2): 421-38

Samhan-Arias AK and Gutierrez-Merino C (2014) Purified NADH-cytochrome b5 reductase is a novel superoxide anion source by apocynin: sensitivity to nitric oxide and peroxynitrite. *Free Radic Biol Med*. 73: 174-89

Samuels DC (2004) Mitochondrial DNA repeats constrain the life span of mammals. *Trends Genet*. 20(5): 226-9

Sánchez-Caballero L, Guerrero-Castillo S and Nijtman L (2016) Unraveling the complexity of mitochondrial complex I assembly: A dynamic process. *Biochim Biophys Acta*. 1857(7): 980-90

Sasarman F, Brunel-Guitton C, Antonicka H, Wai T, Shoubridge EA and LSFC Consortium (2010) LRPPRC and SLIRP interact in a ribonucleoprotein complex that regulates posttranscriptional gene expression in mitochondria. *Mol Biol Cell*. 21(8): 1315-23

Sasarman F and Shoubridge EA (2012) Radioactive labeling of mitochondrial translation products in cultured cells. *Methods Mol Biol*. 837: 207-17

Sazanov LA (2015) A giant molecular proton pump: structure and mechanism of respiratory complex I. *Nat Rev Mol Cell Biol*. 16(6): 375-88

Scheper GC, van der Klok T, van Andel RJ, van Berkel CG, Sissler M, Smet J, Muravina TI, Serkov SV, Uziel G, Bugiani M, Schiffmann R, Krägeloh-Mann I, Smeitnik JA, Florentz C, Van Coster R, Pronk JC and van der Knaap MS (2007) Mitochondrial aspartyl-tRNA synthetase deficiency causes leukoencelopathy with brain stem and spinal cord involvement and lactate elevation. *Nat Genet*. 39(4): 534-9

Schultz MB and Sinclair DA (2016) When stem cells grow old: phenotypes and mechanisms of stem cell aging. *Development*. 143(1): 3-14

Scialò F, Sriram A, Fernández-Avala D, Gubina N, Lõhmus M, Nelson G, Logan A, Cooper HM, Navas P, Enríquez JA, Murphy MP and Sanz A (2016) Mitochondrial ROS Produced via Reverse Electron Transport Extend Animal Lifespan. *Cell Metab*. 23(4): 725-34

Sessions OM, Barrows NJ, Souza-Neto JA, Robinson TJ, Hershey CL, Rodgers MA, Ramirez JL, Dimopoulos G, Yang PL, Pearson JL and Garcia-Blanco MA (2009) Discovery of insect and human dengue virus host factors. *Nature*. 458(7241): 1047-50

Sheftel AD, Stehling O, Pierik AJ, Netz DJ, Kerscher S, Elsässer HP, Wittig I, Balk J, Brandt U and Lill R (2009) Human ind1, an iron-sulfur cluster assembly factor for respiratory complex I. *Mol Cell Biol*. 29(22): 6059-73

Shyh-Chang N and Daley GQ (2013) Lin28: primal regulator of growth and metabolism in stem cells. *Cell Stem Cell*. 12(4): 395-406

Simon AF, Shih C, Mack A and Benzer S (2003) Steroid control of longevity in Drosophila melanogaster. *Science*. 299(5611): 1407-10

Sjostrand FS (1953) Electron microscopy of mitochondria and cytoplasmic double membranes. *Nature*. 171(4340): 30-2

Smogorzewska A, Desetty R, Saito TT, Schlabach M, Lach FP, Sowa ME, Clark AB, Kunkel TA, Harper JW, Colaiácovo MP and Elledge SJ (2010) A genetic screen identifies

FAN1, a Fanconi anemia-associated nucleasse necessary for DNA interstrand crosslink repair. *Mol Cell*. 39(1): 36-47

Stadtman ER (1992) Protein oxidation and aging. *Science*. 257(5074): 1220-4

Steenweg ME, Ghezzi D, Haack T, Abbink TE, Martinelli D, van Berkel CG, Bley A, Diogo L, Grillo E, Te Water Naudé J, Strom TM, Bertini E, Prokisch H, van der Knaap MS and Zeviani M (2012) Leukoencephalopathy with thalamus and brainstem involvement and Hugh lactate “LTBL” caused by EARS2 mutations. *Brain*. 135(Pt 5): 1387-94

Tan AS, Baty JW, Dong LF, Bezawork-Geleta A, Endaya B, Goodwin J, Bajzikova M, Kovarova J, Peterka M, Yan B, Pesdar EA, Slobol M, Filimonenko A, Stuart S, Vondrusova M, Kluckova K, Sachaphibulkij K, Rohlena J, Hozak P, Truksa J, Eccles D, Haupt LM, Griffiths LR, Neuzil J and Berridge MV (2015) Mitochondrial genome acquisition restores respiratory function and tumorigenic potential of cancer cells without mitochondral DNA. *Cell Metab*. 21(1): 81-94

Tatar M, Bartke A and Antebi A (2003) The endocrine regulation of aging by insulin-like signals. *Science*. 299(5611): 1346-51

Teixeira FK, Sanchez CG, Hurd TR, Seifert JR, Czech B, Preall JB, Hannon GJ and Lehmann R (2015) ATP synthase promotes germ cell differentiation independente of oxidative phosphorylation. *Nat Cell Biol*. 17(5): 689-96

Tennessen JM, Baker KD, Lam G, Evans J and Thummel CS (2011) The Drosophila estrogen-related receptor directs a metabolic switch that supports developmental growth. *Cell Metab*. 13(2): 139-48

Todorova T, Bock FJ and Chang P (2014) PARP13 regulates cellular mRNA post-transcriptionally and functions as a pro-apoptotic factor by destabilizing TRAILR4 transcript. *Nat Commun*. 5: 5362

Todorova T, Bock FJ and Chang P (2015) Poly(ADP-ribose) polymerase-13 and RNA regulation in immunity and cancer. *Trends Mol Med*. 21(6): 373-84

Triepels RH, Hanson BJ, van den Heuvel LP, Sundell L, Marusich MF, Smeitink JA and Capaldi RA (2001) Human complex I defects can be resolved by monoclonal antibody analysis into distinct subunit assembly patterns. *J Biol Chem*. 276(12): 8892-7

Tu MP, Yin CM and Tatar M (2002) Impaired ovarian ecdysone synthesis of Drosophila melanogaster insulin receptor mutants. *Aging Cell*. 1(2): 158-60

Tu YT and Barrientos A (2015) The Human Mitochondrial DEAD-Box Protein DDX28 Resides in RNA Granules and Functions in Mitoribosome Assembly. *Cell Rep*. S2211-1247(15):00058-3

Tuppen HA, Blakely EL, Turnbull DM and Taylor RW (2010) Mitochondrial DNA mutations and human disease. *Biochim Biophys Acta*. 1797(2): 113-28

Uchiumi T, Ohgaki K, Yagi M, Aoki Y, Sakai A, Matsumoto S and Kang D (2010) ERAL1 is associated with mitochondrial ribosome and elimination of ERAL1 leads to mitochondrial dysfunction and growth retardation. *Nucleic Acid Res*. 38(16): 5554-68

Vafai SB and Mootha VK (2012) Mitochondrial disorders as windows into an ancient organelle. *Nature*. 491(7424): 374-83

van Geldermalsen M, Wang Q, Nagarajah R, Marshall AD, Thoeng A, Gao D, Ritchie W, Feng Y, Bailey CG, Deng N, Harvey K, Beith JM, Selinger CI, O'Toole SA, Rasko JE and Holst J (2016) ASCT2/SLC1A5 controls glutamine uptake and tumor growth in triple-negative basal-like breast cancer. *Oncogene*. 35(24): 3201-8

Van Raamsdonk JM and Hekimi S (2009) Deletion of the mitochondrial superoxide dismutase sod-2 extends lifespan in Caenorhabditis elegans. *PLoS Genet*. 5(2): e1000361

Venema J and Tollervey D (1999) Ribosome synthesis in Saccharomyces cervisiae. *Annu Rev Genet*. 33: 261-311

Venneti S, Dunphy MP, Zhang H, Pitter KL, Zanzonico P, Campos C, Carlin SD, La Rocca G, Lyashchenko S, Ploessi K, Rohle D, Omuro AM, Cross JR, Brennan CW, Weber WA, Holland EC, Mellinghoff IK, Kung HF, Lewis JS and Thompson CB (2015) Glutamine-based PET imaging facilitates enhanced metabolic evaluation of gliomas in vivo. *Sci Transl Med*. 7(274): 274ra17

Vinogradov AD and Grivennikova VG (2016) Oxidation of NADH and ROS production by respiratory complex I. *Biochim Biophys Acta*. 1857(7): 863-71

Vinothkumar KR, Zhu J and Hirst J (2014) Architecture of mammalian respiratory complex I. *Nature*. 515(7525): 80-4

Wallin I (1992) On the nature of mitochondria. III. The demonstration of mitochondria by bacteriological methods. IV. A comparative study of the morphogenesis of root-nodule bacteria and chloroplasts. *American Journal of Anatomy*. 30(4): 451-71

Wang DD, Shu Z, Lieser SA, Chen PL and Lee WH (2009) Human mitochondrial SUV3 and polynucleotide phosphorylase form a 330-kDa heteropentamer to cooperatively degrade double-stranded RNA with a 3'-to-5' directionality. *J Biol Chem*. 284(31): 20812-21

Warburg O, Wind F and Negelein E (1927) The Metabolsim of Tumors in the Body. *J Gen Physiol*. 8(6): 519-30

Webb CT, Gorman MA, Lazarou M, Ryan MT and Gulbis JM (2006) Crystal structure of the mitochondrial chaperone TIM9.10 reveals a six-bladed alpha-propeller. *Mol Cell*. 21(1): 123-33

Wheaton WW, Weinberg SE, Hamanaka RB, Soberanes S, Sullivan LB, Anso E, Glasauer A, Dufor E, Mutlu GM, Budinger GS and Chandel NS (2014) Metformin inhibits mitochondrial complex I of cancer cells to reduce tumorigenesis. *Elife*. 3: e02242

Whelan SP and Zuckerbraun BS (2013) Mitochondrial signaling: forwards, backwards, and in between. *Oxid Med Cell Longev*. 2013:351613

Wiedenabb N, Pfanner N and Ryan MT (2001) The three modules of ADP/ATP carrier cooperate in receptor recruitment and translocation into mitochondria. *EMBO J*. 20(5): 951-60

Wise DR, DeBerardinis RJ, Mancuso A, Sayed N, Zhang XY, Pfeiffer HK, Nissim I, Daikhin E, Yudkoff M, McMahon SB and Thompson CB (2008) Myc regulates a transcriptional program that stimulates mitochondrial glutaminolysis and leads to glutamine addiction. *Proc Natl Acad Sci USA*. 105(48): 18782-7

Wise DR and Thompson CB (2010) Glutamine addiction: a new therapeutic target in cancer. *Trends Biochem Sci*. 35(8): 427-33

Wittig I, Braun HP and Schägger H (2006) Blue native PAGE. *Nature Protocols*. 1: 418-28

Wolf AR and Mootha VK (2014) Functional genomic analysis of human mitochondrial RNA processing. *Cell Rep*. 7(3): 918-31

Wu MC, Arimura GK and Yunis AA (1978) Mechanism of sensitivity of cultured pancreatic carcinoma to asparaginase. *Int J Cancer*. 22(6): 728-33

Wydro M, Bobrowicz A, Temperley RJ, Lightowlers RN and Chrzanowska-Lightowlers ZM (2010) Targeting of the cytosolic poly(A) binding protein PABPC1 to mitochondria causes mitochondrial translation inhibition. *Nucleic Acids Res*. 38(11): 3732-42

Xia J and Wishart DS (2010) MetPA: a web-based metabolomics tool for pathway analysis and visualization. *Bioinformatics*. 26: 2342-44

Yanagida O, Kanai Y, Chairoungdua A, Kim DK, Segawa H, Nii T, Cha SH, Matsuo H, Fukushima J, Fukasawa Y, Tani Y, Taketani Y, Uchino H, Kim JY, Inatomi J, Okayasu I, Miyamoto K, Takeda E, Goya T and Endou H (2001) Human L-type amino acid transporter 1 (LAT1): characterization of function and expression in tumor cell lines. *Biochim Biophys Acta*. 1514(2): 291-302

Yang W and Hekimi S (2010a) Two models of mitochondrial dysfunction lead independently to lifespan extension in Caenorhabditis elegans. *Aging Cell*. 9(3): 433-47

Yang W and Hekimi S (2010b) A mitochondrial superoxide signal triggers increased longevity in Caenorhabditis elegans. *PLoS Biol*. 8(12):e1000556

Yang Y, Song Y and Loscalzo J (2007) Regulation of the protein disulfide proteome by mitochondria in mammalian cells. *Proc Natl Acad Sci USA*. 104(26): 10813-7

Yasukawa T, Yang MY, Jacobs HT and Holt IJ (2005) A bidirectional origin of replication maps to the major noncoding region of human mitochondrial DNA. *Mol Cell*. 18: 651-62

Yu J, Lan X, Chen X, Yu C, Xu Y, Liu Y, Xu L, Fan HY and Tong C (2016) Protein synthesis and degradation are essential to regulate germline stem cell homeostasis in Drosophila testes. *Development*. 143(16): 2930-45

Zarse K, Schmeisser S, Groth M, Priebe S, Beuster G, Kuhlow D, Guthke R, Platzer M, Kahn CR and Ristow M (2012) Impaired insulin/IGF1 signaling extends life span by promoting mitochondrial L-proline catabolism to induce a transient ROS signal. *Cell Metab*. 15(4): 451-65

Zhang Y, Ikeno Y, Qi W, Chaudhuri A, Li Y, Bokov A, Thorpe SR, Baynes JW, Epstein C, Richardson A and Van Remmen H (2009) Mice deficient in both Mn superoxide

dismutase and glutathione peroxidase-1 have increased oxidative damage and a greater incidence of pathology but no reduction in longevity. *J Gerontol A Biol Sci Med Sci*. 64(12): 1212-20

Zhao R, Xuan Y, Li X and Xi R (2008) Age-related changes of germline stem cell activity, niche signaling activity and egg production in Drosophila. *Aging Cell*. 7(3): 344-54

Zhu Y and Gao C (2008) ZAP-mediated mRNA degradation. *RNA Biol*. 5(2): 65-7

Zhu Y, Chen G, Lv F, Wang X, Ji X, Xu Y, Sun J, Wu L, Zheng YT and Gao G (2011) Zinc-finger antiviral protein inhibits HIV-1 infection by selectively targeting multiply spliced viral mRNAs for degradation. *Proc Natl Acad Sci USA*. 108(38): 15834-9

Zickermann V, Wirth C, Nasiri H, Siegmund K, Schwalbe H, Hunte C, Brandt U (2015) Structural biology. Mechanistic insight from the crystal structure of mitochondrial complex I. *Science*. 347(6217): 44-9